UNIVERSITY OF TURKU

Retinal plasticity in the context of a partially rescued retinitis pigmentosa mouse model

Master's thesis
University of Turku
MSc Degree Programme in
Biomedical Sciences
Drug Discovery and Development
03/2022

Peppi Raunioniemi

Supervisors
Susanne F. Koch, PhD
Professor of Molecular Pharmacology, Principal Investigator
Department of Pharmacy
Faculty of Chemistry and Pharmacy
Ludwig Maximilian University of Munich

Ullamari Pesonen, PhD
Professor of Pharmacology and Drug Development
Institute of Biomedicine
Faculty of Medicine
University of Turku

The originality of this thesis has been checked in accordance with the University of Turku quality assurance system using the Turnitin Originality Check service.

Master's thesis

Subject: Institute of Biomedicine, MDP in Biomedical Sciences, Drug Discovery and Development
Author: Peppi Raunioniemi
Title: Retinal plasticity in the context of a partially rescued retinitis pigmentosa mouse model
Supervisors: Prof. Susanne F. Koch (1st), Ludwig Maximilian University of Munich
Prof. Ullamari Pesonen (Formal), University of Turku
Number of pages and Supplementary materials: 86 pages, 5 supplementary figures
Date: 21.03.2022

Retinitis pigmentosa (RP) is a major cause of hereditary blindness and visual disability. The prevalence of RP is estimated to be 1/4000, affecting approximately 2.5 million people worldwide. RP is a very slow-progressing disease, and its symptoms start usually during adolescence. Mutations in over 70 different genes can cause photoreceptor cell degeneration leading to retinitis pigmentosa. A common RP-related gene is *PDE6B* which encodes a β-subunit of PDE6-enzyme which has a crucial function in rod-mediated vision.

No cure is available currently for RP patients. Treatment options are few, but the most promising one is gene therapy. Since retinal gene therapy is delivered by a single sub-retinal injection, it does not rescue all the diseased photoreceptor cells. The impact of the non-rescued photoreceptor cells on the rescued ones is not fully understood. This remains a challenge for the therapy.

The project aimed to study the retinal morphology and the function of the retinal pigment epithelium (RPE) in 48-week-old diseased (RP) and partially rescued mice. *Pde6b*$^{ST/WT}$ mice have a functional *Pde6b* allele and were used as a control in the experiments. *Pde6b*$^{ST/ST}$ mice have a *loxP*-flanked stop cassette in the intron 1 of both loci of the *Pde6b* gene. The stop cassette contains multiple polyadenylation signals which prevent gene expression. *Pde6b*$^{ST/ST}$ exhibit progressive rod degeneration. In *Pde6b*$^{ST/ST}$ *Pax6αCre* mice, stop cassettes are partially removed by the Cre recombinase which is expressed under a *Pax6α* promoter. Both *Pde6b* alleles are functional in the distal retina whereas the non-recombined retina in the center remains mutant.

Retinal sections were stained with multiple antibodies to study the retinal morphology. RPE morphology was studied by quantifying fluorescence images from RPE wholemounts. Apoptotic cell death in the RPE cells was studied by using a commercial TUNEL assay. In normal physiology, RPE cells phagocytose photoreceptor cell outer segments and this process was studied by using an *ex vivo* assay.

According to the results, the partially rescued retina of *Pde6b*$^{ST/ST}$ *Pax6αCre* showed signs of retinal remodelling. This can be seen as beneficial for the retinal gene therapies conducted by a single injection if the partially rescued retina can regenerate and expand the rescued area. The diseased retina of *Pde6b*$^{ST/ST}$ showed large-scale retinal degeneration and revealed heterogeneity of the RPE.

Keywords: retinitis pigmentosa, retinal pigment epithelium, retina, retinal remodelling, Pde6b mutation, Cre recombinase

Contents

1 Introduction

1.1 Human vision and the function of the retina

The major unit behind the human vision is the retina which contains several cell layers lining at the back of the eyeball (Fig.1). When light travels through the lens into the retina, it is first detected by two types of photoreceptor cells, cones and rods. After phototransduction in photoreceptor cells, the signal continues first to bipolar cells and then to ganglion cells which axons form the optic nerve and finally, the signal achieves the brain. Then, visual experience occurs. Furthermore, the retina consists

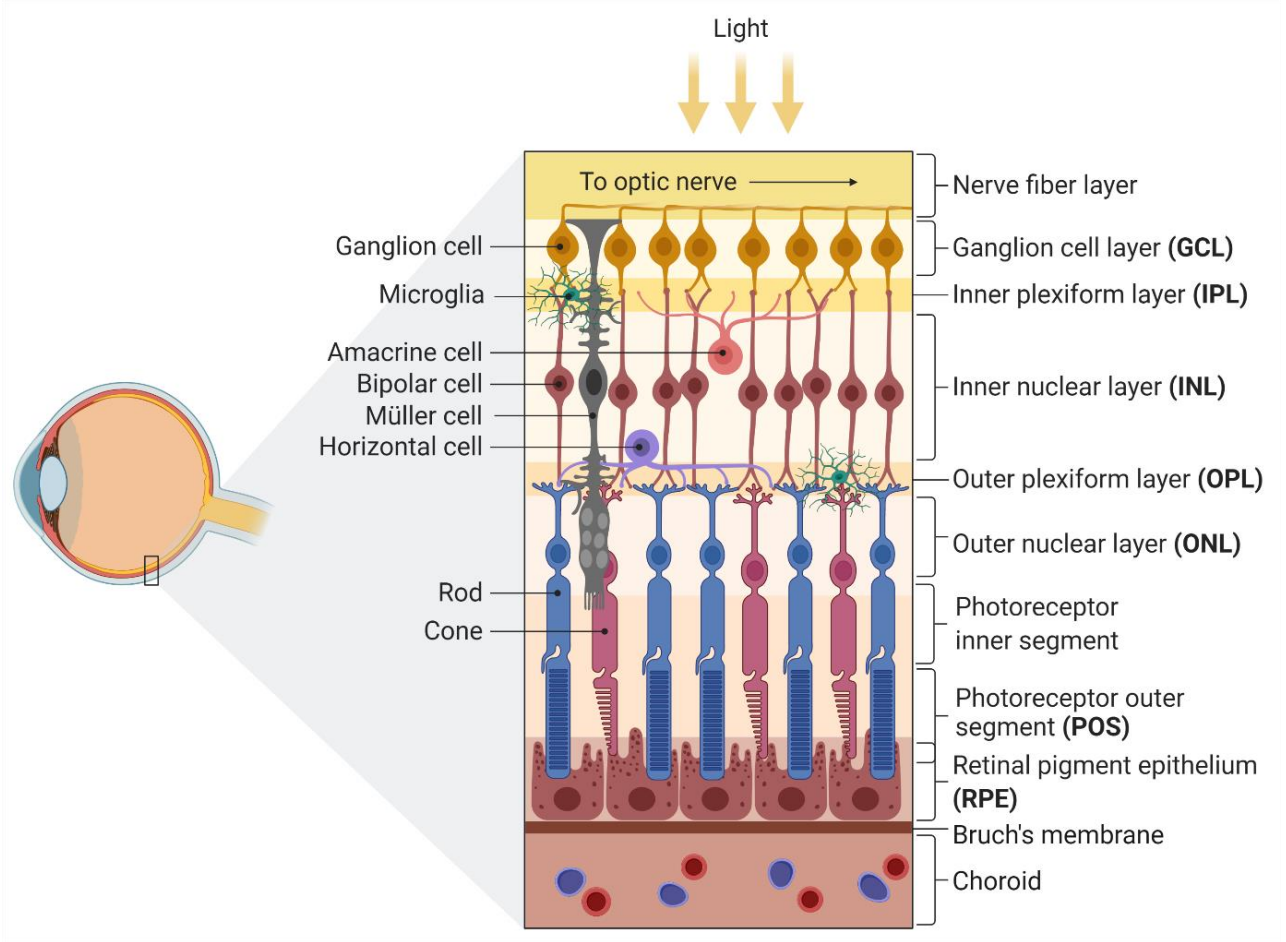

Figure 1. Structure of the human retina. The retina contains many different cell types all of them have a unique function to maintain the retinal homeostasis and ensure the function of vision. The outer nuclear layer (ONL) contains the nuclei and the cell bodies of photoreceptor cells. Cell bodies of bipolar cells, horizontal cells, Müller glia cells and amacrine cells form the inner nuclear layer (INL). Ganglion cell layer (GCL) contains ganglion cells and some amacrine cells. The axons of ganglion cells form the optic nerve. Two synaptic (plexiform) layers separate these three nuclear layers which contain dendrites and synapses. Between the GCL and the INL is the inner plexiform layer (IPL) and between the INL and the ONL is the outer plexiform layer (OPL). In the IPL, ganglion cells, amacrine cells and the bipolar cell axons are connected. In the OPL, photoreceptor cells, bipolar cells and horizontal cells interact. Additionally, microglia cells lay in the GCL, IPL and OPL. Müller cells have long cell bodies, and they extend throughout the whole retina. Retinal pigment epithelium (RPE) lays right below the photoreceptor outer segments, POS. *Created with BioRender.com.*

of diverse cell types, all of which have an essential function to maintain retinal homeostasis. (Wilkinson et al., 2018) Human and mouse retinae have similar, well-organized structures and the same retinal cell types are found in both retinae. However, the mouse retina seems to have a higher rods density than the human retina (Jeon et al., 1998). While the human retina consists of three types of cones, the mouse retina has two (Nikonov et al., 2006). Another main difference is that the mouse retina does not contain a macula, which is a small, pigmented area in the central retina responsible for high-resolution and colour vision. It contains a high density of cones in its central part, the fovea (Volland et al., 2015).

1.1.1 Cone and rod photoreceptors cells

A human retina consists of approximately 100 million rods and 6 million cones. The ratio can be explained by the different functions; cones are responsible for colour vision and rods for peripheral and night vision. Rods and cones are sensory neurons that are capable to convert photons of light into an electrical signal that can be detected by the nervous system. (Baylor et al., 1979) On a cellular level, rods are more sensitive than cones. Even a single photon can reach the limit of phototransduction cascade through rods, but cones are about 100 times less sensitive. (Burkhardt, 1994)

Cones differ morphologically and functionally from rods. A major part of cones is in the fovea, which is a central area of the retina specialized for high acuity vision. Cones express several types of visual pigments, called opsins, which spectral sensitivity defines the subtype of the cone. In humans, three cone subtypes exist: short-, middle- and long-wavelength cones (S, M and L). This classification defines in which wavelength the cone is most sensitive: For the S-cones, the sensitivity peak is 445 nm (blue), for M-cones 543 nm (green) and L-cones 566 nm (red). The minority of cones corresponds to blue S-cones (~10%), whereas the majority is red L-cones. The sum of the impulses from rods and cones eventually defines our visual experience. (Shevell and Kingdom, 2007) Cones are less sensitive to photons and thus function mainly during daylight. Their response time is short which enables them to detect moving objects. Rods are highly sensitive to photons, but their response time is much longer which adapts them to function in the dark. Rods have a stable distribution around the retina, with an exception in the fovea where cones have a majority. (Kawamura and Tachibanaki, 2008)

Photoreceptor cells are both highly polarized cells and can be divided into four subcellular regions: the outer segment (OS), the inner segment (IS), the nucleus, and the synaptic terminal (Fig. 2). The OS contains discs where photons are captured as starting the phototransduction cascade. Rods have cylinder-shaped OS whereas cones have shorter, approximately half of the length of rod OS, and

shape is thinner on the tip. OS contains discs with a major protein content of opsins. In rods, opsin is rod opsin (rhodopsin when the protein is bound to 11-*cis* retinal). Despite the dense packaging of rhodopsin on the disc membranes, it is functional only as a monomer. (Pugh and Lamb, 2000) The IS contains organelles for protein synthesis (Golgi apparatus and endoplasmic reticulum) and metabolism (mitochondria, lysosomes). The synaptic terminal contains glutamate vesicles which are released into the synaptic cleft constantly in the dark. When light falls, cyclic guanosine monophosphate (cGMP) levels decrease and cGMP gated cation channels (CNG) close leading to hyperpolarization of the cell membrane and finally a reduction of glutamate release at the synapse. This signal is detected by bipolar and horizontal cells. (Sung and Chuang, 2010; Wilkinson et al., 2018) Rods and cones are connected by gap junctions which allow the electrical and chemical coupling between these two cell types (Asteriti et al., 2014; Raviola and Gilula, 1973).

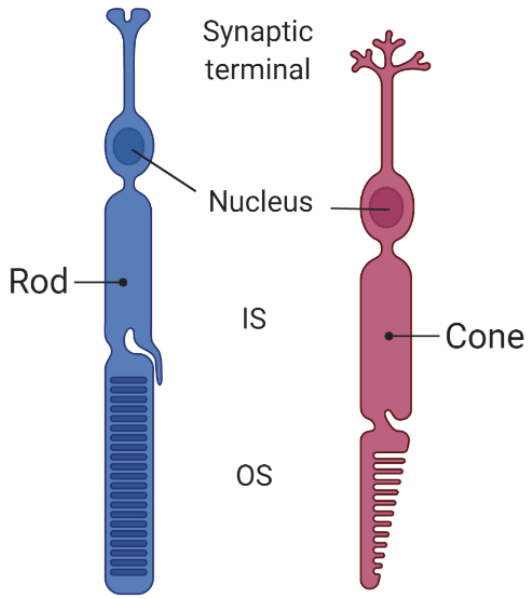

Figure 2. Structure of cone and rod photoreceptor cells. Rods and cones contain four subcellular regions: the outer segment (OS), the inner segment (IS), the nucleus, and the synaptic terminal. *Created with BioRender.com.*

Photoreceptor cells play a key role in the glucose metabolism between them and the retinal pigment epithelium (RPE). Once glucose is transported from the choroid through the RPE to the photoreceptor cells, most of it is converted to lactate through aerobic glycolysis. Aerobic glycolysis produces adenosine triphosphate (ATP) to photoreceptor cells. Lactate is transported back to the RPE and Müller cells for their energy metabolism. RPE cells produce fatty acids and ketone bodies which are delivered to photoreceptor cells which use them to the Krebs cycle and oxidative phosphorylation to produce ATP. (Kanow et al., 2017; Viegas and Neuhauss, 2021) Glucose transporter 1 (GLUT1) is the major glucose transporter in the RPE and photoreceptor cells (Gospe et al., 2010; Mantych et al., 1993).

1.1.2 Bipolar, horizontal and ganglion cells

Cones and rods send signals into bipolar and horizontal cells (Fig. 3). Horizontal cells (HCs) are interconnecting neurons located in the INL. HCs are extensively coupled cells which increases their receptive field enormously. The function of HCs is not fully understood, but the current consensus is that they provide negative feedback signals for cones and rods. (Twig et al., 2003) In the light, the hyperpolarization of photoreceptor cells causes HCs to hyperpolarize continuously (Kaneko, 1970). Upon the hyperpolarization, HCs send feedback signals for photoreceptor cells which induce the calcium channels to open and let calcium ions flow inside the cell. This allows glutamate to release into the synaptic cleft between photoreceptor and bipolar cell. The feedback cascade causes surrounding photoreceptor cells to depolarize. (Kamermans and Spekreijse, 1999; Thoreson et al., 2008)

Bipolar cells are glutamatergic interneurons having similar glutamate ribbons near synapses as photoreceptors (Fig. 3). Additionally, bipolar cells can be divided into two groups: rod bipolar cells

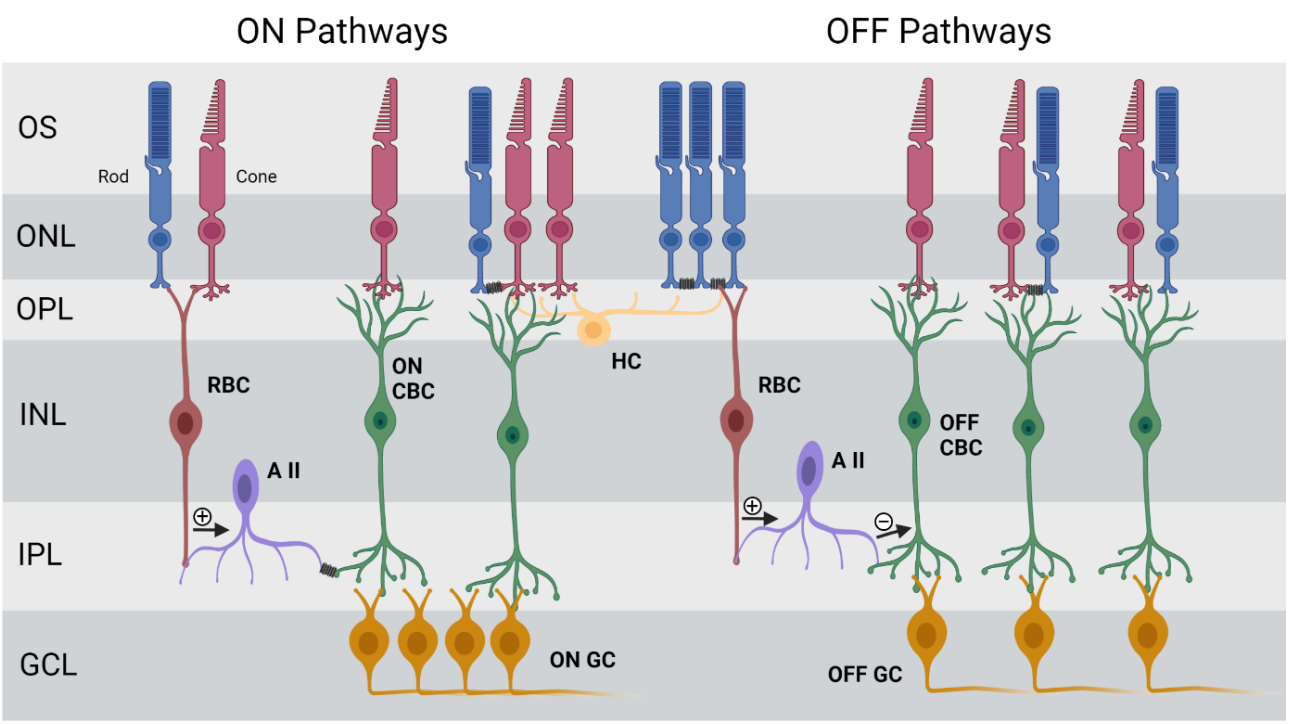

Figure 3. Bipolar cell pathways in the retina. ON pathways include rod bipolar cells (RBCs) and ON cone bipolar cells (ON CBCs). RBCs receive signals mainly from rods but also from cones. They depolarize by light and send glutamatergic signals onto AII amacrine cells. Amacrine cells are connected via gap junctions with ON CBCs which synapse onto the ON ganglion cells (ON GCs). OFF pathways include (ON) RBCs and OFF CBCs. OFF CBCs receive glutamatergic signals mostly from cones but also some of the OFF CBC subtypes and additionally from rods. RBCs send glutamatergic signals to AII amacrine cells as in the ON pathway but in the OFF pathway amacrine cells make inhibitory glycinergic signals onto OFF CBCs. Since rods and cones have gap junctions between them, rods can send signals indirectly through both ON and OFF CBCs. HC, horizontal cell. Adapted from Fain & Sampath, 2018. *Created with BioRender.com.*

(RBCs) and cone bipolar cells (CBCs). Vertebrates have two types of bipolar cells: ON and OFF bipolar cells. Cone bipolar cells have 9-12 ON- and OFF subtypes depending on the species. The length of the different subtypes varies, and they can end in various depths of the IPL. ON and OFF CBCs are defined by the types of postsynaptic glutamate receptors on their dendrites. OFF CBCs express α-amino-3-hydroxy-5-methyl-4-isoxazole propionic acid (AMPA)/kainate receptors in their dendrites. Whereas, ON CBCs and RBCs have metabotropic glutamate receptor 6 (mGluR6) receptors. (Shekhar et al., 2016; Ghosh et al., 2004)

ON pathways include RBCs and ON CBCs. Until this day, only one type of RBC has been characterized in mammals (Masu et al., 1995). RBCs receive signals mostly from rods but also from cones. In the light, RBCs depolarize and send glutamate signals for AII amacrine cells, which have gap junctions with ON CBCs. Furthermore, ON CBCs contact with ON-type ganglion cells (ON GCs). Rods are known to share signals with other rods by gap junctions, but also with cones that export the signal onto the ON CBCs. Light causes a depolarization of ON CBCs. In the darkness, ON CBCs are hyperpolarized due to the constant glutamate release from the photoreceptors. Currently, there has been published evidence showing that ON CBCs might have input also from rods (Whitaker et al., 2021).

OFF pathways include (ON) RBCs and OFF CBCs. OFF CBCs are hyperpolarized by light, similarly to cones. The synapse between a cone and an OFF CBC is like the synapse between a cone and a horizontal cell. In the OFF pathway, RBCs behave as in the ON pathway but AII amacrine cells make inhibitory glycinergic synapses onto OFF CBCs. These cells have synapses onto the OFF-ganglion cells (OFF GCs). Most of the OFF CBCs receive input from cones but at least three OFF CBC subtypes have shown additional contact with rods (mice, primates). Additionally, indirect signals from rods to cones by gap junctions reach the OFF CBCs. (Fain and Sampath, 2018; Wilkinson et al., 2018)

Ganglion cells (GCs) are the retina output neurons; they receive signals from both the ON and the OFF CBCs by glutamatergic AMPA receptors. In addition, amacrine cells have synapses and gap junctions also to GCs but these mechanisms are not well understood. Currently, 40 different ON and OFF GC subtypes have been identified from mouse retina (Baden et al., 2016). The major neurotransmitter in GCs is glutamate. GC axons form the optic nerve which runs across the vitreal surface. In contrast to other inner retinal cells, GCs send action potentials that fits better for relatively long distance to the brain. (Dacey, 2004)

1.1.3 Amacrine and glial cells

While horizontal cells get input from photoreceptor cells, amacrine cells are in contact with bipolar cells (Fig. 3). Amacrine cells can be divided into two groups by their dendritic size: narrow- and wide-field amacrine cells. Narrow-field amacrine cells are mainly glycinergic and wide-field cells GABAergic (Lin and Masland, 2006; Majumdar et al., 2009). 30 morphologically different mammalian amacrine cells are known (Lin and Masland, 2006; MacNeil and Masland, 1998). AII amacrine cells are the major transporters of signals from the RBCs to the CBCs (Fig. 3). They have inhibitory synapses into the CBCs in the OFF pathway, and gap junctions into the CBCs in the ON pathway. AII amacrine cells are in contact with all the retinal bipolar cells forming a dense connectome. Different connections can be divided into four categories including postsynaptic relation with RBCs, gap junctions with most ON CBCs, and then both postsynaptic and gap junctions with either CBC subclass 7 or all OFF CBCs. (Marc et al., 2014) AII cells are highly coupled cells having abundant gap junctions between each other. (Mills and Massey, 1995) Although AII amacrine cells impact mostly rod-mediated vision, due to the two-dimensional AII-AII gap junctions, also cone vision is shown to be affected. (Van Wyk et al., 2009).

The human retina consists of diverse glial cells including microglia and two types of macroglia: Müller cells and astrocytes (Fig. 1). Microglia are phagocytes and antigen-presenting cells. Resting microglia cells are found in the plexiform and ganglion cell layers. They constantly clear their microenvironment by phagocytosing metabolic products and cellular debris. (Fontainhas et al., 2011) Once microglia detect a pathogenic stimulus, it becomes activated, proliferates, and moves into the region of damage. (Ferrer-Martín et al., 2015) Microgliosis (increased microglia in the pathogenic site) is common in many retinopathies such as retinal detachment or proliferative vitreoretinopathy (Hollborn et al., 2008). Microglia and immune cells (monocytes/macrophages, neutrophils) delivered from the bloodstream mediate the inflammation and fibrinolysis in the site of pathogenesis. (Rashid et al., 2019) Chronic, dysregulated inflammation commonly generates secondary tissue damage. Activated microglia produce multiple pro-inflammatory agents such as prostaglandins, matrix metalloproteases (MMPs), reactive radicals, Fas-ligand and proinflammatory cytokines like IL-1β and TNF-α. (Wilkinson et al., 2018) In addition, activated microglia secretes a protein called endothelin-2 which induces ganglion cell death, astrogliosis and vasoconstriction. These factors increase the risk of glaucoma. (Howell et al., 2011)

Müller glia span the complete retina and represent about 90% of the retinal glial cell population (Vecino et al., 2016). Their cell bodies are found in the INL, and two vertical axons radiate in opposite

directions. Müller cells have a crucial role in the visual cycle of cone photoreceptors. They convert cone-driven *trans*-retinol to 11-*cis* retinal which then can be reused in the phototransduction cascade. (Xue et al., 2017) By uptake of the neurotransmitters glutamate and GABA, Müller glia regulate synaptic activity of the inner retina (Bringmann et al., 2013). Glutamate is needed to produce antioxidant glutathione in Müller cells. Glutathione is released rapidly from Müller cells in response to oxidative stress, such as ischemia and provided to the neurons. In general, the retina needs a lot of antioxidative protection due to its high light exposure and high oxygen consumption. (Pow and Crook, 1995; Schütte and Werner, 1998) Another important function of Müller cells is to maintain the osmotic and potassium homeostasis in the retina. Extracellular potassium is taken up by Müller cells mainly passively through Kir4.1 channels (Kofuji et al., 2000). Maintenance of osmotic homeostasis occurs through aquaporin-4 (AQP4) receptors, specialized transporters for water molecules (Nagelhus et al., 1998).

Astrocytes contribute most of its glia functions together with Müller cells. They maintain retinal water homeostasis through AQP4 receptors (Bosco et al., 2005). Together, astrocytes and Müller cells also regulate extracellular pH, remove carbon dioxide and excess potassium, and clear extracellular fluid originated from neurotransmitter activity. (Fernández-Sánchez et al., 2015; Reichenbach and Bringmann, 2013) Also, they maintain retinal vascular stability together with microglia and pericytes by inhibiting vascular endothelial cell proliferation. On the other hand, astrocytes are also the main vascular endothelial growth factor (VEGF) producers in the retina (Stone et al., 1995). The distribution of astrocytes follows mainly the retinal blood vessels. Astrocytes get activated in response to ischemia, increased intraocular pressure or excitotoxicity (prolonged activation of excitatory receptors such as glutamate receptors). (Bringmann et al., 2006; Vecino et al., 2016) Age-related astrocyte degeneration is associated with the degeneration of the blood-retinal barrier (Chan-Ling et al., 2007).

1.1.4 Retinal pigment epithelium

The retinal pigment epithelium is the outermost layer of the retina (Fig. 4). The basal side of the RPE is connected to Bruch's membrane and choroid, and the apical side to the outer segments of photoreceptor cells (POSs). RPE consists of a single layer of cuboidal epithelial cells which are joined together by tight junctions (Rizzolo, 2007). RPE constitutes the outer blood-retinal barrier. The human eye consists of approximately 3.5 x 10^6 RPE cells (Panda-Jonas et al., 1996). A specific feature of RPE cells is that they are postmitotic, meaning that the RPE cell population remains stable during adult life except in certain diseases. The apical part contains numerous microvilli (3-7 μm) whereas

the basolateral membrane is flat and lies on the top of the Bruch´s membrane. (Sparrow et al., 2010) The Bruch´s membrane contains mainly collagen and elastin and is located between the RPE and choroid capillaries (Benedicto et al., 2017).

The nuclei number of RPE cells varies but the reason for multi-nucleate RPE cells is not fully understood. However, it has been proposed that multi-nucleate cells may have a protective role against stress or cancer cells (Pandit et al., 2013). RPE cells become multi-nucleated by ageing. Also, the size of the cell increases. Multinucleation does not seem to be due to cell fusion, but to incomplete cell division. Interestingly, phagocytosis capacity is identical regardless of the nuclei number. POS exposure promotes multinucleation *in vitro* and suppresses cell proliferation. Additionally, exposure to POSs induces the formation of reactive radicals and DNA oxidation in RPE cells. (Chen et al., 2016)

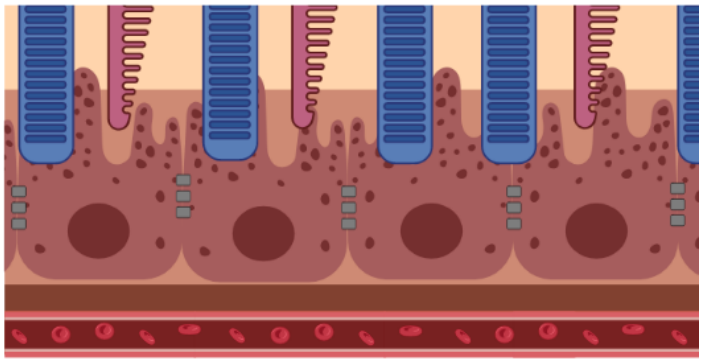

Figure 4. RPE cell layer of the retina. The RPE consists of a single layer of cuboidal epithelial cells which are joined together by tight junctions. RPE cells are highly polarized having the basal side right above the Bruch´s membrane (brown layer) and the apical part with microvilli in contact with POS. Choroidal capillaries transport nutrients to and metabolic waste from the retina, and they are found right below the Bruch´s membrane. *Created with BioRender.com.*

The energy metabolism of the RPE is largely dependent on lactate produced by photoreceptor cells. Glucose is taken in by RPE from choroidal capillaries and transported for photoreceptor cells, which then convert it to lactate via aerobic glycolysis. Lactate is transported for RPE and Müller cells. RPE cells use lactate to the Krebs cycle and oxidative phosphorylation to produce ATP. RPE cells use a minimal amount of glucose in their energy metabolism through glycolysis. Lactate seems to inhibit glycolysis in the RPE, and thus it has been proposed that this may be due to the enhanced glucose transportation to photoreceptor cells. Phagocytosis of POSs by the RPE cells leads to increased intracellular levels of fatty acids which are converted into ketone bodies via β-oxidation. Further, the ketone bodies can be metabolized and used for the Krebs cycle for ATP production. (Kanow et al., 2017; Viegas and Neuhauss, 2021) It has been shown *in vitro* that oxidative stress induces RPE cells to produce citrate via reductive carboxylation of α-ketoglutarate. In the cytosol, citrate participates to change of $NADP^+$ to NADPH. The cytosolic NADPH can be used to protection of oxidative stress. (Du et al., 2016).

RPE has many essential functions to maintain the homeostasis of the retina. RPE maintains the ion balance in the subretinal space. Sodium/potassium adenosine triphosphatase (Na^+/K^+-ATPase) mediates the active outflux of Na^+- and the influx of K^+-ions. Na^+/K^+-ATPase is located in the apical membrane of the RPE. High Na^+-ion concentration in subretinal space is essential for the function of photoreceptor cells. During the dark current, cGMP-gated channels are open and Na^+ ions can enter and depolarize photoreceptor cells. Another critical function of the RPE related to the phototransduction cascade is the re-isomerization of *trans*-retinal into the *cis* configuration. In addition, RPE transports water and Cl^- ions from photoreceptor cells into the bloodstream, and vitamin A and glucose from the bloodstream into the photoreceptor cells, respectively. (Strauss, 2005; Sparrow et al., 2010) The most abundant organelle in RPE cells is the melanosome, a lysosome-like structure producing melanin. Melanin acts as a light-absorbing pigment but also protects the retina by quenching reactive radicals. (Glickman et al., 2001)

One of the major roles of the RPE is to phagocytose the POSs. RPE cells are the most actively phagocytosing cells in the human body. Phagocytosis takes place daily via diurnal rhythm, about 1 hour after light onset (Milićević et al., 2021). This process is essential for the long-term functionality and viability of photoreceptor cells. (Kwon and Freeman, 2020) It is estimated that 7-10% of the POS population is phagocytosed per day meaning that the whole POS population is replaced every two weeks. When the old discs are phagocytosed at the tip of the POS, new discs are formed simultaneously by the photoreceptor cells. Recognition, internalization, and degradation are different phases of the phagocytosis process. (Kevany and Palczewski, 2010)

Recognition. Engulfment of the POSs into the RPE cell is driven by actin polymerization. Phosphatidylserine (PtdSer) is a phospholipid that is expressed in the tip of the POS facing the RPE. (Ruggiero et al., 2012) First, PtdSer residues bind to the MerTK membrane receptors on the RPE cells with the help of specific bridging molecules, such as Tubby and Gas6 (Caberoy et al., 2010; Hall et al., 2005). It has been shown that at least some of these bridging molecules are expressed by the RPE cells in a circadian fashion (Milićević et al., 2019). After PtdSer residues have bound to MerTK receptors, complex intracellular pathways finally activate both branched and linear actin polymerization inside the RPE cells (Eden et al., 2002; Patel et al., 2002). Also, the RPE transmembrane integrins, mainly αvβ5 get activated on the cell membrane and further bind to the PtdSer phospholipids via MFG-E8 protein. MerTK-PtdSer- and αvβ5-PtdSer -complexes act as a bridge between intracellular actin filaments and POSs. (Kwon and Freeman, 2020) Long before the internalization process, apical microvilli of the RPE have their membrane branches deep in the POSs, nearly halfway up to the whole POS length (Steinberg et al., 1977; Almedawar et al., 2020).

Internalization. After the PtdSer-binding, polymerized actin filaments change their organization by forming pseudopods, an arm-like projection of cell membrane (Matsumoto et al., 1987). Further, the RPE plasma membrane expands around the POSs and forms mature phagosomes (Chaitin and Hall, 1983). Internalization is mediated by the receptor tyrosine kinase, c-mer, and its ligand Gas6. One essential protein in the membrane ensheathment is Rac (Mao and Finnemann, 2012b). However, the exact mechanisms of pseudopodia fusing are not fully understood. It has been seen that the fused pseudopods, also known as nascent phagosomes are regular in size, being 1-2 μm in diameter (Mao and Finnemann, 2016). Thus, it has been proposed that cellular mechanisms of the RPE related to sealing the pseudopodia may be similar to the endocytosis due to this regular-sized pattern. (Mazzoni et al., 2014) After sealing from the RPE plasma membrane, nascent phagosomes fuse first with endosomes and after all with lysosomes, finally forming mature phago(lyso)somes (Bosch et al., 1993). During the fusion, phagosomes are transported from the apical to the basal side by microtubules. (Kwon and Freeman, 2020)

Degradation. Once in the basal side, phagosomes fuse with lysosomes (phagolysosome) and then the degradation process starts. Noteworthy is that the pH of the cell decreases from 7.4 to 4.5 when going from the apical to the basal side. The main reason for the low pH is the ATPase enzyme which hydrolyzes ATP as producing protons into the lumen. Many of the lysosomal enzymes get activated in low pH, and thus acidification is important for the POS degradation process. Cathepsin D and S are the most important lysosomal enzymes since they degrade rhodopsin (Bosch et al., 1993; Deguchi et al., 1994) Hydrolyzed small molecules diffuse either out from the RPE cell or are reused within the cell. Diffused molecules are transported out by the choroid capillaries. (Kwon and Freeman, 2020)

If the phagocytosis function did not function properly, POSs might accumulate into the RPE cells. Accumulated POSs include mainly oxidized proteins and lipids which are called lipofuscin. Lipofuscin forms granular structures and many of its ingredients have autofluorescence. The most common lipofuscin fluorophore is A2E, N-retinylidene-N-retinylethanolamine (Sakai et al., 1996; Guan et al., 2020). When lipofuscin-containing RPE granules are excited by a 488 nm wavelength, the emission peak is 600 nm (Guan et al., 2020). For a long time, it has been suspected that accumulated lipofuscin might have an impact on retinal diseases, such as age-related macular degeneration (Petrukhin, 2013). However, lipofuscin accumulates by age in all healthy individuals. (Sparrow and Boulton, 2005)

1.1.5 Rod phototransduction cascade

1.1.5.1 Signal activation

The process by which light is converted into electrical signals is called a phototransduction cascade (Fig. 5). It is a G-protein-coupled receptor signalling pathway. (Langlois et al., 1996)

The cascade begins when a photon of light is absorbed by a transmembrane glycoprotein, rhodopsin (R). Rhodopsin is found in disc-shaped membranes in the POSs. Rhodopsin consists of seven looped helices, a glycosylated N-terminus and cytosolic C-terminus. Inside the rhodopsin is 11-*cis* retinal chromophore which is the actual photon-absorbing molecule. The absorption of a photon induces isomerization of 11-*cis* retinal to its *trans*-configuration. This leads to a conformational change of R to its activated form (R*). Next, R* interacts with heterotrimeric G-protein, transducin (T) which

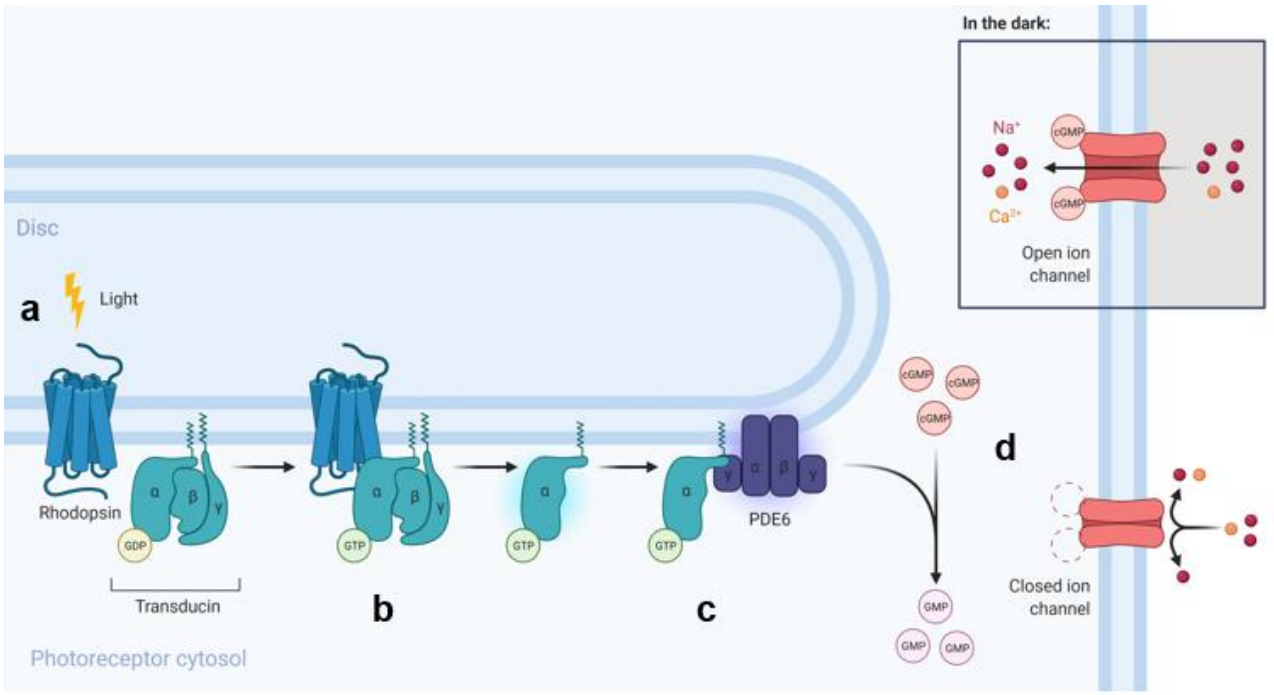

Figure 5. Phototransduction in rod photoreceptors. a) A photon of light induces an isomeric change in cis-11 retinal to trans configuration inside the transmembrane glycoprotein rhodopsin (R) on the disc of the outer segment of rod photoreceptor cell. b) This leads to a conformational change of R to its activated form (R*). Next, R* interacts with heterotrimeric G-protein called transducin (T) which consists of alpha (α), beta (β), and gamma (γ) subunits together with GDP. Interaction with R* leads to an exchange of GDP to GTP and the T complex dissociates into Tα-GTP and Tβγ subunits. c) Tα-GTP binds and removes the inhibitory γ-subunit of the cGMP- phosphodiesterase-6 (PDE6) complex. Then, activated PDE* hydrolyzes cytosolic cGMP to GMP decreasing the cytosolic concentration of cGMP. d) The decrease in the cytosolic cGMP concentration leads to a closure of the cGMP-gated (CNG) cation channels in the plasma membrane resulting to a significant reduction in the influx of Na^+ and Ca^{2+} -ions. CNG channels close also in the rod photoreceptor cell axon terminal. The decrease in Ca^{2+} influx at the synaptic terminal reduces glutamate release into the synapse. The situation is opposite in the dark when the CNG channels are open allowing constant influx of Na^+ and Ca^{2+} ions. Thus, glutamate is released constantly into the synapse. *Created with BioRender.com.*

consists of alpha (α), beta (β), and gamma (γ) subunits together with guanosine diphosphate (GDP). Interaction leads to an exchange of bound GDP to guanosine triphosphate (GTP), and the T complex dissociates into Tα-GTP and Tβγ subunits. R* is then free to activate more T complexes. It is estimated that one R* can activate 100 transducin molecules. (Fung et al., 1981)

Next, Tα-GTP binds and removes an inhibitory γ-subunit from the phosphodiesterase-6 (PDE6) complex. PDE6 requires two Tα molecules to get fully activated (Qureshi et al., 2018). Rod PDE6 holoenzyme (Fig. 6) consists of α and β catalytic subunits both of them having an identical inhibitory γ subunit ($\alpha\beta\gamma_2$) (Deterre et al., 1988; Baehr et al., 1979; Gulati et al., 2019; Lehtonen et al., 2004).

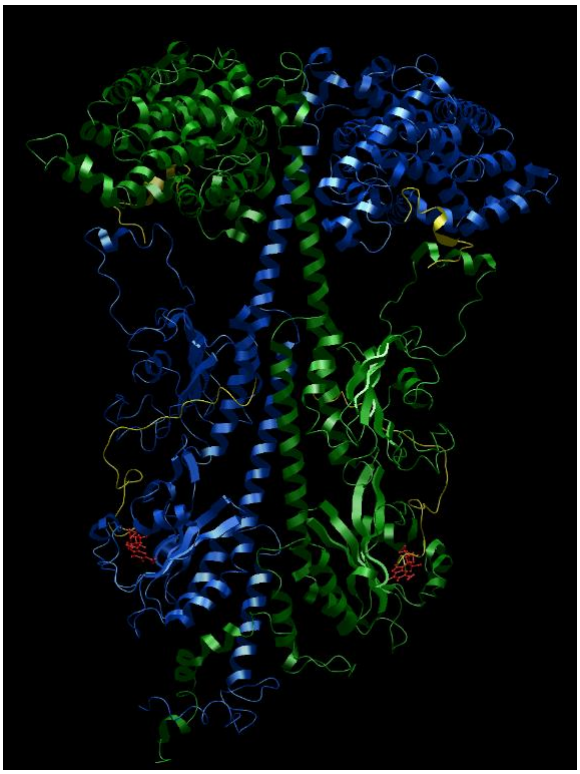

Figure 6. 3D view of rod PDE6 holoenzyme with two cGMP molecules as its ligands. Rod PDE6 holoenzyme consists of α and β catalytic subunits both having an identical inhibitory γ subunit (αβγ2). Once activated, PDE6 starts to hydrolyze cGMP to GMP. α- and β-subunits have their own binding site for cGMP. Green, β-subunit. Blue, α-subunit. Yellow, γ-subunits (2). Red, cGMP. Image created by Bodil (Lehtonen et al., 2004) using PDB ID 6MZB as a cryo-EM structure of PDE6 (Gulati et al., 2019).

α- and β-subunits have their binding site for cGMP (Gulati et al., 2019). Cone PDE6 has two identical α-subunits and its inhibitory γ-subunits have different amino acid structures compared to rods (Gillespie and Beavo, 1988). Once activated, PDE6* starts to hydrolyze cGMP to GMP decreasing the cytosolic concentration of cGMP and increasing the concentration of GMP, respectively. One PDE6* molecule can hydrolyze thousands of cGMP molecules. The decrease in the cytoplasmic cGMP concentration leads to a closure of cGMP gated (CNG) cation channels in the cell membrane, resulting in a significant reduction in the influx of Na^+ and Ca^{2+} ions. (Yee and Liebman, 1978) The decrease in the cation influx leads to hyperpolarization of the cell membrane and a decrease in glutamate release into the synapse (Schmitz and Witkovsky, 1997).

The situation is opposite in the dark when the CNG channels are open allowing a constant influx of Na^+ and Ca^{2+} ions. Therefore, glutamate release is also constant. In the dark, the efflux of Na^+ is managed by Na^+/K^+ ATPase pumps in the IS. Circulating Na^+ ions are the basis for the dark current in rod photoreceptors. (Schneider et al., 1991) Efflux of the Ca^{2+} ions occurs through Na^+/Ca^{2+}, K^+ exchangers (Reilander et al., 1992).

The signal from rod photoreceptor cells is first detected by bipolar and horizontal cells after which the signal continues to ganglion cells of which axons form the optic nerve. Through the optic nerve impulse achieves to the brain and the experience of vision is created. (Wilkinson et al., 2018)

1.1.5.2 Signal deactivation

Deactivation of R* and PDE6*, and resynthetization of cGMP are required to suppress the phototransduction cascade. This allows photoreceptors to return to the resting state and then start the cycle again. R* deactivation begins in its C-terminus where rhodopsin kinase (GRK1) phosphorylates Ser and Thr residues of R* (Ohguro et al., 1993). GRK1 is inhibited by a protein called recoverin (Rv) which is controlled by Ca^{2+} ions. When CNG channels close after R activation, Ca^{2+} concentration falls and Rv is not inhibiting GRK1 anymore and it can phosphorylate R*. (Klenchin et al., 1995) Then, a protein called arrestin (Arr) binds to phosphorylated R* and the catalytic activity of R* is quenched. (Burns, 2010)

Quenching of PDE6* occurs through the deactivation of Tα. Transducin gets deactivated when it hydrolyses GDP to GTP. In the GTP hydrolysis, an RGS-9 protein complex binds to the transducin and stimulates the hydrolysis to happen. The RGS9 complex consists of the RGS9 subunit, Gβ5 subunit and membrane-anchoring protein called R9AP. After transducin is deactivated, PDE6* cannot hydrolyse cGMP. (Wilkinson et al., 2018)

Returning to the resting state also requires resynthesis of the cGMP to open the CNG channels. cGMP is resynthesized by retinal guanylyl cyclase (RetGC). RetGCs are regulated by the guanylyl cyclase activating proteins 1 and 2 (GCAPs). When Ca^{2+} concentration falls after the closure of CNG channels, RetGC's activity increases which lead to a restoring of resting cGMP and reopening of CNG channels. (Gorczyca et al., 1995)

1.2 Retinitis pigmentosa

1.2.1 Etiology, pathophysiology, and clinical symptoms

Retinitis pigmentosa (RP) is a group of inherited retinal degenerative diseases and a major cause of hereditary blindness and visual disability. The prevalence of RP is estimated to be 1/4000, affecting approximately 2.5 million people worldwide. Despite that RP cannot be cured yet, different treatment options exist and especially gene therapy is a potential approach for future therapies. (Hamel, 2006; Tuohy and Megaw, 2021) RP is a very slow-progressing disease. The first symptoms are experienced usually during adolescence. Patients are diagnosed typically between 25-40 years of age. (Tsujikawa et al., 2008) The pathogenesis of RP starts with the degeneration of rod photoreceptors. At this stage, clinical symptoms are night-blindness and visual field constriction ("tunnel vision"). At an early stage, fundus photography does not show any changes. (Hamel, 2006)

Further, also cone cells start to degenerate and vision deteriorates more (loss of central vision, blindness). The first signs in fundus are arteriolar narrowing and a change in pigmentation. (Brancati et al., 2018) Another clinical hallmark is deteriorated or absent a- and b-waves in the electroretinogram (Ma et al., 2012). The function of the macula, a section in the center of the retina responsible for high-resolution and colour vision, remains normal until the later stages of the disease. The optic nerve head in the fundus has been reported to have a waxy pallor in RP patients but the reason is unknown. (Verbakel et al., 2018) Cataract characterized by yellowish crystalline changes at the posterior side of the lens is common in all forms of RP. Patients with advanced RP have more narrowed retinal vessels. The cause of the retinal vessel narrowing is not known but it seems to be a secondary change and not the primary cause of the disease. (Jackson et al., 2001)

Mutations in over 70 different genes can cause retinitis pigmentosa. Over 20 of the non-syndromic RP types inherit autosomal dominantly, representing 20-25% of patients. Other non-syndromic types are autosomal recessive (15-20%), X-linked recessive (10-15%) or sporadic RP. Other rarer types include mitochondrial, X-linked dominant and digenic (mutations in two different genes) types. However, about 40% of the RP patients cannot be classified by a genetic mutation. (Parmeggiani et al., 2011) 20-30% of RP patients have a syndromic disease that causes visual impairment. The most common type of syndromic RP is Usher syndrome, which is a genetic disorder causing chronic hearing loss and progressive visual impairment. (Petit, 2001)

One of the first RP associated genes was *PDE6B* which has a main role in phototransduction cascade in rod photoreceptors expressing the β-subunit of the phosphodiesterase-6 enzyme. Mutation in

PDE6B leads first to an accumulation of cGMP, and further to rod degeneration. (Bowes et al., 1990) Genetically, mutations in *PDE6B* are usually either missense mutations or splicing defects, and they are inherited as autosomal recessive. (Kuehlewein et al., 2021; Kim et al., 2020)

1.2.2 Current therapeutic options

Currently, there is no cure against retinitis pigmentosa, but some treatments are available.

Only one gene therapy product against RP is authorized by both the European Medicines Agency (EMA) and the U.S. Food and Drug Administration (FDA) while multiple is still in clinical trials. Luxturna® (voretigene neparvovec) is an adeno-associated virus (AAV) vector -based gene therapy product for RP patients who have mutations in the *RPE65* gene. Viral vectors deliver copies of the *RPE65* gene into the photoreceptor cells. The treatment is given as a single subretinal injection per eye. Additional immunosuppressant medication before and after the injections are necessary. (Kang and Scott, 2020) Multiple common adverse effects have been reported, such as headache, dizziness, eye inflammation, eye swelling, retinal detachment, increased intraocular pressure and nausea (Gao et al., 2020).

The Argus device is currently the only approved prosthesis device for the treatment against RP. Its first-generation device was approved by the FDA already in 2002, and the newer technology in 2011 by the EMA. Argus is designed for patients with advanced RP. The device consists of three parts: eyeglasses with a video camera, a video processing unit attached to a waist belt, and a microelectrode-array implant with an antenna transplanted to the patient´s retina. The video camera detects signals which are transferred into a brightness map. Brightness values are sent as pulse amplitudes for the electrode array, and finally, the patient´s brain processes receiving signal. (da Cruz et al., 2016; Finn et al., 2018)

1.2.3 Current clinical pipeline

Retinitis pigmentosa is classified as an orphan disease by the EMA and the FDA. Thus, medicinal product development against retinitis pigmentosa is supported financially. Currently, 224 clinical trials associated with retinitis pigmentosa can be found at clinicaltrials.gov (U.S.), and 31 at clinicaltrialsregister.eu (Europe). A major part of the clinical trials uses gene therapy as an approach (Table 1).

1.2.3.1 Gene therapy

Typically, gene therapy treatments are planned to be used with AAVs as carriers to deliver the functional gene, such as *RPGR* for patients with X-linked RP. These therapies are characterized as mutation-specific gene therapies. Typically, the target cells of mutation-specific gene therapies are photoreceptor cells. Currently, similar clinical studies using AAV-vectors are multiple, the main difference being a different treatable gene. When the viral vectors are delivering copies of a functional gene to photoreceptor cells, a disadvantage is that patients need to have functional photoreceptor cells left and thus the therapy cannot be used for late-stage RP patients. Whereas gene therapies targeting bipolar or ganglion cells can be used for late-stage RP patients since these cell types seem to survive for long after photoreceptor degeneration (Lin and Peng, 2013; Gilhooley et al., 2021). Gene therapies targeting bipolar or ganglion cells are usually mutation-independent. These therapy options would provide help for wide-range RP patients regardless of the stage of the disease. Since gene therapy is conducted by a single (sub)retinal injection, only a fraction of the target cells can be treated. (Carrella et al., 2020) This is one of the major challenges since, after the injection, the retina is a mosaic consisting of both treated and non-treated cell areas (Koch et al., 2017).

Intravitreal injection of a multi-characteristic opsin (MCO) is one of the experimental mutation-independent gene therapies. *MCO* encodes a light-sensitive opsin molecule and is delivered by a single AAV-intravitreal injection to bipolar cells. Following the injection, bipolar cells become light-sensitive neurons, and can partially store the vision. (Tchedre et al., 2021) Another experimental mutation-independent gene therapy approach is AAV-delivered *NR2E3.* Although mutations in this gene cause both autosomal dominant and recessive types of retinitis pigmentosa (Escher et al., 2009), preclinical studies have shown that a single AAV-delivered subretinal injection of *NR2E3* restores vision in multiple RP models. *NR2E3* encodes a photoreceptor-specific nuclear receptor, and its gene therapy targets are remaining photoreceptor cells. *NR2E3* is a key regulator of multiple networks responsible for apoptosis, phototransduction and oxidative stress. (Li et al., 2021a) Currently, RP patients with either autosomal recessive or dominant *NR2E3* mutations, or autosomal dominant *RHO* mutations are being recruited to clinical studies. GS030-DP is a mutation-independent, experimental gene therapy product that delivers a channel rhodopsin gene (*ChrimsonR-tdTomato*) to retinal ganglions cells via a single intravitreal AAV injection. The therapy includes also stimulating goggles which encode images of the surrounding visual world and amplify a light source for the genetically engineered retina. (Sahel et al., 2021)

1.2.3.2 Stem cell-based therapy

Stem cell-based therapies have shown their capability as a mutation-independent therapy option. Umbilical cord-derived mesenchymal stem cells can release immunomodulatory and paracrine factors which are like the ones expressed by the RPE. (He et al., 2014; Uy et al., 2013) Multiple different administration routes have already been tested in clinical trials including intravenous (Zhao et al., 2020), subretinal (Oner et al., 2016), suprachoroidal (Kahraman and Oner, 2020), intravitreal (Tuekprakhon et al., 2021) and sub-tenon (Özmert and Arslan, 2020). Umbilical cord-derived mesenchymal stem cells seem to restore RP patients´ vision, but the best administration route remains still under research and potential treatment interval need to be defined for long-term use (Florido, 2021).

1.2.3.3 Small molecule drugs

Multiple small molecule -targets have been studied in preclinic, such as cannabinoid system, Wnt/β-catenin/GSK3β pathway, apoptosis modulators (PARP-1), growth factors (VEGF, BDNF), Gpr124 protein and HDAC enzyme. (Carullo et al., 2020) However, only a few drug molecules have reached a clinical phase. N-acetylcysteine is one of these promising small molecule candidates. It is a derivate of L-cysteine and plays a role in the biosynthesis of glutathione. The mechanism of action is based on neutralizing reactive oxygen radicals (Dekhuijzen, 2004). After rod degeneration, cones suffer from oxidative damage and antioxidants have been seen as a potential option to increase the survival of cones. (Tohari et al., 2016; Komeima et al., 2006) N-acetylcysteine is planned to be administered orally and its target group is RP patients with moderate loss of vision. Other small molecules in clinical trials are minocycline and hydroxychloroquine. Both are designed to be taken orally and for long-term use. Minocycline is a highly lipophilic antibiotic, which has shown anti-apoptotic, anti-inflammatory and antioxidant effects (Chen et al., 2012). Whereas hydroxychloroquine is a drug already in the market in the EU and the U.S., but with indications in malaria, lupus, and rheumatoid arthritis. Mechanism of action of hydroxychloroquine in the treatment of autosomal dominant RP relies on the hypothesis that by altering the autophagy pathway of photoreceptor cells, retinal degeneration could be slowed (Yao et al., 2018).

1.2.3.4 Other therapy approaches

Umbilical cord blood platelet-rich plasma (CB-PRP) contains growth factors and neurotrophins which have the potential to slow retinal degeneration and cell death (Giovanna Valentini et al., 2019;

Arslan et al., 2018). A phase III trial delivers CB-PRP via a single sub-retinal injection for patients with rod-driven, early to intermediate stage RP.

1.2.4 Animal models in retinitis pigmentosa research

There are multiple animal models which are either genetically modified or carry a spontaneous mutation leading to RP.

The most common RP model is the Retinal degeneration 1 (*rd1*) mouse which represents an autosomal recessive RP. *Rd1* mouse has a viral insertion in the reverse orientation in the intron 1 of the *Pde6b* and a non-sense mutation in the exon 7 of the *Pde6b.* *Rd1* is homozygous for both mutations. Deficient β-subunit of the PDE6 leads to an accumulation of cGMP in the rods. (Farber et al., 1994; Pittler and Baehr, 1991) In the *rd1* mouse, a progressive photoreceptor degeneration begins around post-natal day 10. All rods are lost at 25 days after birth, and all the cones around at 100 days after birth. (Kalloniatis et al., 2016) Another common RP mouse model is Retinal degeneration 10 (*rd10)* mouse which has a missense mutation R560C in the *Pde6b* which leads to an autosomal recessive retinal degeneration. It has a slower retinal degeneration process compared to *rd1* for an unknown reason. However, it has been suggested that the missense mutation in the *rd10* decreases PDE6 stability and transportation which may be the cause of a decrease in the maximal and the basal activity of the PDE6. (Wang et al., 2018)

Canines are common in pre-clinical studies since some dog breeds have spontaneous mutations leading to inherited retinal degeneration. Briard dog has a naturally occurring autosomal recessive RPE65$^{-/-}$genotype which leads to a severe type of RP (Veske et al., 1999). Other larger species commonly used are non-human primates and genetically modifies pigs. Large animal models have many advantages compared to rodents such as the size of the eye, higher cone density and higher photoreceptor packing thus being closer to the human eye. (Winkler et al., 2020)

Table 1. Clinical pipeline for the treatment of retinitis pigmentosa. Majority of retinitis pigmentosa -specific investigational drug candidates in clinical trials are gene therapy products. The table represents the active RP-related clinical trials on 02/2022 which have been registered at clinicaltrials.gov.

Indication, gene	Investigational drug	Administration route, (*drug class*)	Phase	NCT-identifier
Early to intermediate stage of X-Linked Retinitis Pigmentosa, *RPGR*	rAAV2tYF-GRK1-hRPGRco	a single sub-retinal AAV-injection (*mutation-specific gene therapy*)	II / III	NCT04850118
Early to intermediate stage of retinitis pigmentosa, *PDE6B*	AAV2/5-hPDE6B		I / II	NCT03328130
Early to intermediate stage of retinitis pigmentosa, *PDE6A*	rAAV.hPDE6A		I / II	NCT04611503
Early to intermediate stage of retinitis pigmentosa, *MERTK*	rAAV2-VMD2-hMERTK		I	NCT01482195
Late-stage retinitis pigmentosa	vMCO-010	a single intravitreal AAV-injection (*mutation-independent gene therapy*)	II	NCT04945772
Early to intermediate stage of retinitis pigmentosa, *NR2E3* or *RHO*	OCU400		I / II	NCT05203939
Late-stage retinitis pigmentosa	GS030-DP combined with GS030-MD (stimulating goggles)		I / II	NCT03326336
Early to intermediate stage of retinitis pigmentosa	Umbilical cord-derived mesenchymal stem cells	a single injection to sub-tenon or suprachoroidal space *(stem cell-based therapy)*	II	NCT04763369
Moderate retinitis pigmentosa	N-Acetylcysteine	orally taken tablets: 2 x 1200 mg/d for 6 months (*small-molecule drug*)	II	NCT04864496
Moderate retinitis pigmentosa	Minocycline	orally taken tablets: 100mg/d for 6-months (*small-molecule drug*)	II	NCT04068207
Early to intermediate stage of autosomal dominant retinitis pigmentosa, P23H-*RHO*	Hydroxychloroquine	orally taken tablets: 4 mg/kg/d or 5 mg/kg/d for 12-months (*small-molecule drug*)	I / II	NCT04120883
Early to intermediate stage of retinitis pigmentosa	CB-PRP	a single sub-retinal injection of CB-PRP *(biological drug)*	III	NCT04636853

1.3 Background of the experimental design

1.3.1 Cre-*loxP* recombination

Sternberg and Hamilton were the first scientists who identified a recombinase enzyme that recombines DNA fragments. The enzyme was isolated from the P1 bacteriophage. They named the recombination enzyme as Cre and called its two binding sites as *lox*P (**l**ocus **o**f **x**-over, P1). (Sternberg and Hamilton, 1981) After decades from Sternberg and Hamilton´s work, the Cre-*loxP* technique is still a powerful gene-editing tool used in biomedical research. The main principle behind the technique is, that by adding the *lox*P sequences to the desired part of the genome, with Cre recombinase enzyme the DNA strand between the *lox*P sites is removed. Cre gene is usually added under a tissue-specific promoter. By crossing a Cre mouse with a mouse having *lox*P sites in its genome, desired DNA strand will be removed. Despite being mainly used in genetic excision, Cre-*lox*P can also be used in the inversion or translocation of DNA depending on the orientation and location of *lox*P sites. (Kim et al., 2018)

1.3.2 Mouse models of the project

In this master thesis project, I used three different mouse models to study the retinal morphology and the function of RPE in diseased (RP) and partially rescued mice. (Fig 7.). *Pde6b*$^{ST/WT}$ mice have a stop cassette in one allele of the *Pde6b* gene which leads to interruption of its expression. However, the other allele with a functional *Pde6b* compensates for this loss and halts rod degeneration. (Koch et al., 2015) *Pde6b*$^{ST/WT}$ mice were used as control and will be referred to as wildtype in the text.

Pde6b$^{ST/ST}$ mouse has a *loxP*-flanked stop cassette in the intron 1 of both loci of the *Pde6b* gene. The stop cassette contains multiple polyadenylation signals which prevent gene expression. *Pde6b*$^{ST/ST}$ exhibit progressive rod degeneration. (Davis et al., 2013) This mouse acts as a retinitis pigmentosa model and will be referred to as a mutant in the text.

In *Pde6b*$^{ST/ST}$ *Pax6αCre* mice, both *Pde6b* alleles are functional in the distal retina due to the Cre-loxP recombination. In the central retina, both *Pde6b* alleles contain a stop cassette which interrupts the expression of PDE6B. Transcription factor Pax6 under a retina-specific regulatory element (α) act as a Cre recombinase promoter. *Pax6*α has an essential role in the development of the eye and is expressed already in the early developing optic vesicle, and later in retinal progenitor cells (RPCs). All retinal cell types are developed from the RPCs. (Bäumer et al., 2002) Due to the distal expression

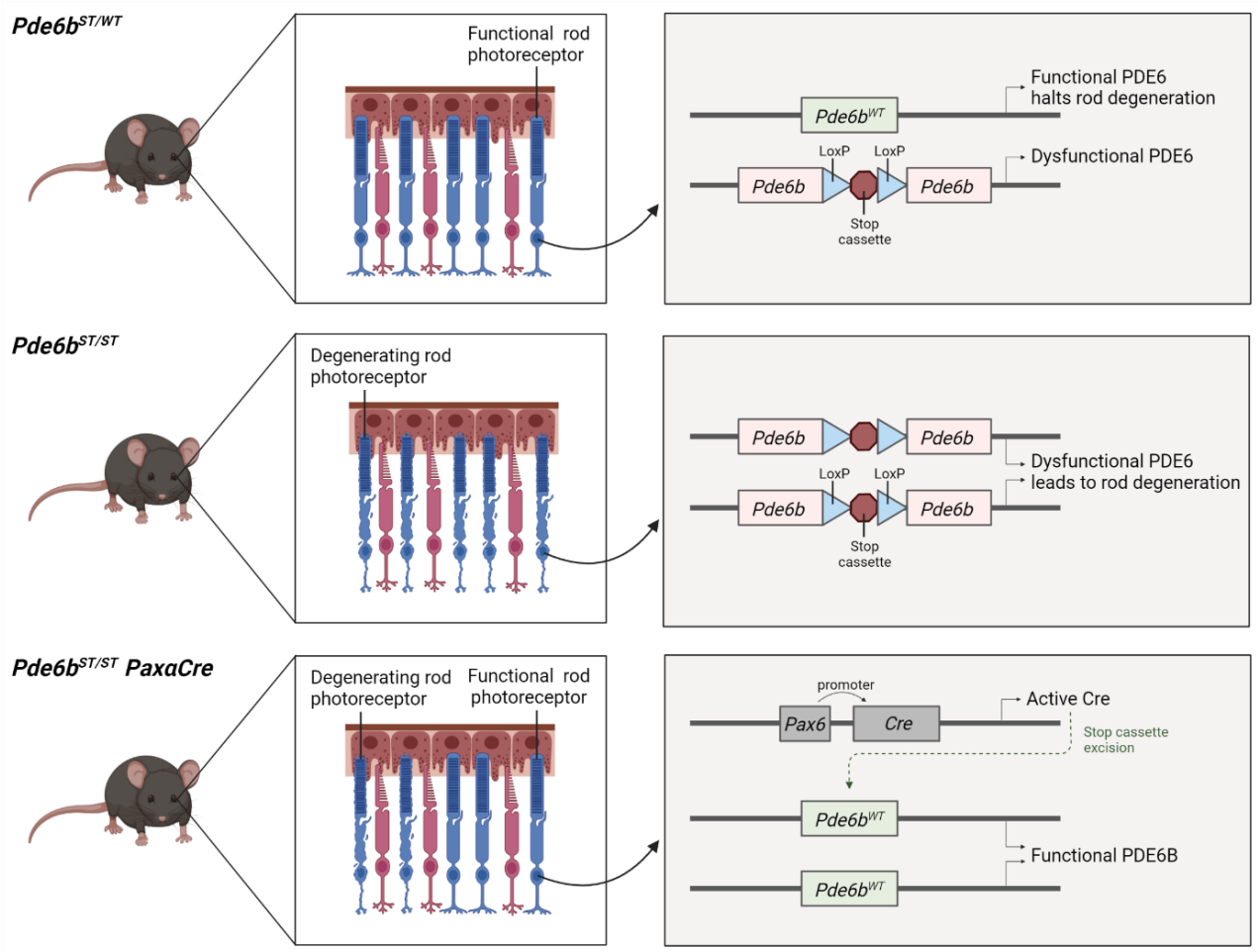

Figure 7. Mouse models of the project. Illustration of rod phenotypes, and *Pde6b*$^{ST/WT}$, *Pde6b*$^{ST/ST}$ and *Pde6b*$^{ST/ST}$ *Pax6αCre* mice. In *Pde6b*$^{ST/WT}$ mice, *Pde6b* allele is functional. In *Pde6b*$^{ST/ST}$ mice, both *Pde6b* alleles contain a stop cassette which interrupts the expression of PDE6B. In *Pde6b*$^{ST/ST}$ *Pax6αCre* mice, both *Pde6b* alleles are functional in the distal retina due to the Cre-*lox*P recombination under a *Pax6α* promoter. In the central retina, both *Pde6b* alleles contain a stop cassette. *Created with BioRender.com.*

of *Pax6α* in the RPCs, also the Cre recombinase is expressed in the corresponding area and stop cassettes are removed by Cre-loxP recombination. (Koch et al., 2017; Marquardt et al., 2001) The deletion of stop cassettes leads to rescued PDE6B expression in the distal retina (Fig. 8). The other, non-recombined area in the center remains mutant. *Pde6b*$^{ST/ST}$ *Pax6αCre* will be referred to as partially treated later in the text. This unique mouse model is a great tool to study the effects of the mosaic retina (health-diseased) on the function of the RPE.

An additional reporter allele, *ROSA*$^{nT\text{-}nG}$ was used to label the Cre-recombined and the non-recombined retinal areas. *ROSA*$^{nT\text{-}nG}$ mice have a *loxP*-flanked tdTomato (red fluorescent) gene upstream of an enhanced green fluorescent protein (EGFP, green fluorescent) gene. Following exposure to Cre recombinase, recombined areas express EGFP and non-recombined areas tdTomato. (Koch et al., 2017; Prigge et al., 2013)

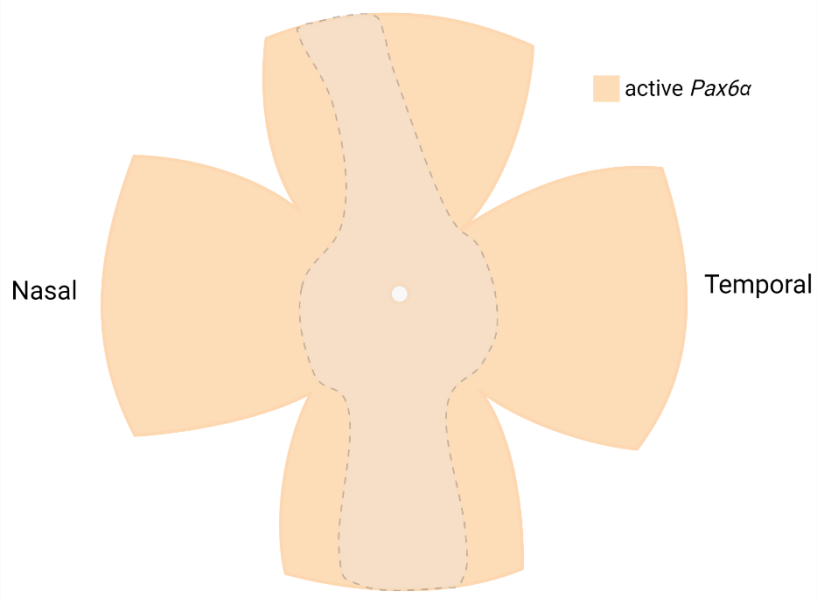

Figure 8. *Pax6α* active area in the retina of *Pde6b*^{STIST} *Pax6αCre* mice. Area of active Pax6 defines where Cre recombinase removes stop cassettes. The non-recombined area in the center remains mutant. *Created with BioRender.com.*

1.4 Summary

RP is a major cause of hereditary blindness and visual disability. It is a very slow-progressing disease, and its symptoms start usually during adolescence. Mutations in over 70 different genes can cause photoreceptor cell degeneration leading to retinitis pigmentosa. A common RP-related gene is *PDE6B* which encodes a β-subunit of PDE6-enzyme which has a crucial function in rod-mediated vision. (Wilkinson et al., 2018)

Currently, no cure is available for RP patients. Treatment options are few, but the most promising one is gene therapy. Since retinal gene therapy is delivered by a single (sub-)retinal injection, it does not rescue all the diseased photoreceptor cells (Koch et al., 2017). Despite the promising, experimental gene therapies which target other than photoreceptor cells as a single injection, the whole retina cannot be achieved by the therapy. The impact of the non-rescued photoreceptor cells on the rescued ones is not fully understood. This remains a challenge for the therapy. (Crane et al., 2021)

New therapeutic approaches against retinitis pigmentosa are needed. Due to the essential role of the RPE for retinal homeostasis, it may be a potential target in future therapies against RP. In other retinal degenerative diseases, RPE-based therapies have shown potential in animal models (Hinkle et al.,

2021). In addition to new approaches, fundamental research about the impact of the non-rescued retina on the rescued one is crucial to understand the long-term effects of gene therapy.

The aim of the project was to study the retinal morphology and the function of the RPE in 48-week-old diseased (RP) and partially rescued mice. Wildtype mice were used as controls in the experiments. Partially rescued retina represented gene therapied human retinitis pigmentosa due to the mosaic-like pattern of rescued and unrescued rods (Koch et al., 2017). Apoptosis assay and photoreceptor cell outer segment (POS) phagocytosis assay were chosen to understand the metabolic state of the RPE in mutant and partially rescued mice. A special interest was also to observe signs of retinal remodelling in the partially rescued retina.

2 Results

2.1 Retinal morphology

2.1.1 Photoreceptor cells are absent in *Pde6b*$^{ST/ST}$ mice and partially degenerated in *Pde6b*$^{ST/ST}$ *Pax6αCre* mice at 48 weeks of age

Photoreceptor cell degeneration rate was studied in 48-week-old wildtype, mutant and partially treated mice by measuring outer nuclear layer (ONL) thickness in retinal sections (Fig. 9). In wildtype retinas, the ONL thickness slightly decreased towards the periphery. In mutant retinas, ONL was almost completely gone due to photoreceptor cell loss. In partially treated retinas, the ONL thickness was decreased in the center compared to wildtype. Further, the morphology of 48-week-old mutant and partially treated retinas were studied and compared to wildtype by using multiple specific antibodies. The mice had an additional *ROSA*$^{nT\text{-}nG}$ allele to illustrate recombined and non-recombined cell areas.

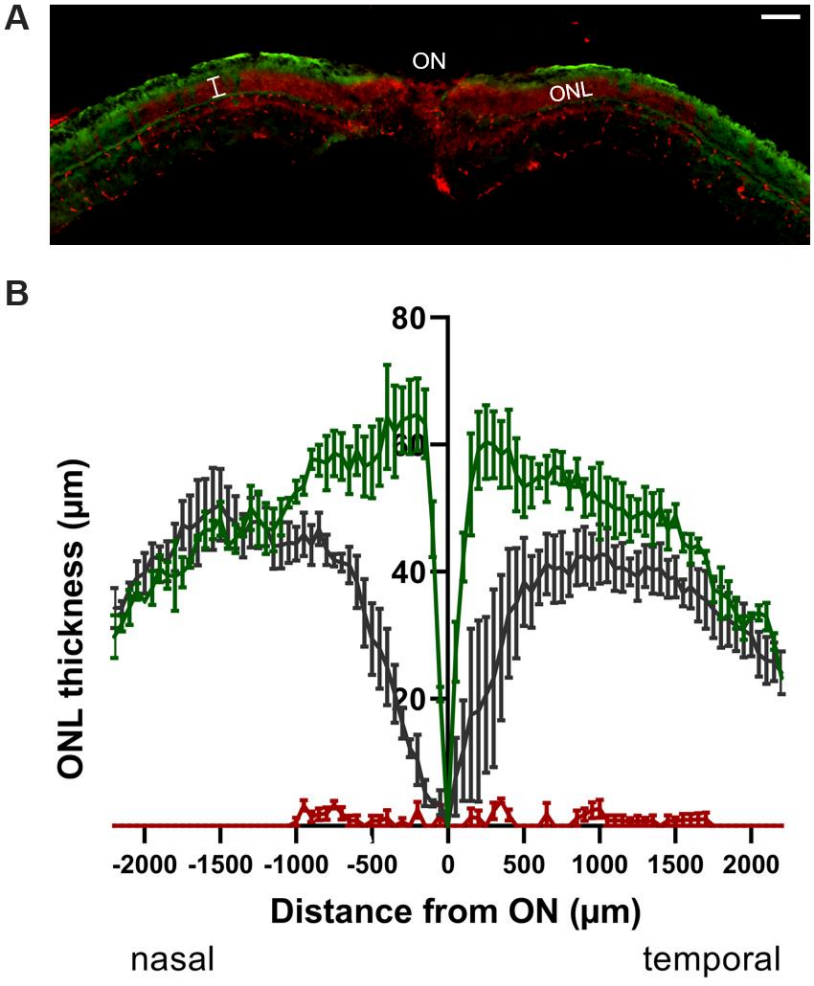

Figure 9. Outer nuclear layer thickness measurements of wildtype, partially treated and mutant mice. A) ONL thickness (µm) measurements were conducted by using 48-week-old retinal sections. Line, measurement point. ON, optic nerve. ONL, outer nuclear layer. Scale bar, 100µm B) Values with SEMs represented in a spider-plot (n= 3 in each group). Green, wildtype; Red, mutant; Grey, partially treated.

2.1.2 Multiple retinal cell types are degenerated in *Pde6b*$^{ST/ST}$ mice, whereas *Pde6b*$^{ST/ST}$ *Pax6αCre* mice show signs of retinal regeneration at 48 weeks of age

To study PDE6 protein expression, the β-subunit of rod PDE6 and γ-subunit of rod/cone PDE6 (PDE6G/H) were labelled (Fig. 10). In wildtype retinas, PDE6B and PDE6G/H were expressed in outer segments (OSs). In mutant retinas, there was no specific PDE6B expression and no PDE6G/H expression. In partially treated retinas, PDE6B was observed in OSs in the recombined area but also potentially in the non-recombined area. Notable is that the PDE6B expression in the recombined area of partially treated retina was not as abundant as in wildtype. In addition, PDE6G/H expression was like wildtype in the recombined area. PDE6G/H had a strong expression in the non-recombined area.

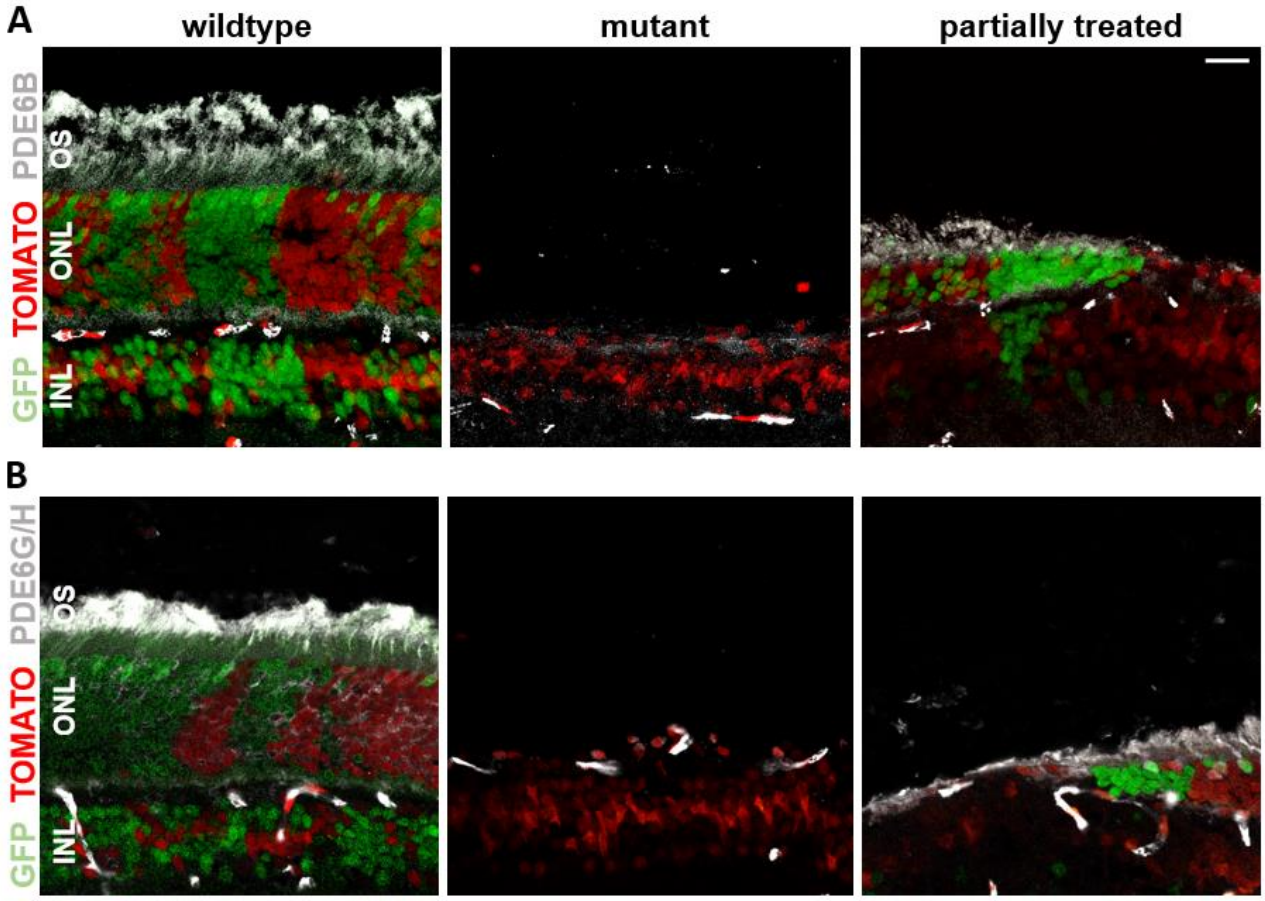

Figure 10. A) 48-week-old mutant lacks PDE6B expression, whereas partially treated retina expresses PDE6B weakly in the non-recombined area. Retinal sections were immunolabelled with Anti-GFP with anti-goat Alexa Fluor 488 and Anti-PDE6B with anti-mouse Alexa Fluor 405. Green, recombined nuclei; red, non-recombined nuclei; white/grey, PDE6B. **B) PDE6G/H expression differs remarkably between mutant and partially treated retina being totally absent in mutant and expressed in partially treated.** Retinal sections were immunolabelled with Anti-GFP with anti-goat Alexa Fluor 488 and Anti-PDE6G/H with anti-mouse Alexa Fluor 647. Green, recombined nuclei; red, non-recombined nuclei; white/grey, γ-subunit of rod/cone PDE6. Scalebar, 20μm.

Cone arrestin, also known as Arrestin-C, is a cone-specific protein and can be used to study cone morphology (Gurevich et al., 1995). In 48-week-old wildtype, cone synapses could be seen as a continuous row below the ONL and cone inner segments (IS)s and OSs above it (Fig. 11). In mutant, cones were absent. In partially treated retina, cone cells seemed to be shorter than in wildtype in both non-recombined and recombined area.

GARP antibody detects a specific region of CNG channels found in rod OSs (Sarfare et al., 2014). In 48-week-old wildtype, rod OSs were abundantly presented (Fig. 12). Due to the degeneration of photoreceptor cells in mutant, also rod OS were lost. The non-recombined area of the partially treated retina seemed to have a stable expression of GARP proving that rod OSs are not fully degenerated. GARP expression in the recombined area of partially treated retina was abundant.

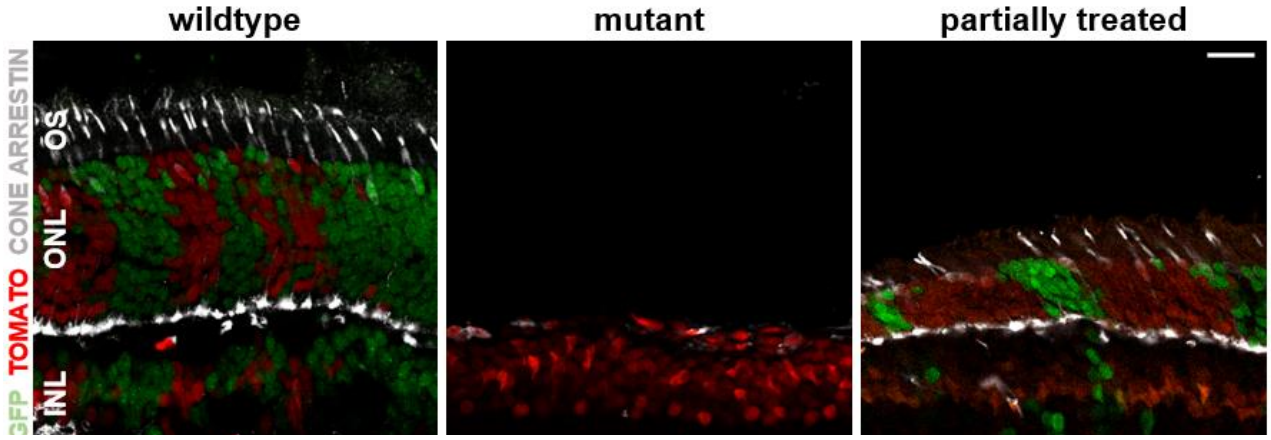

Figure 12. Cones are lost in 48-week-old mutant and shortened in partially treated retina. Sections were immunolabelled with Anti-GFP with anti-goat Alexa Fluor 488 and Anti-CONE ARRESTIN with anti-rabbit Alexa Fluor 647. Green, recombined nuclei; red, non-recombined nuclei; white/grey, cones. Scalebar, 20µm.

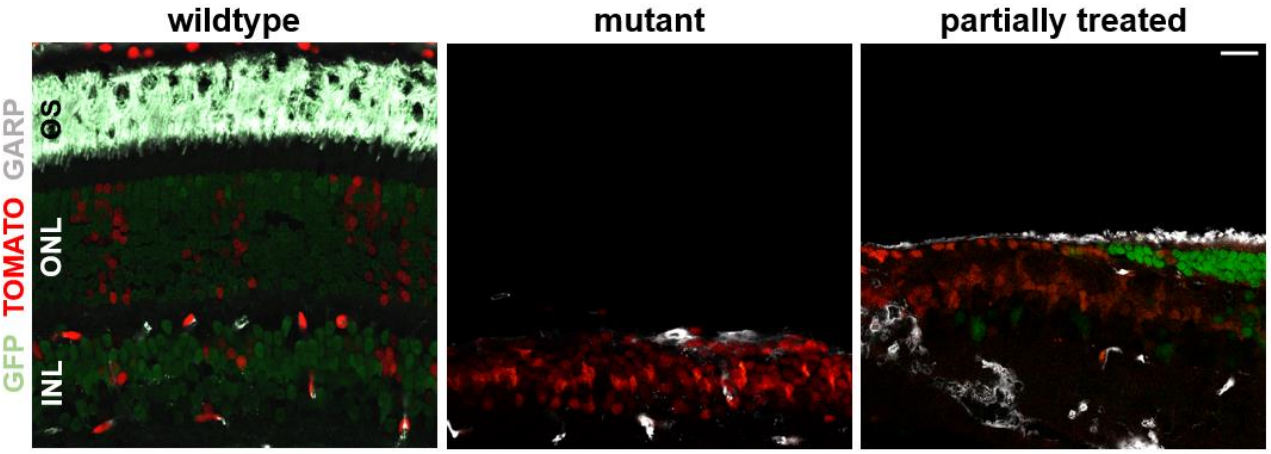

Figure 11. Rod OS are absent in mutant due to the total degeneration of rods but have stable expression in partially treated retina. Sections were immunolabelled with Anti-GFP with anti-goat Alexa Fluor 488 and Anti-GARP with anti-mouse Alexa Fluor 647. Green, recombined nuclei; red, non-recombined nuclei; white/grey, rod OS. Scalebar, 20µm.

Cone bipolar cells (CBCs) and rod bipolar cells (RBCs) were stained with separate antibodies to study whether photoreceptor cell loss in mutant or partial rod-cone degeneration in partially treated retinae has had an impact on bipolar cells. PKCα antibody binds to Protein kinase C α which is widely expressed in RBCs (Greferath et al., 1990; Xiong et al., 2015). In wildtype, RBC dendrites, cell bodies, axons and axon terminals could be observed (Fig. 13A). In mutant, RBC dendrites were lost, and axon terminals were partially degenerated. In partially treated retinae, RBC dendrites and axon terminals were partially degenerated in the non-recombined area (Fig. S2). In the recombined area, there were no signs of RBC degeneration.

SCGN antibody binds to secretagogin which is a calcium-binding protein expressed in both ON and OFF CBCs (Puthussery et al., 2010). In wildtype, CBCs had multi-branched axons and abundant dendrites (Fig. 13B, Fig. S3). In mutant mice, CBC dendrites were lost, and CBC axons and axon

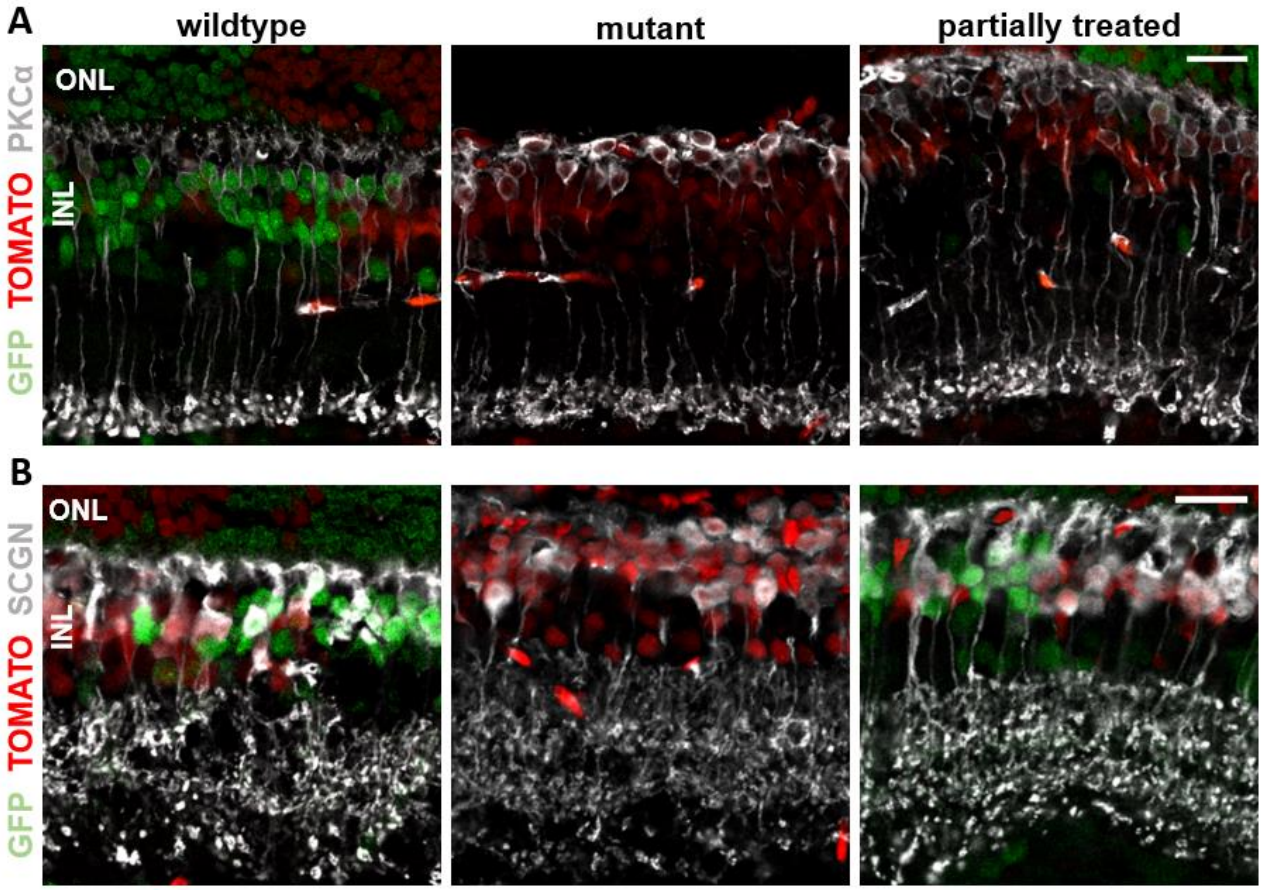

Figure 13. A) RBC dendrites are lost in mutant and partially degenerated in partially treated mouse retina at 48 weeks of age. Retinal sections were immunolabelled with Anti-GFP with anti-goat Alexa Fluor 488 and Anti-PKCα with anti-mouse Alexa Fluor 647. Green, recombined nuclei; red, non-recombined nuclei; white/grey, rod bipolar cells (RBCs). Scalebar, 20µm. **B) CBC dendrites are lost in mutant and partially degenerated in partially treated mouse retina at 48 weeks of age.** Retinal sections were immunolabelled with Anti-GFP with anti-goat Alexa Fluor 488 and Anti-SCGN with anti-rabbit Alexa Fluor 647. Green, renominated nuclei; red, non-recombined nuclei; white/grey, cone bipolar cells (CBCs). Scalebar, 20µm.

terminals seemed to be degenerated. In partially treated mice, CBC dendrites were partially lost in the non-recombined area. In the recombined area, CBC morphology represented wildtype.

Horizontal cells (HCs) are interconnecting neurons that participate in receiving signals from both rods and cones (Twig et al., 2003). HC morphology was studied by using an antibody against Calbindin D28k which is a major calcium-binding protein in HCs (Mitchell et al., 1995). In wildtype, HCs seemed to form a continuous layer in the OPL and have dendrites against the ONL (Fig. 14). In mutant, HCs were degenerated almost completely. In partially treated retinae, HCs had a wildtype-like continuous layer in the OPL. However, in the non-recombined area, the amount of HC dendrites seemed to be decreased. Additional, long ectopic branches of HCs could be observed in mutant retinae and in the non-recombined area of the partially treated retina (Fig. S4).

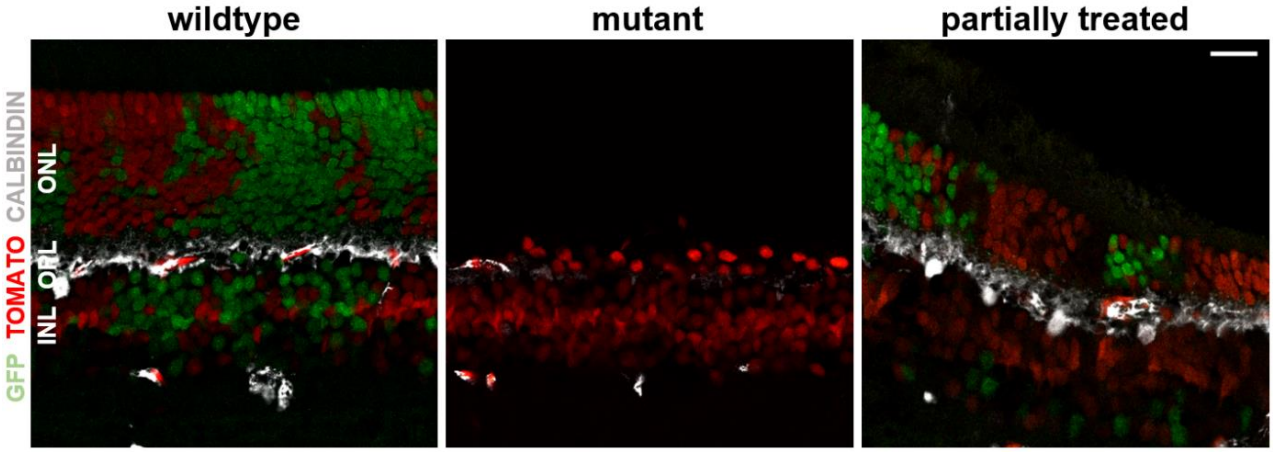

Figure 14. Horizontal cell number and connecting branches have decreased notably in mutant, and less prominently in treated mouse retina at 48 weeks of age. Sections were immunolabelled with Anti-GFP with anti-goat Alexa Fluor 488 and Anti-CALBINDIN D-28k with anti-mouse Alexa Fluor 647. Green, recombined nuclei; red, non-recombined nuclei; white/gray, horizontal cells. Scalebar, 20µm.

Further, morphology studies continued with microglia (Fig. 15A) and Müller cell (Fig. 15B) specific antibodies. IBA1 (Ionized calcium-binding adaptor molecule 1) is a microglia/macrophage specific calcium-binding protein that participates in phagocytosis function in activated microglia (Ohsawa et al., 2004). In wildtype, microglia were mainly expressed in the outer plexiform layer (OPL), but some were found also in the inner plexiform layer (IPL). In mutant, (activated) microglia expression was increased in the IPL. Additionally, microglia were localized in the INL. In partially treated retina, microglia expression was like in wildtype in both recombined and non-recombined area.

Glutamine synthetase is a cytosolic enzyme located in Müller cells (Riepe and Norenburg, 1977; Rauen and Wießner, 2000). In wildtype, Müller cells seemed to have a well-organized, tight structure from the ONL to the GCL in which ends it formed limiting membranes. In mutant retina, Müller cells formed a glial seal above the INL. In partially treated retina, a wildtype-like, well-organized pattern of Müller cells was observed except that a glial seal was formed above the ONL in the non-recombined area.

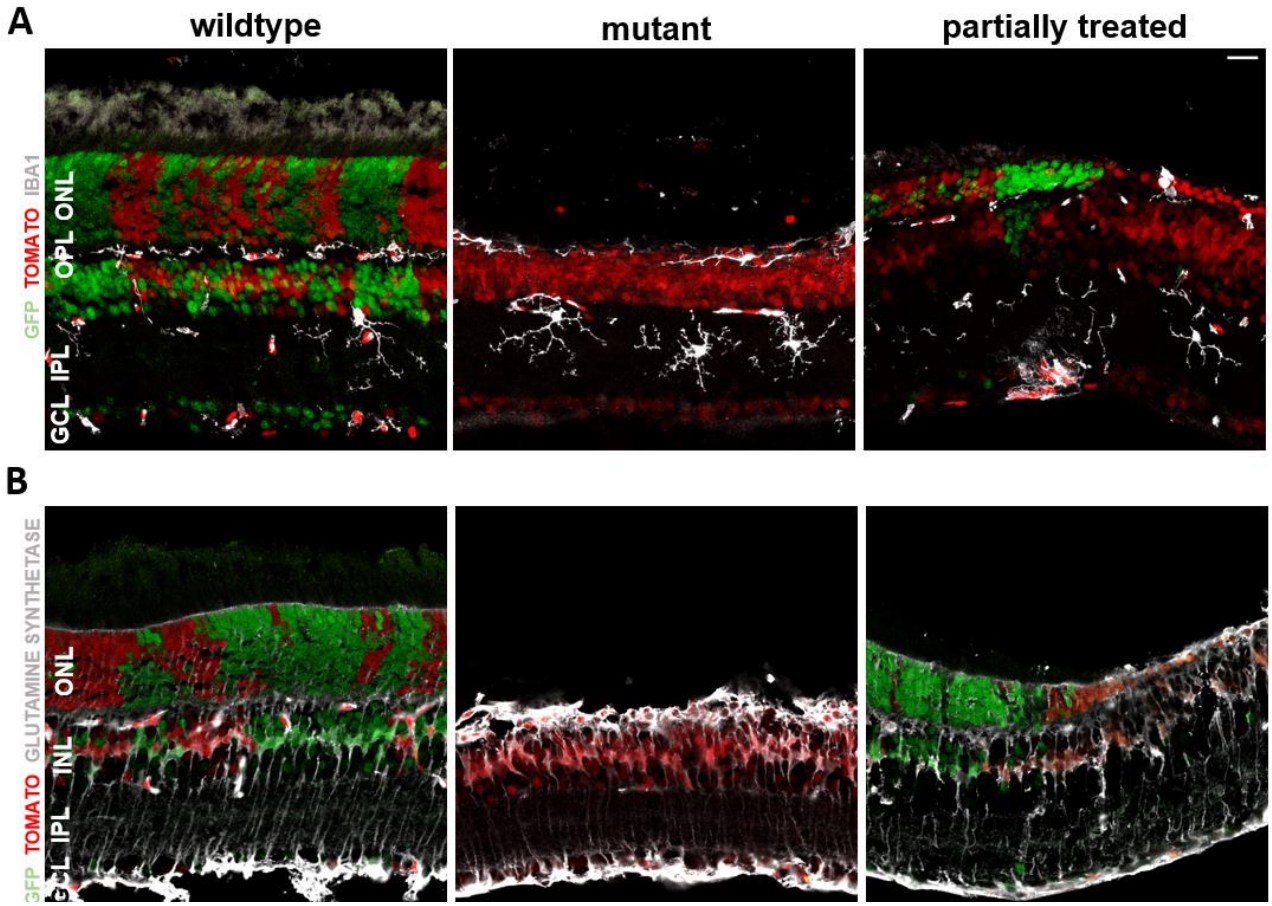

Figure 15. A) Microglia expression is increased in mutant retina at 48 weeks of age. Sections were immunolabelled with Anti-GFP with anti-goat Alexa Fluor 488 and Anti-IBA1 with anti-rabbit Alexa Fluor 647. Green, recombined nuclei; red, non-recombined nuclei; white/gray, microglia. Scalebar, 20µm. **B) Müller cells form a glial seal above the INL in mutant retina at 48-weeks of age.** Sections were immunolabelled with Anti-GFP with anti-goat Alexa Fluor 488 and Anti-GLUTAMINE SYNTHETASE with anti-rabbit Alexa Fluor 647. Green, recombined nuclei; red, non-recombined nuclei; white/gray, Müller cells. Scalebar, 20µm

Glucose transporter 1 (GLUT1) is the main glucose transporter in the retina and the RPE (Gospe et al., 2010; Mantych et al., 1993). To study the retinal glucose metabolism, 48-week-old retinal sections were stained for GLUT1 antibody (Fig. 16). In wildtype, GLUT1 was expressed in the ONL, and in the apical and the basal sides of the RPE. In mutant, GLUT1 was expressed in both sides of the RPE but the apical side seemed to partially contain two separate layers of GLUT1. In partially treated

retina, GLUT1 had a wildtype-like expression in the basal side of the RPE, but had increased expression in the apical side of the RPE. The increased GLUT1 expression in the apical side of the RPE was seen in both recombined and non-recombined areas. Additionally, GLUT1 expression was increased in the ONL of the non-recombined area.

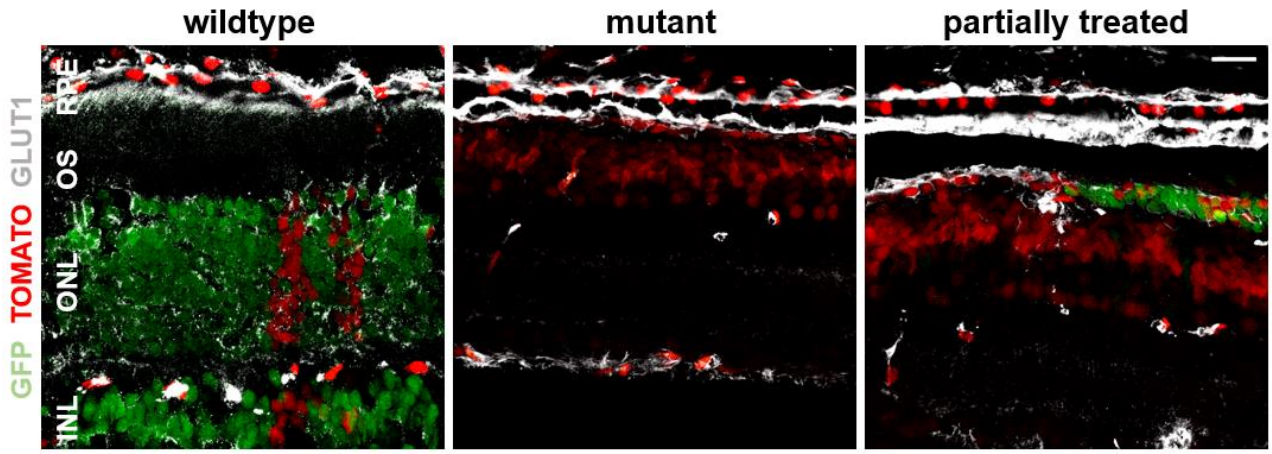

Figure 16. Partially treated mice have an increased GLUT1 expression in the apical side of the RPE, and in the ONL of the non-recombined area of retina at 48 weeks of age. Sections were immunolabelled with Anti-GFP with anti-goat Alexa Fluor 488 and Anti-GLUT1 with anti-mouse Alexa Fluor 647. Green, recombined nuclei; red, non-recombined nuclei; white/grey, GLUT1 receptors. Scalebar, 20µm.

2.2 RPE morphology

2.2.1 *Pde6b*$^{ST/ST}$ has a site-specific and heterogenous RPE morphology, whereas *Pde6b*$^{ST/ST}$ *Pax6αCre* shows signs of RPE regeneration in the area of non-recombined retina

After the morphological studies with retinal sections, a deeper look into the RPE was taken by using RPE wholemounts. β-catenin is a part of a protein complex that forms adherens junctions between RPE cells (Burke, 2008). It is a valuable marker to study RPE morphology as expressed in the cell membrane. Anti-β-catenin was used to define the morphology of the RPE of 48-week-old mutant and partially treated mice.

Wildtype RPE consisted of hexagonal and well-organized epithelial cells (Fig. 17). A remarkable difference between wildtype and mutant in both central and peripheral RPE could be seen. Mutant RPE consisted of tiny and elongated cells in the center, whereas in the periphery the cells looked bigger and elongated. Both areas have completely lost an organized, hexagonal pattern. Temporal

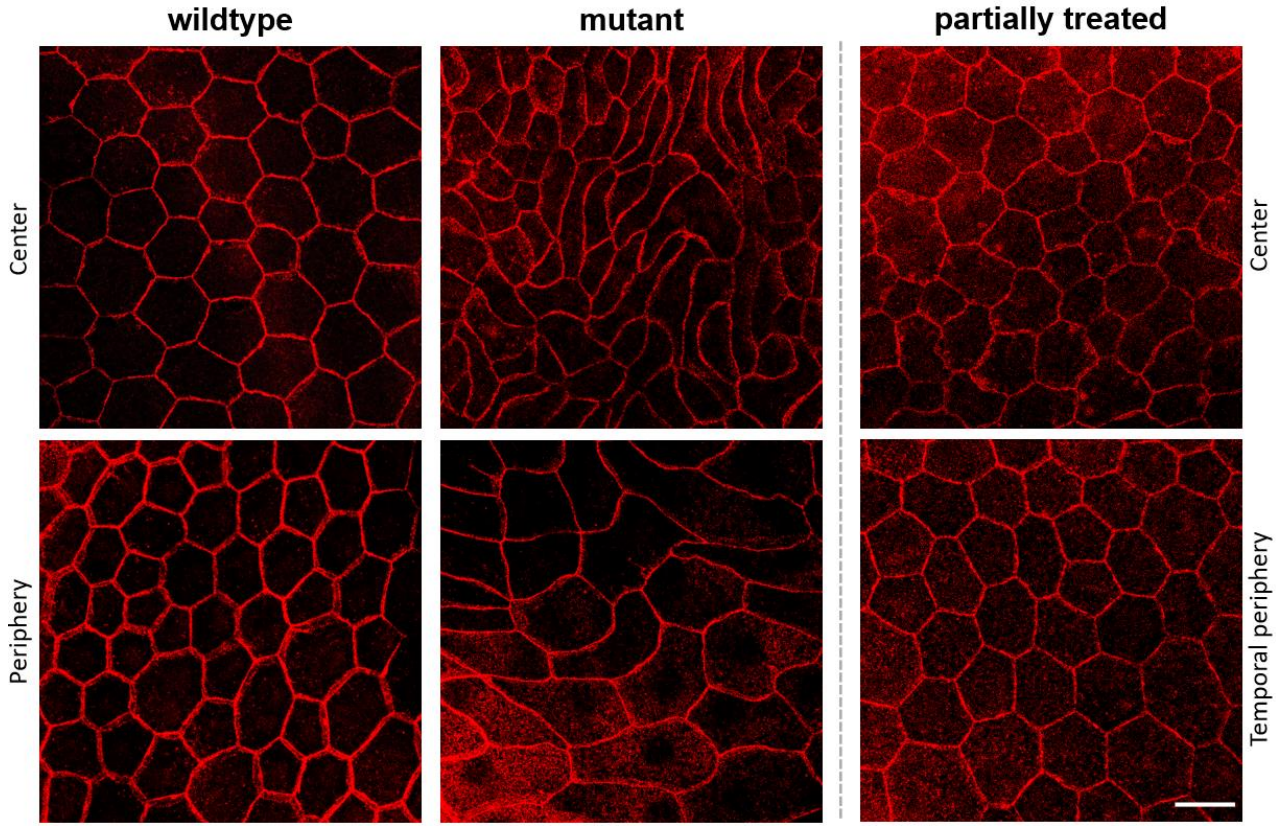

Figure 17. Overview of central and (temporal) peripheral RPE cell morphology of 48-week-old wildtype, mutant and partially treated mice. RPE wholemounts were immunolabelled with anti- β-CATENIN with anti-rabbit Alexa Fluor 647. Red, β-CATENIN. Scalebar 20µm.

peripheral RPE of the partially treated mice was identical to the wildtype. Interestingly, central RPE of partially treated mice had a wildtype-like morphology as having hexagonal shape partially left and also cell size did not seem to be changed notably. Further, research continued by defining RPE cell size and shape and finally, a relative number of nuclei per RPE cell was quantified.

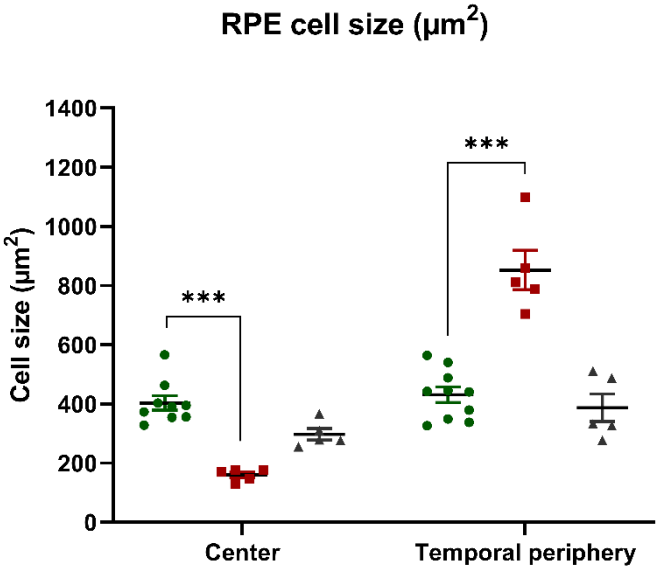

Figure 18. Mutant has significantly larger epithelial cells in periphery than in central RPE, whereas partially treated resembles wildtype as having similar-sized cells in both areas at 48 weeks of age. RPE cell values with SEMs. In center, significant difference between wildtype and mutant was shown (wildtype, n = 9; mutant, n = 5, treated, n = 5) with 2-way ANOVA, $p<0.0001$. In temporal periphery, significant difference between wildtype and mutant was shown (wildtype, n = 10; mutant, n = 5, treated, n = 5; 2-way ANOVA, $p<0.0001$). Green, wildtype; red, mutant; grey, partially treated.

Wildtype had similar RPE cell size in center (mean: 403.2 μm^2) and periphery (mean: 431.2 μm^2) (Fig. 18). Whereas mutant mice had significantly smaller cells in central (mean: 159.5 μm^2) than in peripheral (mean: 852.0 μm^2) RPE. In center, mutant mice had statistically significantly smaller RPE cells than wildtype. Whereas in the periphery, mutant mice had statistically significantly bigger RPE cell size than wildtype. Partially treated mice did not differ statistically significantly from wildtype in center (mean: 342.3 μm^2) nor in temporal periphery (mean: 387.0 μm^2).

RPE cell shape was studied by using the parameters eccentricity (Fig. 19A) and solidity (Fig. 19B). Eccentricity describes the relationship between the opposite diameters of an item. The closer the values are to each other; the closer the eccentricity value is to zero. (Ayoub, 2003) Solidity defines the density of the object as giving a value between zero to one. A value less than one means that an object has an irregular boundary. (Zdilla et al., 2016)

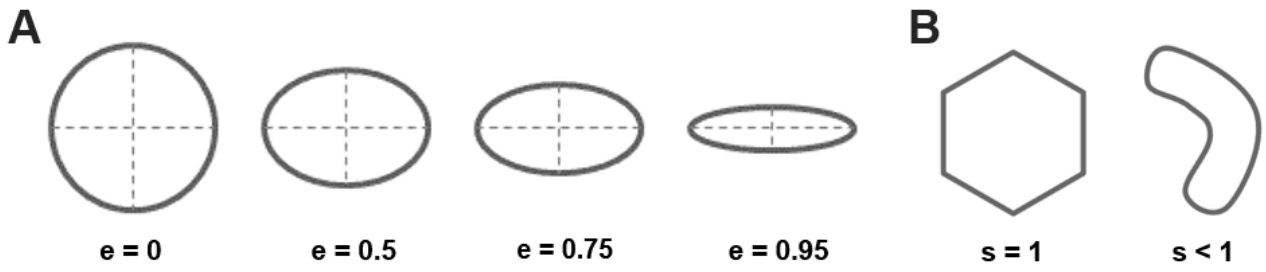

Figure 19. A) Eccentricity of circle and different ellipses. B) Solidity of hexagonal and irregular cylinder shapes.

Quantification of the eccentricity of RPE cells showed that 48-week-old mutant mice had significantly bigger values in center and periphery than wildtype (Fig. 20). Partially treated mice did not differ significantly from wildtype in center nor in temporal periphery. In solidity, wildtype had significantly bigger values than mutant and partially treated in center as confirming that wildtype RPE cells resembled more hexagonal shape (Fig. 21). In periphery, wildtype had also bigger values than mutant mice. Partially treated did not differ statistically significantly from wildtype in temporal periphery.

It was assumed that wildtype mice would have had the solidity values closer to one. Thus, an additional (manual) measurement was conducted by using ImageJ instead of automatic calculation by CellProfiler (Fig. S5). With this approach, wildtype reached a solidity value of 1 with its replicate means in both center and periphery.

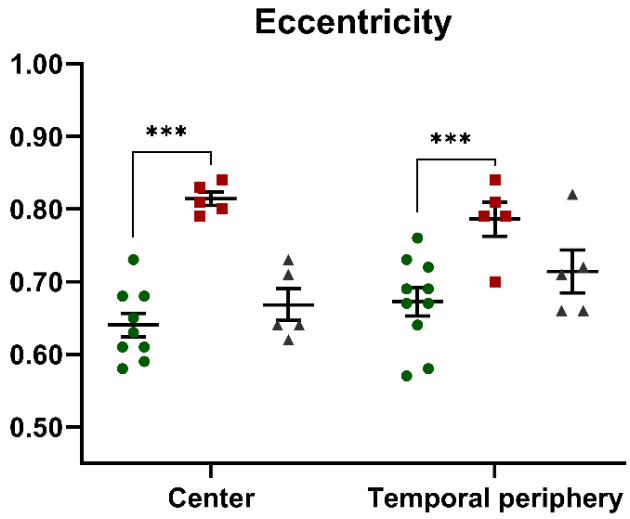

Figure 20. Mutant RPE cells show significantly increased eccentricity in central and peripheral RPE, whereas partially treated resembles wildtype in both areas at 48 weeks of age. Means with SEMs. In center, statistically significant difference between wildtype and mutant ($p<0.0001$), and between mutant and treated ($p=0.0003$) was shown (wildtype, n = 9; mutant, n = 5, treated, n = 5) with 2-way ANOVA. In temporal periphery, statistically significant difference between wildtype and mutant ($p=0.0012$) was shown (wildtype, n = 10; mutant, n = 5, treated, n = 5; 2-way ANOVA). Green, wildtype; red, mutant; grey, treated.

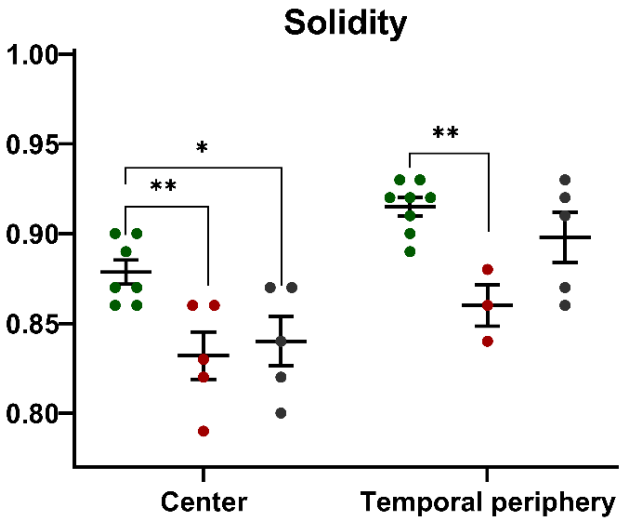

Figure 21. Mutant RPE cells show significantly decreased solidity in central and peripheral RPE, whereas partially treated resembles wildtype in temporal periphery and mutant in center at 48 weeks of age. Means with SEMs. In center, statistically significant difference between wildtype and mutant ($p=0.0066$), and between wildtype and treated ($p=0.0261$) was shown (wildtype, n = 7; mutant, n = 5, treated, n = 5) with 2-way ANOVA. In temporal periphery, statistically significant difference between wildtype and mutant ($p=0.0055$) was shown (wildtype, n = 8; mutant, n = 3, treated, n = 5; 2-way ANOVA). Green, wildtype; red, mutant; grey, treated

2.2.2 Nuclei number is shifted to one in the central RPE of *Pde6b*$^{ST/ST}$ whereas *Pde6b*$^{ST/ST}$ *Pax6αCre* has a wildtype-like nucleus pattern in both central and peripheral regions of the RPE at 48 weeks of age

RPE morphology studies of 48-week-old mutant and treated mice continued with nuclei number definition. Fluorescence images of RPE wholemounts were observed by ImageJ and relative numbers of nuclei were defined (Fig. 22). Neither in center nor in temporal periphery statistically significant difference in relative nuclei number per RPE cell could be seen between wildtype and mutant or wildtype and partially treated at 48 weeks of age (Fig. 23).

In center, mutant replicates had wide-range variance between relative numbers of cells having one or two nuclei. Almost none of the mutant mice had three or more nuclei in the center, whereas wildtype and partially treated mice had. Partially treated mice resembled wildtype mice in center as having the most of the RPE cells with two nuclei, the second-most with one nucleus and the minority with three or more nuclei. In temporal periphery, wildtype, mutant and partially treated mice showed large

variance in a relative number of RPE cells having one or two nuclei. Whereas none of them had three or more nuclei in the temporal periphery.

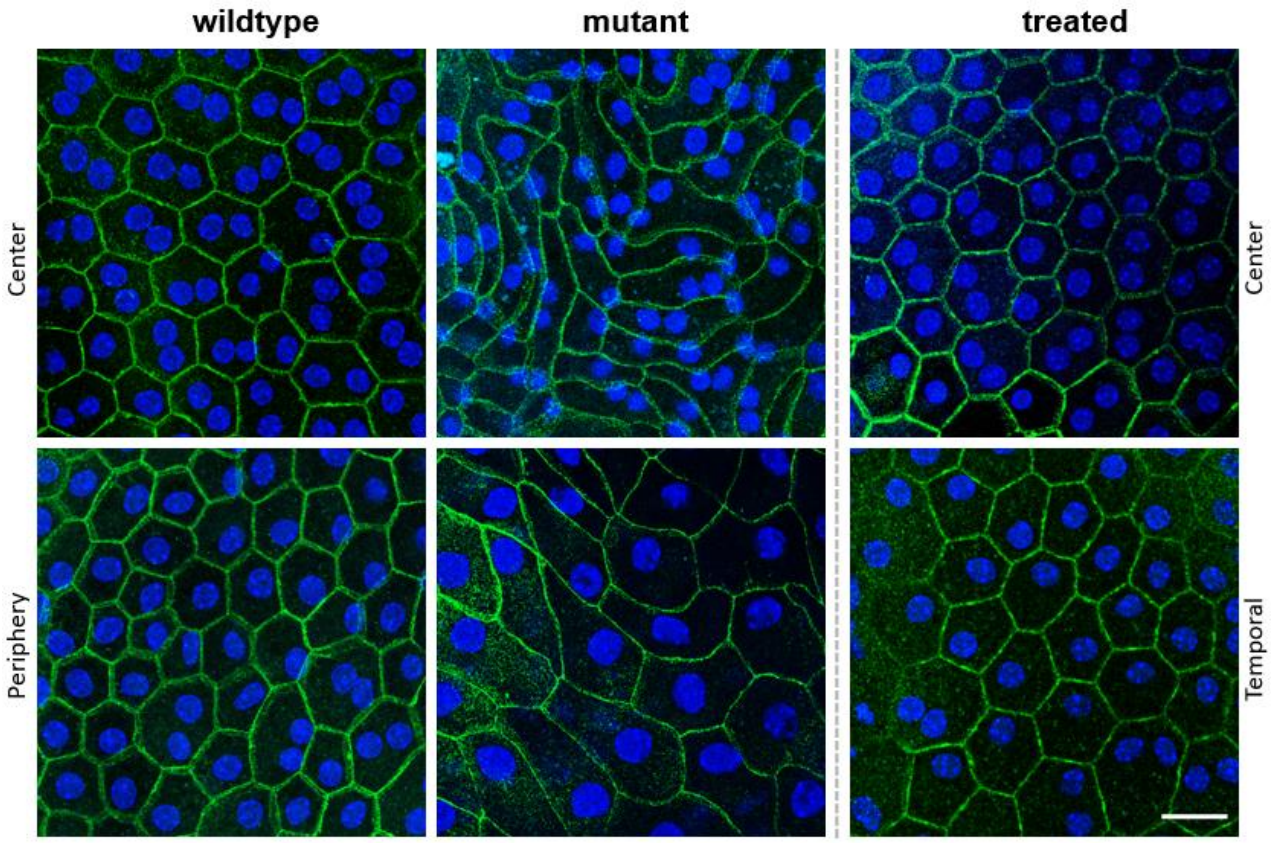

Figure 21. Representative fluorescence images of RPE wholemounts from 48-week-old wildtype, mutant and partially treated mice illustrating the nuclei number of RPE cells. RPE wholemounts were stained for anti-β-CATENIN with anti-rabbit Alexa 647 and for Hoechst. Green, β-catenin; Blue, nuclei. Scalebar, 20 µm.

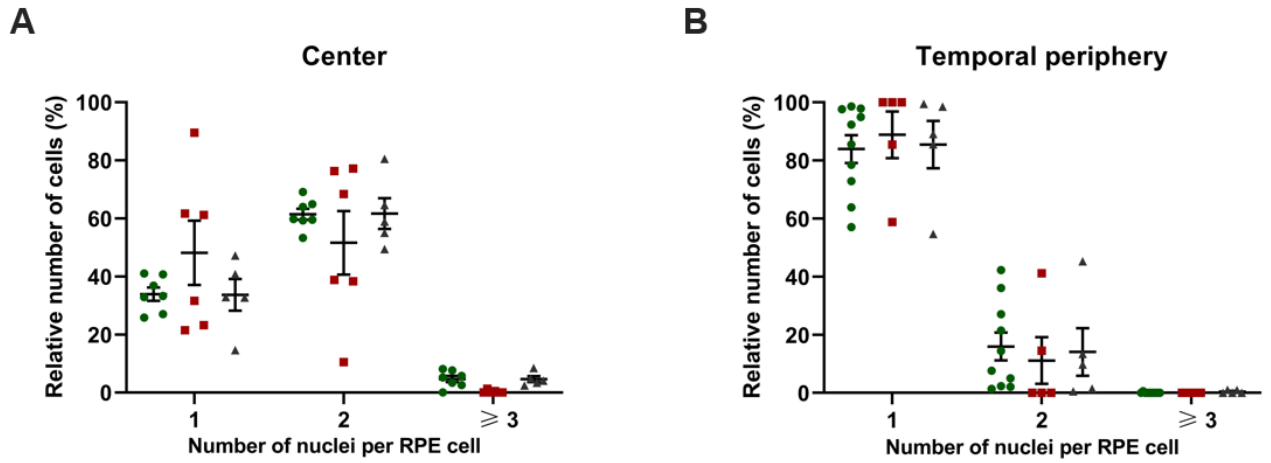

Figure 23. A) No statistically significant difference in nuclei number between wildtype, mutant or treated mouse RPE in center can be seen at 48 weeks of age. Means with SEMs. Wildtype, n = 7; mutant, n = 6, treated, n = 5. 2-way ANOVA. **B) No statistically significant difference in nuclei number between wildtype, mutant or treated mouse RPE in termporal periphery can be seen at 48 weeks of age.** Means with SEMs. Wildtype, n = 7; mutant, n = 6, treated, n = 6. 2-way ANOVA. Green, wildtype; red, mutant; grey, treated.

From research with RPE wholemounts from 48-week-old mutant, four different cell areas could be observed (Fig.24). Around the ON, RPE cells could not be seen at all. In the next distal area, RPE cells seemed to be small and elongated. Then, the cell morphology changed to represent wildtype RPE as cells had partially hexagonal shape and regular size. In the most peripheral RPE, cells were large and elongated. Relative lengths of the cell areas in nasal and temporal sites were defined (Fig. 25) by using fluorescence images from 48-week-old mutant RPE wholemounts. As a result, no significant difference in relative cell area lengths between nasal and temporal sites could be seen.

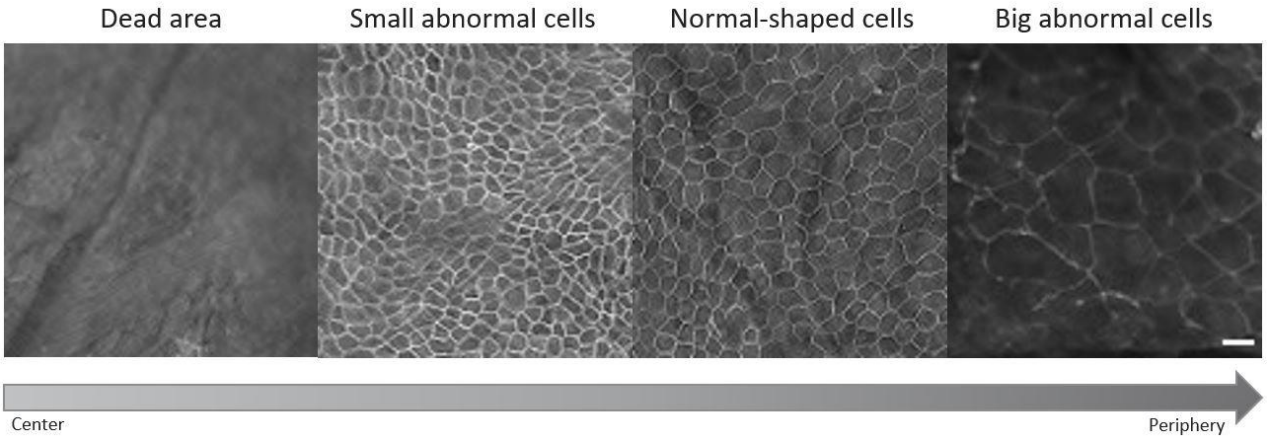

Figure 24. Four different cell areas in 48-week-old mutant RPE can be observed. RPE wholemounts were immunolabelled with anti-β-CATENIN with anti-rabbit Alexa Fluor 647. Scalebar, 25 µm.

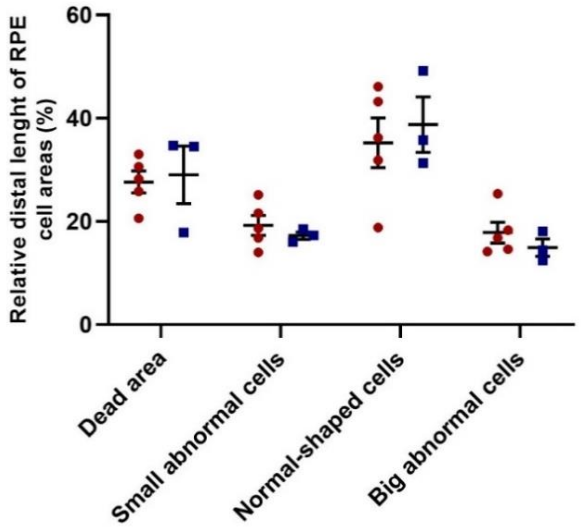

Figure 25. Relative distal lengths of four morphologically different RPE cell areas do not differ significantly between temporal and nasal sites of 48-week-old mutant mice. Relative values with SEMs. No significance difference was observed in any cell area between nasal (blue) and temporal (red) sites (2-way ANOVA, n=3 in nasal, n=5 in temporal). Red, temporal; blue, nasal.

2.3 RPE apoptosis

The RPE cell apoptosis rate in 48-week-old mutant and partially treated mice was studied by a TUNEL assay which was conducted for RPE wholemounts *ex vivo*. During apoptosis, DNA is cleaved. In the TUNEL assay, free 3´-OH termini of cleaved DNA are labelled by using FITC-fluorescent labelled nucleotides. The polymerization reaction is catalyzed by Terminal deoxynucleotidyl transferase (TdT) enzyme. Results can be observed with a fluorescent microscope. (Negoescu et al., 1996)

Wildtype did not show any sign of apoptosis in central nor in peripheral RPE. A tiny, dotted pattern of TUNEL signal could be seen. Mutant showed a strong TUNEL signal in the central RPE, but the pattern represented accumulated matter and not the nucleus-localized DNA fragments. Mutant had seemingly less TUNEL signal in the peripheral RPE where the pattern was tiny-dotted. Partially treated mice had a mutant-like accumulated pattern of TUNEL in the central RPE but in the temporal periphery, the TUNEL signal represented wildtype.

Negative and positive controls were conducted for wildtype RPE wholemounts to confirm the functionality of the assay (Fig. 27). A weak, tiny-dotted pattern of TUNEL signal could be observed in the negative control. Positive control had a TUNEL signal which colocalized with nuclei in periphery but not in the center.

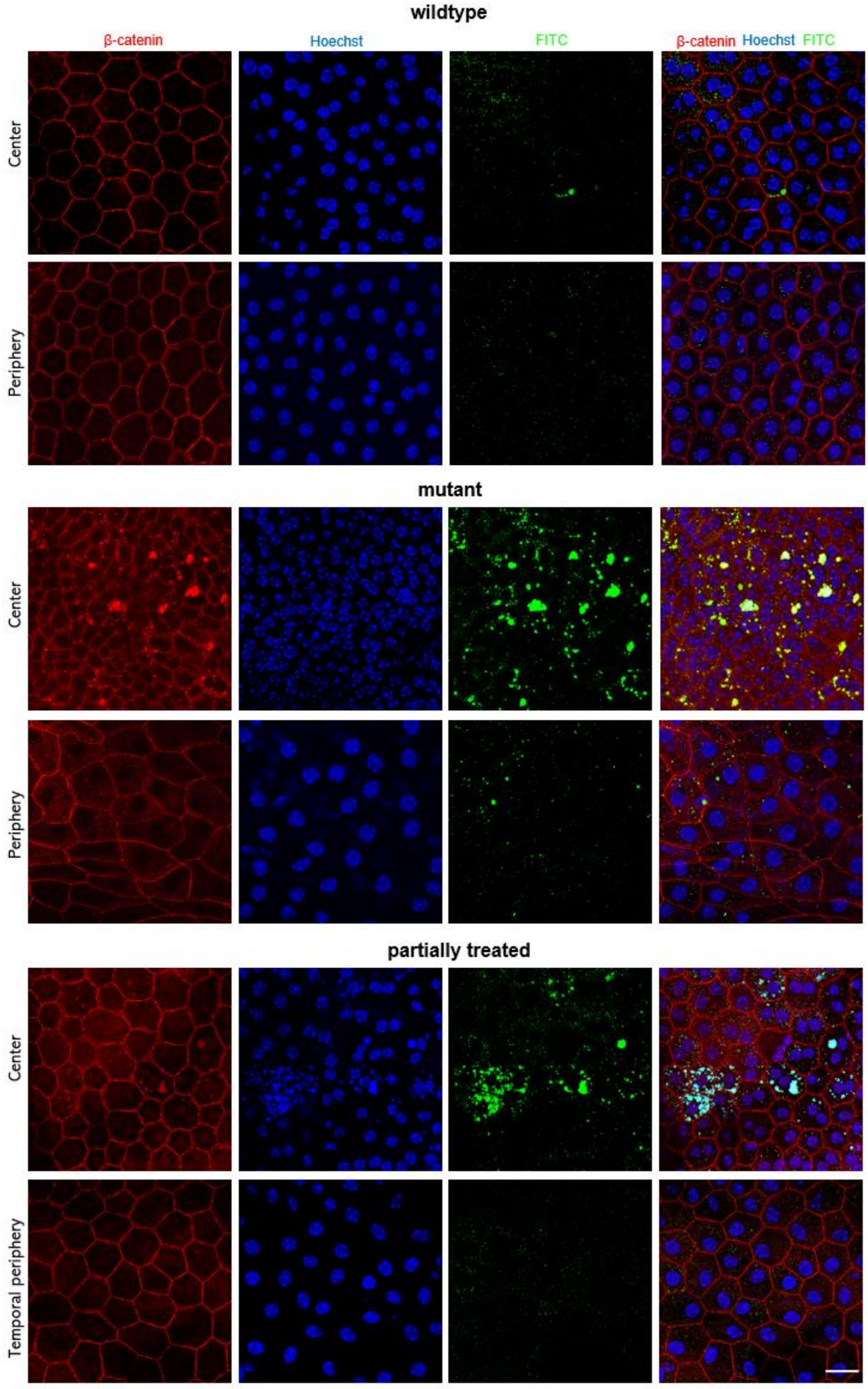
wildtype
β-catenin
Hoechst
FITC
β-catenin Hoechst FITC
Center
Periphery
mutant
Center
Periphery
partially treated
Center
Temporal periphery

Figure 26. Representative confocal images of TUNEL assay results from central and temporal peripheral areas of 48-week-old RPE wholemounts from wildtype, mutant and partially treated mice. TUNEL assay was conducted for RPE wholemounts after which they were stained with anti-β-catenin with anti-rabbit Alexa Fluor 647 and Hoechst. Red, β-CATENIN; green, FITC-labelled nucleotides (TUNEL); blue, nuclei (Hoechst). Scalebar, 20μm.

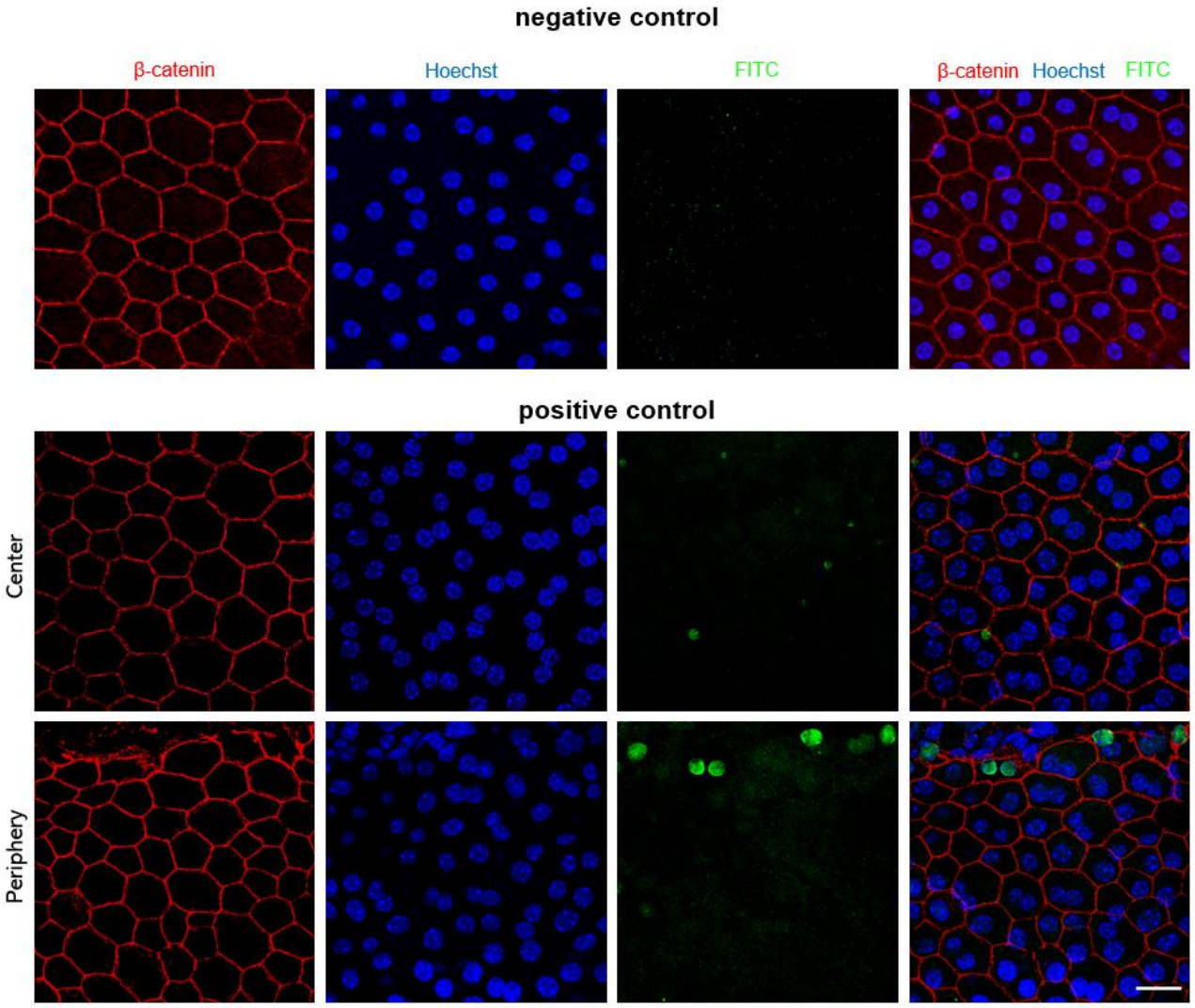

Figure 27. Negative and positive controls of TUNEL assay. In negative control, TUNEL assay was conducted without the TdT enzyme. In positive control, in prior to TUNEL assay, RPE wholemounts were challenged with DNAse enzyme. Both negative and positive controls were conducted for wildtype RPE wholemounts. Red, β-catenin; green, FITC-labelled nucleotides; blue, nuclei (Hoechst). Scalebar, 20μm.

2.4 POS phagocytosis by the RPE

POS phagocytosis is one of the major functions of RPE cells. Recognition, internalization, and degradation can be recognized as different phases of the process. An *ex vivo* POS phagocytosis assay was used to study the process in 48-week-old partially treated and mutant mice. In the experiments, RPE wholemounts were challenged with FITC-labelled porcine-POSs and later labelled also with anti-rhodopsin to localize mouse-originated POSs. *In vitro* POS phagocytosis assay by Mao & Finnemann was used as a template but some minor changes were made due to the use of RPE wholemounts instead of RPE cell culture (Mao and Finnemann, 2012a).

After isolating and labelling porcine-POSs with FITC-fluorescent dye, a feasible POS amount per RPE wholemount was defined. A starting point for the definition was that mouse RPE contains approximately 55,000 cells (Jiang et al., 2013), and the feasible amount of POS particles per RPE cell *in vitro* has been 10 (Mao and Finnemann, 2012a). Eventually, three different amounts were chosen: 16.2 x 10^6, 2.43 x 10^6 and 8.1 x 10^6 POS per RPE wholemount (Fig. 28).

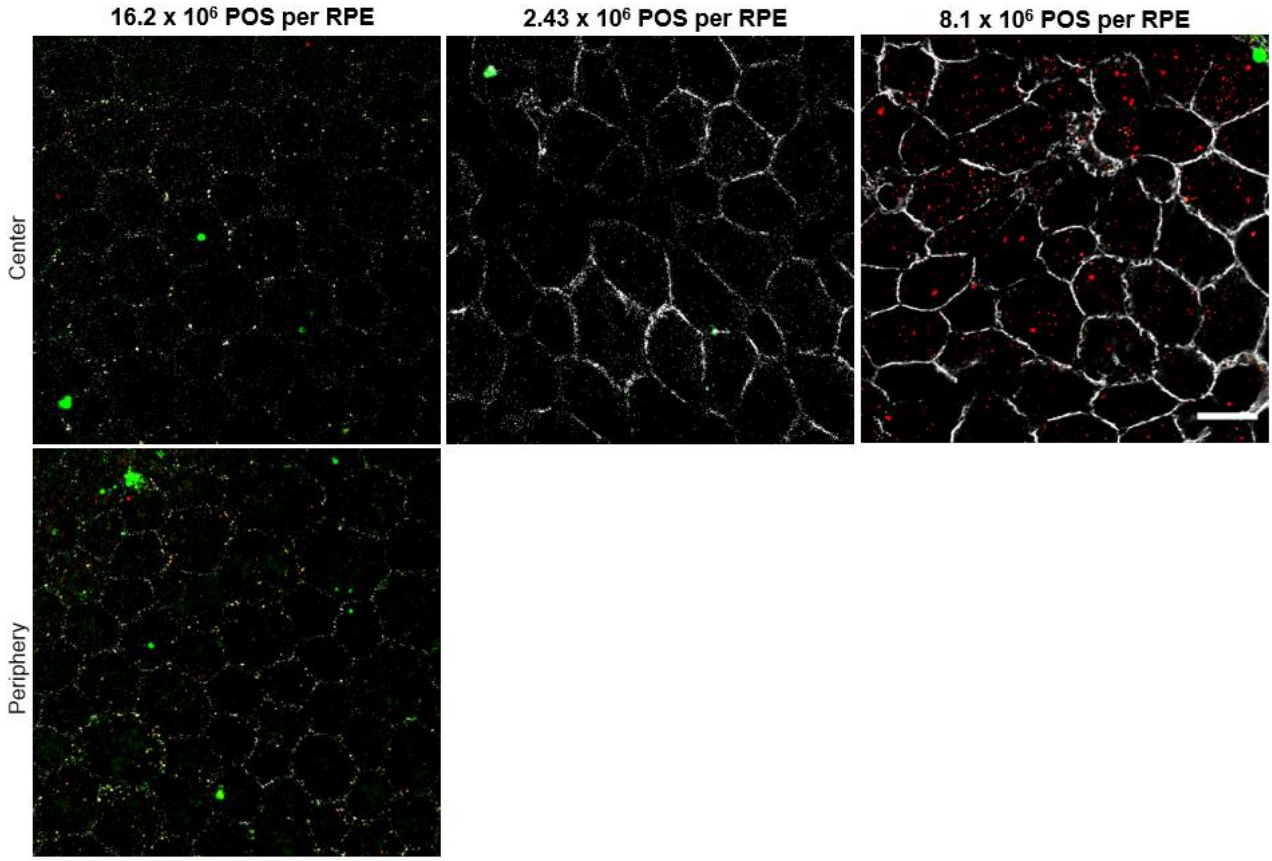

Figure 28. POS phagocytosis assay was conducted for wildtype RPE wholemounts to define the feasible number of POS per RPE for the experiments. RPE wholemounts were challenged for FITC-labelled porcine-POS after which they were stained for anti-RHODOPSIN with anti-mouse Alexa Fluor 555 and anti- β-CATENIN with anti-rabbit Alexa Fluor 647. Grey; β-CATENIN; red, mouse- and porcine-POS; green, FITC-labelled porcine POS, yellow (merge), membrane-bound porcine-POS. Scalebar, 20μm.

After the three POS phagocytosis assays, 16.2 x 10^6 POS per PRE was selected to use in the experiments since it seemed to show the most feasible pattern for defining the activity of POS phagocytosis. In the first assay (16.2 x 10^6 POS per PRE), 25 min incubation at RT for anti-β-catenin was not enough which could be seen as a weak expression in the RPE cell membrane. Thus, the incubation time was changed to be overnight. In addition, the confocal microscope was changed to a regular fluorescence microscope (Keyence) since the latter showed a better pattern for β-catenin.

POS phagocytosis assay was conducted for 48-week-old RPE wholemounts from mutant and partially treated mice (Fig. 29). According to Mao & Finnemann, the following meanings for different fluorescence signals are defined: green represents both membrane-bound and internalized FITC-labelled porcine-POSs, and if they overlap with anti-rhodopsin (red), the POSs are membrane-bound. Thus, FITC-labelled POSs not overlapping with anti-rhodopsin are internalized. However, since the protocol by Mao & Finnemann was carried out *in vitro*, no mouse-originated POS existed. Since the assay used in this project was *ex vivo*, anti-rhodopsin antibody labels also the mouse-originated POS which could be seen as red in a merged image.

The RPE of partially treated mice seemed to have internalized more FITC-POS particles in the temporal periphery than in the center. Expression of RHODOPSIN was abundant in the central RPE but very low in the temporal periphery. A minority of FITC-POSs was membrane-bound in the center and temporal periphery.

Mutant mice had an abundant expression of internalized FITC-POS particles in the central RPE whereas in the periphery the expression was really low. Multiple FITC-POSs were membrane-bound in the center, and also the amount of membrane-bound mouse-POSs seemed to be abundant.

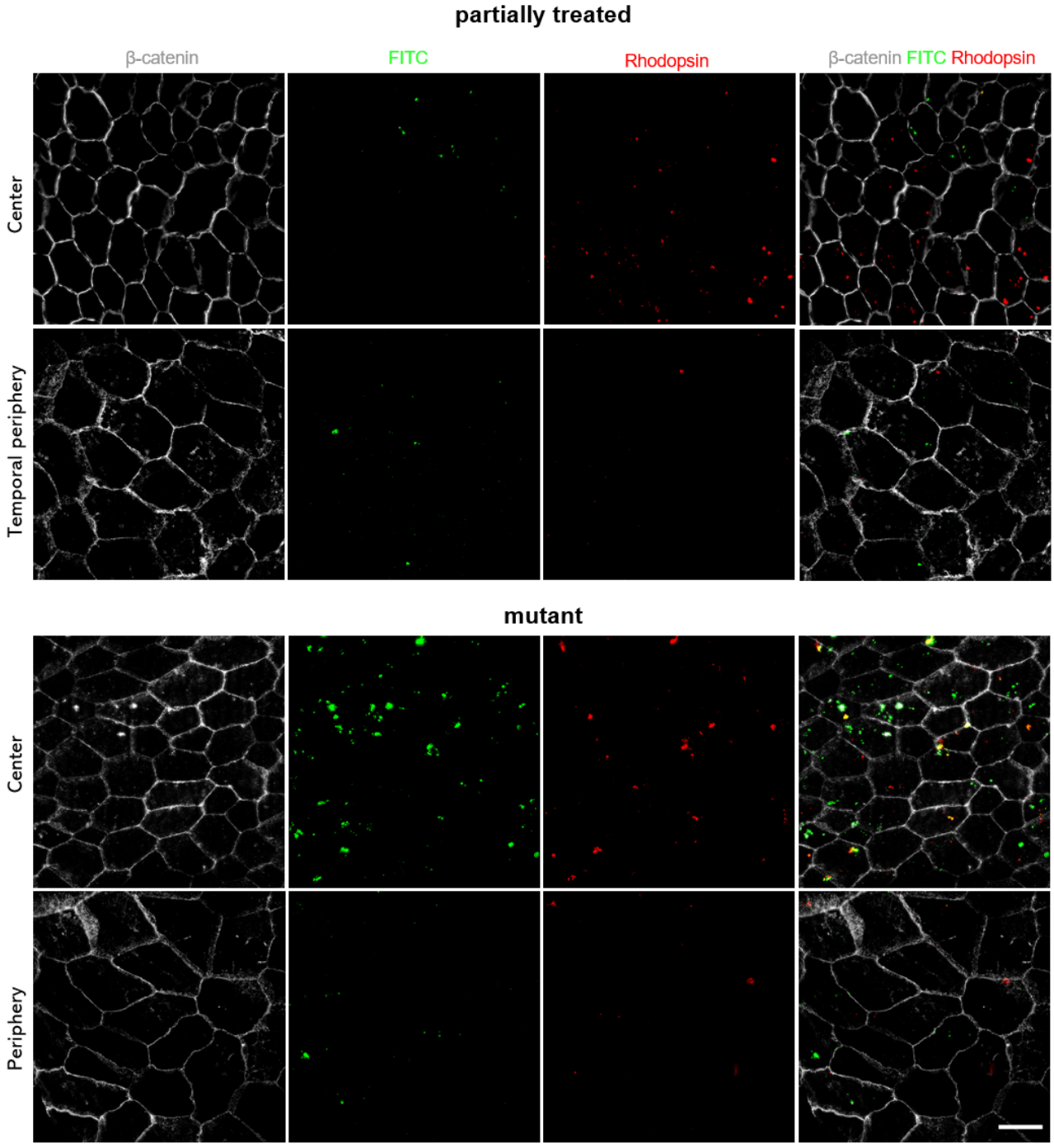

Figure 29. Representative images resulting *ex vivo* POS phagocytosis assay conducted for 48-week-old RPE wholemounts from treated and mutant mice. RPE wholemounts were challenged for FITC-labelled porcine-POS after which they were stained for anti-RHODOPSIN with anti-mouse Alexa Fluor 555 and anti- β-CATENIN with anti-rabbit Alexa Fluor 647. Grey; β-CATENIN; red, mouse- and porcine-POS; green, FITC-labelled porcine POS, yellow (merge), membrane-bound porcine-POS. Scalebar, 20μm.

3 Discussion

3.1 Retinal morphology

3.1.1 *Pde6b*$^{ST/ST}$

In the retinae of 48-week-old *Pde6b*$^{ST/ST}$, rods and cones were completely degenerated and this could be seen to have led to the degeneration of rod (RBC) and cone bipolar cells (CBCs). RBCs and CBCs did not have any dendrites left and their axons and axon terminals were degenerated. Similar RBC degeneration has been seen in the *rd10* mice which showed degenerated RBC dendrites already at 30 days of age, but axons remained unchanged. Also, CBC dendrite loss has been seen in the *rd10* mice at a later timepoint. (Gargini et al., 2007).

Horizontal cells (HCs) get signals mainly from photoreceptor cells and after the total loss of them, HCs were almost completely degenerated in 48-week-old *Pde6b*$^{ST/ST}$. HCs had additional neuronal branches which entered to inner plexiform layer (IPL). This is called neuronal sprouting and it is seen as a remodelling attempt of HCs (Marc et al., 2003). A similar HC pattern has been seen in the *rd1* mice which also showed absent dendrites and additional neuronal branches (Kalloniatis et al., 2016; Phillips et al., 2010).

Müller glia formed a dense glial seal above the INL where rods and cones were degenerated. The glial seal provides mechanical protection for the remaining retinal cells. In normal physiology, Müller glia get lactate from photoreceptor cells which convert it from glucose (Viegas and Neuhauss, 2021). After the cone and rod degeneration, the lactate supply for Müller cells decreases. However, except the glial seal, Müller cells seemed to remain stable and have an organized structure in the mutant retina. In addition to glutamine synthetase, multiple other proteins and small molecule targets have been used to study the morphology of Müller cells such as taurine, glutamate, glutamine, CRALBP (cellular Retinaldehyde binding protein 1) and glutathione. It has been proposed that in degenerating retina, additional glutamate pathways exist in addition to glutamine synthetase (Pfeiffer et al., 2016).

Rod degeneration has been proposed to be a stimulating factor to activate retinal microglia (Gupta et al., 2003). The number of activated microglia was increased in the IPL, and above the INL. Microglia phagocyte cell debris and thus increased microglia activity in the INL is likely to be due to the photoreceptor cell degeneration and in the IPL due to the bipolar cell axon and axon terminal degeneration. In the long run, the cytokines and chemokines produced by microglia cause a state of chronic inflammation. This is harmful for the surrounding retinal tissue as increasing tissue damage.

(Rashid et al., 2019) Modulating retinal microglia activity may be a potential therapeutic target in future therapies against RP (Gupta et al., 2018).

Photoreceptor cells have an essential role in the glucose metabolism between them and the RPE. Photoreceptors intake glucose from the RPE and convert it to lactate which is then intaken by the RPE and Müller cells. (Viegas and Neuhauss, 2021) Surprisingly, GLUT1 expression did not differ remarkably from wildtype. Despite the total loss of photoreceptor cells, potentially only a little increase in GLUT1 expression in the apical and basal sides of the RPE was seen. This may be due to the alternative energy strategy. However, since the morphology of the RPE differed remarkably between central and peripheral regions, more site-specific research about GLUT1 expression is needed.

3.1.2 *Pde6b$^{ST/ST}$ Pax6αCre*

Signs of retinal remodelling could be seen in 48-week-old *Pde6b$^{ST/ST}$ Pax6αCre.* Rod-specific anti-PDE6B antibody showed a little PDE6B expression in the non-recombined area of *Pde6b$^{ST/ST}$ Pax6αCre* retina at least in the very border of the recombination. PDE6B may have been transported from the recombined rods to non-recombined ones. Expression levels of a rod specific α-subunit of PDE6 may provide information about cellular compensating strategy due to the potential asymmetric cGMP binding to the PDE6 enzyme (Guo et al., 2005). Rods OSs showed a stable expression in the non-recombined area. The recombined area may have had a positive impact on *Pde6b*-deficient rods as potentially slowing the rod degeneration.

Cones seemed to be shorter in *Pde6b$^{ST/ST}$ Pax6αCre.* The cone shortening started already in the recombined area and increased in the non-recombined area. Shortening may be due to the cone cell death and thus thinner cone cell layer could create an illusion about the cell shortening. On the other hand, cone OS and IS shortening has been observed in early AMD patients (Baraas et al., 2021) and thus, the shortening might be a hallmark of cone degeneration. Despite the cone shortening, cone synapses remained as a stable line. Also, γ-subunit of PDE6 in rod and cone OSs remained expressed actively in the non-recombined area of *Pde6b$^{ST/ST}$ Pax6αCre* although the total number of photoreceptor cells was lower.

In ONL thickness measurements, the recombined area could be seen to have a positive impact on photoreceptor cell number in the central retina. Although ONL thickness was decreased in the center, it could reach the wildtype levels in the periphery. Also, there was no total loss of photoreceptor cells in the central retina. It could be proposed that rescued photoreceptor cells potentially with the RPE

can slow the degeneration of non-rescued photoreceptor cells. Although it seemed that the temporal periphery of *Pde6b*$^{ST/ST}$ *Pax6αCre* ONL was thinner than in the nasal periphery, no conclusion between potential differences between nasal and temporal retinal degeneration cannot be made due to the small n-number (3).

Bipolar cells and horizontal cells (HCs) get input from both photoreceptor cells. A partial photoreceptor cell degeneration seemed to have an impact on HCs in the non-recombined area where HCs had fewer dendrites. However, the number of HCs seemed to remain stable despite the photoreceptor cell degeneration. After rod and cone cell death, signals to HCs decrease and neuronal sprouting is seen as a remodelling attempt of HCs (Marc et al., 2003). This means that HCs create neuronal branches which typically enter the inner nuclear layer. Neuronal sprouting of HCs was seen in the non-recombined area of *Pde6b*$^{ST/ST}$ *Pax6αCre.* A partial photoreceptor cell loss had an impact also to rod and cone (ON and OFF) bipolar cells. Both had a partial loss of dendrites and decreased synaptic activity in the non-recombined area. However, despite these minor defects, both cell types had dendrites and active synapses also in the non-recombined area closest to the recombined area.

A partial degeneration of the retina was assumed to have an impact on glial cell activation. Indeed, there was a potential increase in the activated microglia number in the non-recombined area. Microglia have been reported to remain active in the remodelling process. Microglia activity can be either harmful or protective. Chronic microglia activity is harmful as promoting tissue damage and inflammation. Protective activity contains cell debris clearing and the release of anti-inflammatory cytokines. (Cherry et al., 2014; Rashid et al., 2019) By defining the activity of pro- and anti-inflammatory agents in the retina would provide more detailed information about the state of the microglia activity. Müller cells had created a glial seal above the non-recombined ONL where photoreceptors were partially degenerated. The glial seal is believed to give mechanic protection for degenerated retina (Di Pierdomenico et al., 2020).

GLUT1 expression was increased in the apical side of RPE in both recombined and non-recombined areas. Also, increased GLUT1 expression was seen above the non-recombined ONL. This atypical GLUT1 expression provides evidence of changed glucose metabolism in both RPE and remaining photoreceptors. Increased GLUT1 expression in the RPE indicates that the intake of glucose from choroid capillaries has increased enormously. Also, an increased GLUT1 expression in the non-recombined ONL means that remaining photoreceptor cells have increased glucose intake. Since the number of lactate-producing photoreceptor cells has decreased, the retina may try to compensate for the loss by increasing the GLUT1 expression.

3.2 RPE morphology

3.2.1 *Pde6b*$^{ST/ST}$

The total photoreceptor cell loss was assumed to have an impact on RPE due to the strong symbiosis between them. The effects are probably both direct and indirect since also the other retinal cell types were degenerated and thus interfering with the retinal homeostasis.

Fig. 32 illustrates the heterogeneous pattern of the RPE of 48-week-old *Pde6b*$^{ST/ST}$ mice. As confirmed with cell size measurements, RPE cells of *Pde6b*$^{ST/ST}$ were seemingly smaller in the center, and larger (double-size compared to wildtype) in the farthest periphery. Around the ON, RPE cells were absent. Between the central cell population consisting of small and elongated cells and the most peripheral large cells, a wildtype-like pattern of hexagonal RPE cells was observed. Parameters describing cell shape (solidity, eccentricity) showed that in both center and the farthest periphery the

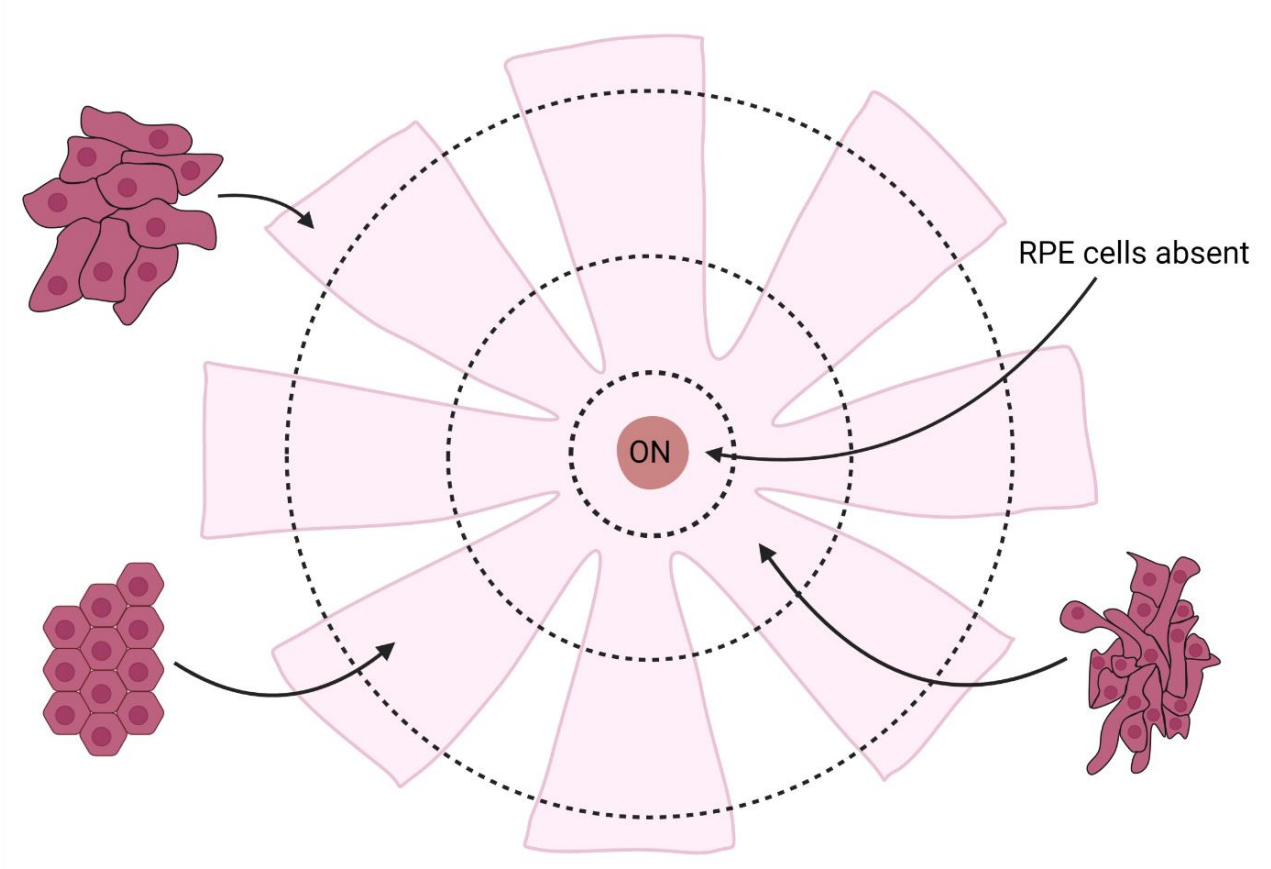

Figure 32. Schematic illustration of RPE of 48-week-old *Pde6b*$^{ST/ST}$ mouse shows the heterogeneity of different RPE cell populations. RPE cells are absent around the ON after which they become small and elongated. When moving more to periphery, cells resemble wildtype as most of them having hexagonal shape and organized pattern. The most peripheral parts of RPE consist large and swollen cells. Nuclei number per RPE can be seen to shifted towards one in a cell population next to dead area. In farthest periphery nuclei number did not seem to differ from wildtype. Created with BioRender.com.

RPE cells have lost their hexagonal shape. Nuclei number per RPE was shifted towards one in the central cell population around the dead area. However, wide-range variation between percentages of one or two nuclei per RPE was seen which might indicate that also the wildtype-like cells have been analysed. Decreased nuclei number per RPE in center may indicate of cell death or decreased cell division. In the farthest periphery, nuclei number did not seem to differ from wildtype.

RPE morphology of 48-week-old *Pde6b*$^{ST/ST}$ is heterogeneous as proving that physiological features have site-specifically changed, and the lack of photoreceptor cells alone does not explain the morphological changes. One explaining factor for the absence of the most central RPE cells, and small and elongated cells around this dead area, is elevated intraocular pressure (IOP). In normal physiology, IOP is higher in the central compared to the peripheral region of the eye (Queirós et al., 2007). Since one cell layer is completely absent (ONL) between the RPE and the vitreous, the impact of the IOP on the RPE may have been increased. Elevated IOP causes a decrease in retinal blood flow affecting especially the central area of the retina and optic nerve (Zhi et al., 2012). Retinal vessel narrowing can be seen as a clinical hallmark in late-stage RP patients as potentially being a cause of elevated IOP. Retinal vessel narrowing leads to decreased retinal blood flow as potentially causing hypoxia and further optic nerve damage. Hypoxia-mediated cell death may be taking place in the central RPE of *Pde6b*$^{ST/ST}$. In addition to retinal vessel narrowing, elevated IOP may be the driving factor for water movement (diffusion) from central RPE to peripheral regions, and thus explain the decreased cellular volume in the center, and larger in the periphery, respectively.

Another perspective to understand the abnormal morphological characteristics of the RPE of *Pde6b*$^{ST/ST}$, is to consider its energy metabolism. Photoreceptors have a crucial role as suppliers of metabolic intermediates of glucose, such as lactate for surrounding cells, like RPE (Kanow et al., 2017). Due to the absence of photoreceptor cells in 48-week-old retinae of *Pde6b*$^{ST/ST}$, lactate supply for RPE cells has collapsed. Despite the photoreceptor cell loss, no remarkable changes in GLUT1 expression could be seen in the RPE of 48-week-old *Pde6b*$^{ST/ST}$. As a conclusion, RPE may have adapted its energy metabolism, and started to produce ATP from glucose itself. However, more research about GLUT1 expression in different morphological areas of *Pde6b*$^{ST/ST}$ RPE is needed to understand the potential glucose metabolism changes. An elevated IOP and its caused retinal vessel narrowing behind the ON challenge the survival of RPE cells even more. The mid-peripheral RPE of *Pde6b*$^{ST/ST}$ containing wildtype-like cells may be a result of adapted energy strategy. Also, the impact of elevated IOP could be assumed to be weaker in more mid-periphery and thus, retinal vessels have not narrowed notably and are capable to transport glucose. Whereas in the far periphery, swollen cell

shape may be a cause of excessive try of intake of glucose or its intermediates from the surrounding environment.

3.2.2 *Pde6b$^{ST/ST}$ Pax6αCre*

As assumed, Cre recombined areas of *Pde6b$^{ST/ST}$ Pax6αCre* retinae including RPE had wildtype-like morphology. Surprising was, how much the RPE of the non-recombined area resembled wildtype although its corresponding retina was partially degenerated. The non-recombined area had a similar RPE cell size and shape as wildtype. Indeed, the surrounding functional retina including vital RPE may have the capability to remodel RPE or prevent it from the degeneration.

The nuclei number per RPE cell varied a lot in both central and temporal peripheral regions of the RPE. However, also wildtype showed a wide-range variation between one or two nuclei per RPE cell in the peripheral regions. This may indicate that despite the morphological similarities in cell shape, incomplete cell division is more prominent in the central regions of the RPE than in the periphery in both wildtype and *Pde6b$^{ST/ST}$ Pax6αCre* mice. Whether the increased nuclei number per RPE in the central regions is due to the incomplete cell division, it may be relevant to study mitosis markers.

The excessive increase of GLUT1 expression in both apical and basal sides of RPE, and above the remaining, thin photoreceptor cell layer may be the prominent factor behind the RPE regeneration. RPE uses lactate for the TCA cycle to produce ATP and thus it is dependent on photoreceptor cells' capacity to convert glucose to lactate. The number of photoreceptor cells is seemingly decreased in the non-recombined area of the *Pde6b$^{ST/ST}$ Pax6αCre* retina. Thus, by increasing GLUT1 expression in the RPE and photoreceptor cells, the retina may be able to compensate for the decrease of lactate-producing photoreceptor cells. With increased GLUT1 expression, RPE can increase the glucose intake from choroidal capillaries, and further transport glucose for photoreceptor cells. Photoreceptors use glucose for their energy metabolism but are essential lactate-producers for RPE, but also for Müller cells.

3.3 RPE apoptosis

TUNEL assay did not show the desired information about apoptosis in the RPEs of 48-week-old *Pde6b$^{ST/ST}$* and *Pde6b$^{ST/ST}$ Pax6αCre* since the FITC-labelled nucleotides did not colocalize with nuclei. The only exception was the positive control in which nucleus-localized FITC could be observed. A reason for the failed assay may be an insufficient tissue permeabilization since the nucleus-localized FITC dye was only seen in the peripheral, damaged part of the RPE wholemount

in the positive control. Previously, TUNEL assays have been conducted for RPE cells *in vitro* and the results were desired as FITC-labelled nucleotides colocalized with nuclei (Elner et al., 2003).

Despite that the TUNEL assay did not show desired results, it indicated that mutant and partially treated mice might have an accumulated matter in either in- or outside the RPE cells. Especially central RPEs of both seemed to contain a lot of FITC-labelled nucleotides which have been attached by something unspecific.

Accumulated matter bound to FITC-nucleotides may be lipofuscin which means granules containing lipid residues. Lipid remains are originated from the phagocytosis of photoreceptor outer segments (POSs). The amount of lipofuscin typically increases with age but lipofuscin accumulation is also related to hypoxia-induced metabolic changes in RPE cells (Kurihara et al., 2016). This would support the hypothesis that an elevated IOP induces retinal vessel narrowing which causes hypoxia for central RPE of *Pde6b*$^{ST/ST}$. Accumulated matter in the central RPE of *Pde6b*$^{ST/ST}$ *Pax6αCre* reveals that despite the morphology of cells that resembles wildtype, their cell metabolism may be unstable.

Another point of view to study apoptosis and cell death, is to study mitochondrial DNA or mitochondrial function in general. Although TUNEL staining has been shown to bind also to cytosolic, mitochondrial DNA *in vitro* (Song et al., 2019), in *Pde6b*$^{ST/ST}$ and *Pde6b*$^{ST/ST}$ *Pax6αCre* unspecific binding is more likely something else. A commonly used apoptosis marker beside the TUNEL assay is an antibody against caspase-3 which is an essential enzyme in apoptosis (Elner et al., 2003). Additionally, other mechanisms leading to cell death exist. It has been shown *in vitro* that RPE cells die mainly via necroptosis and photoreceptors via apoptosis in response to oxidative stress. Necroptosis can be detected by using an antibody against its specific cytokine, HMGB1. (Hanus et al., 2016).

Stronger RPE tissue permeabilization before the TUNEL assay might be the key to achieving better results. Lee & Kim. have proposed a permeabilization solution containing 0.5% Triton X-100, 1% BSA solution in 0.01% sodium acid diluted with PBS for the whole retina-RPE tissue (Lee and Kim, 2021).

3.4 POS phagocytosis by the RPE

The *ex vivo* POS phagocytosis assay results can be seen as preliminary since they represented such a small n-number and did not have wildtype corresponds included.

The procedure behind the *ex vivo* POS phagocytosis assay was the *in vitro* assay by Mao & Finnemann. According to the authors, the following meanings for different fluorescence signals were defined: green represents both membrane-bound and internalized FITC-labelled porcine-POS, and if they overlap with anti-rhodopsin (red), they are membrane-bound. Rhodopsin is normally digested as a part of POS and therefore it is not assumed to be visible with fluorescence imaging after internalization. Thus, FITC-labelled POSs that do not overlap with anti-rhodopsin are internalized. (Mao and Finnemann, 2012a) However, since the protocol by Mao & Finnemann was carried out *in vitro*, no mouse-originated POSs existed. In the *ex vivo* assay, anti-rhodopsin antibody labels also the mouse-originated POSs which could be seen as red in the merged image.

Abundant expression of both membrane-bound and internalized FITC-POS in the central RPE of 48-week-old *Pde6b*$^{ST/ST}$ mice showed that the RPE cells are capable to recognize and internalize POSs. However, it cannot be known whether the internalized POSs are also degraded or will they accumulate into the cell (lipofuscin). To study the accumulation of POSs or simply the amount of lipofuscin inside the RPE cells, lipofuscin can be stained with an antibody against a lipofuscin pigment, A2E (Abeywickrama et al., 2007). The amount of A2E in mouse RPE can also be measured quantitatively by using high-performance liquid chromatography (Sparrow et al., 2013). It has been seen that the A2E inhibits phagolysosomal degradation which is part of the POS degradation process (Finnemann et al., 2002). Since the RPE of *Pde6b*$^{ST/ST}$ has a site-specific morphology, it may be beneficial to observe results of POS phagocytosis assay also in the wildtype-like area in addition to center and periphery.

Partially treated mice did not show striking differences between central and temporal peripheral RPE in the number of internalized POSs. An interesting finding was that the central RPE which corresponding photoreceptor cells have partially degenerated, had seemingly more mouse-originated membrane-bound POSs than the temporal peripheral RPE. Also, it could be seen that the RPE cells that had membrane-bound mouse-POSs, did not have internalized FITC-POSs.

Multiple methods to quantify results of POS phagocytosis exist, especially for the *in vitro* assays. Artero-Castro et al used flow cytometry as quantitative analysis for *in vitro* POS phagocytosis assay, and confocal imaging as a qualitative method. To confirm internalized POSs, RPE cells were labelled for F-actin (phalloidin) and sectioned vertically to illustrate whether POSs are bound to RPE microvilli and thus defined as internalized. (Artero-Castro et al., 2021). Inana et al. used FICT-labelled bovine-POS for isolated human RPE cells and quantified internalized FITC-POSs based on

the shape and size of the POS particle. They described internalized FITC-POSs as being small, mostly circular and sharply demarcated. The rest were seen as membrane-bound (Inana et al., 2018).

3.5 Summary

3.5.1 48-week-old *Pde6b*$^{ST/ST}$ represents late-stage retinitis pigmentosa

In 48-week-old *Pde6b*$^{ST/ST}$ mice, photoreceptors were absent and retinal degeneration was observed in RBCs, ON and OFF CBCs and HCs. Degenerated HCs had additional neuronal branches by which they try to adapt to the signal loss from photoreceptor cells. Increased expression of activated microglia was observed in inner and outer plexiform layers. The degenerated ONL was covered with a glial seal by Müller cells.

RPE showed site-specific morphology as potentially revealing an impact of physical factors (increased intraocular pressure, hypoxia). The central retina may be affected by increased intraocular pressure due to the degeneration of retinal layers between the RPE and the vitreous. Increased intraocular pressure could cause retinal vessel narrowing and thus lead to hypoxia and starvation of central RPE cells. This would explain the abnormal RPE cell morphology in central regions and the RPE cell death around the ON.

Since photoreceptor cells were absent, mice are blind as representing a late-stage retinitis pigmentosa. Results from this project together with previous findings with *Pde6b*$^{ST/ST}$ mice (Zhang et al., 2018) suggest that *Pde6b*$^{ST/ST}$ has a similar retinal degeneration speed with *rd10* mice.

Although retinal section staining did not reveal any changes in GLUT1 expression in *Pde6b*$^{ST/ST}$, site-specific research is needed due to the site-specific morphology of the RPE cells (Fig. 32). The RPE cells are assumed to be adapted their energy strategy since lactate-producing photoreceptor cells are absent. Alternative energy strategy may be the β-oxidation of lipids.

3.5.2 48-week-old *Pde6b*$^{ST/ST}$ *Pax6αCre* shows signs of retinal regeneration

The non-recombined retina of *Pde6b*$^{ST/ST}$ *Pax6αCre* showed degeneration in photoreceptor cells, RBCs, ON and OFF CBCs, HCs and the RPE whereas the recombined retina resembled wildtype as not having retinal degeneration. However, many of the retinal cell types showed signs of remodelling in the non-recombined area closest to the recombined area. PDE6B was expressed in the non-recombined rods and rod OS expression remained stable. Also, the dendrite loss of bipolar and

horizontal cells was partially rescued. However, also opposite effects were seen. Cones seemed to be shorter already in the recombined area and shortened more in the non-recombined area.

RPE cells showed perhaps the biggest regeneration capacity since they had almost identical morphology compared to wildtype in the non-recombined area of the retina. Increased GLUT1 expression in both apical and basal sides of the RPE and in the remaining non-recombined photoreceptor cells may partially explain the rescued morphology of the RPE.

3.5.3 Future aspects for retinitis pigmentosa research

A deeper understanding of the mitochondria of the RPE cells would provide more information about the cell death and energy metabolism. The role of mitochondria is emphasized during hypoxia and oxidative stress. RPE cells are capable to adapt their energy metabolism, and during oxidative stress, the major pathway to produce energy is reductive carboxylation. The process starts in the mitochondria where citrate is produced after which it is transported to the cytosol where it increases the concentration of NADPH as protecting the cell from oxidative stress. (Du et al., 2016) Mitochondrial DNA (mtDNA) encodes essential proteins participating in the production of the ATP. mtDNA defects have been linked to the potential mechanisms behind retinal degenerations. MtDNA defects can be studied by defining deletions and point mutations in mtDNA and the expression of mitochondrial oxidative phosphorylation enzymes. (Karunadharma et al., 2010).

Dysfunctional autophagy in the RPE cells have been related to AMD (Golestaneh et al., 2017) but it has been proposed that impaired autophagy in the RPE cells may contribute also to the pathogenesis of RP (Moreno et al., 2018). Autophagy is a process by which the cell removes dysfunctional or unnecessary components such as misfolded proteins or damaged organelles by degrading them with lysosomes (Glick et al., 2010). In addition to RPE, proteins related to autophagy have been found in photoreceptor cells, bipolar cells and ganglion cells (Moreno et al., 2018). RPE cells have been shown to degrade damaged mitochondria by using autophagy as a result of oxidative stress (Flores-Bellver et al., 2014). According to the current knowledge, impaired autophagy of the RPE cells leads to angiogenesis and the recruitment of macrophages, and increases the caspase-3 dependent apoptosis (Liu et al., 2016). LC3 is a protein associated with autophagosomes and autolysosomes, and thus it has been widely used as a target to study autophagy activity (Wang et al., 2009; Tanida et al., 2008).

Metabolomics is a study that quantitatively measures metabolites in a biological system, such as blood, cells or solid tissues. Metabolomics is a promising tool to define new biomarkers that may improve the understanding of retinal degenerations, such as RP. (Li et al., 2021b; Tan et al., 2016)

Retinal tissues from mice have been studied successfully for different metabolites using either nuclear magnetic resonance (NMR) (Murenu et al., 2021) or liquid-chromatography-mass spectrometry (Sato et al., 2018) -based methods. Also, mouse RPE tissue has been used (Sparrow et al., 2013). Metabolomics may serve as a potential tool to study glucose metabolism in the retina, and glucose metabolites from mouse retinal tissue have been able to detect by using NMR (Murenu et al., 2021). Untargeted assays to discover retinal metabolome may provide also new discoveries.

In addition to GLUT1, monocarboxylate transporters (MCTs) have an essential role in the glucose metabolism between photoreceptor cells and the RPE. MCTs are responsible for transporting lactate and other important metabolites related to the energy production of the outer retina. Photoreceptors encode MCT1 whereas the RPE encodes MCT1 in the apical membrane but MCT3 in the basolateral membrane. (Han et al., 2020)

4 Materials and methods

All solutions were diluted in ddH_2O if not indicated differently.

4.1 Mice

RPE morphology studies, TUNEL assay and POS phagocytosis assay were conducted by using 48-week-old *Pde6b*$^{ST/WT}$, *Pde6b*$^{ST/ST}$ and *Pde6b*$^{ST/ST}$ *Pax6αCre* mice with no gender bias. In retinal section staining, mice had an additional reporter allele *ROSA*$^{nT\text{-}nG}$ and *Pde6b*$^{ST/WT}$ had Cre gene (*Pde6b*$^{ST/WT}$ *Pax6αCre*). Mice had water and food ad libitum while being kept in 12h light/dark circle. All animal experiments were conducted with permission from local authorities and in the accordance with the animal welfare laws of Germany.

4.1.1 Genotyping

Ear biopsies were incubated with 50 mM NaOH at +95°C for 10 min. 50µl of 1 M Tris-HCl, pH 8.0 was added to the mixture, vortexed and centrifuged at 13,200 rpm at +4°C for 10 min. DNA extract was added to a master mix of primer solution (primers, 10xDreamTaq buffer, ddH_2O, DreamTaq DNA Polymerase, Thermo Scientific dNTP mix). PCR was conducted with a nexus X2 cycler (Eppendorf) using a reaction volume of 15µl. Primers are listed in Table 2.

Table 2. Primers used in genotyping. Primes from Metabion international AG, Germany.

Target	Forward primer	Reverse primer	Internal primer	Annealing temperature (°C)
Pax6α	CGTATGAAGG GGGCAATAGA	AGGCAAATTT TGGTGTACGG	-	59,6
Pde6b^{STOP}	TGCTCTGTGG TGTTGCTCTGC	TGGCGATGCA GAGTGTCCTGA	GTCCTGCACG ACGCGAGCTG	65
ROSA26	AAAGTCGCTC TGAGTTGTTAT	GGAGCGGGAG AAATGGATATG	CCAGGCGGGCC ATTTACCGTAAG	60

After PCR run, samples were run by agarose gel electrophoresis (2% agarose in 1M TAE solution: 1mM EDTA, 40mM Tris, 20mM Acetic acid). The electrophoretic profile was visualized in UV light and genotypes were identified. Genotyping was done by Michelle Jentzsch.

4.2 Retinal morphology

4.2.1 Section staining

4.2.1.1 Preparation of the retinal sections

Preparation of the eyecup was done as described in 4.4.1 without separating the retina from the RPE. The eye cup was incubated in 30% sucrose (Carl Roth GmbH, #4621.1) until sank to the bottom. Prior to embedding the eyecup in embedding medium (Tissue-Tek® O.C.T. Compound, 4583, Sakura Finetek), it was dried gently by using with forceps and tissue. Embedded eye cup was frozen with dry ice and stored in −80°C. 10-12 µm thick sections in temporal-nasal orientation were cut on a cryostat. All retinal sections were from Michelle Jentzsch and prepared by her.

4.2.1.2 Antibodies

Primary antibodies (Table 3) were diluted in 5% ChemiBlocker; 0,3% Triton X-100 in 1xPBS and incubated on slides on a shaker at +4°C overnight. After three times washing with 1xPBS, secondary antibodies (Table 4) diluted in 3% ChemiBlocker in 1xPBS were added and incubated at RT for 1.5 h. Following three times washing with 1xPBS, 5 µg/ml Hoechst 33342 (ThermoFisher, #H3570) was added and incubated 5 min at RT. Slides were washed with 1xPBS and mounted with mounting medium (Polysciences, #18606-20).

Table 3. Primary antibodies used for retinal sections. All antibodies diluted in 1:1 glycerol. M = mouse, R = rabbit, G = goat.

Name	Host	Dilution	Manufacturer, #
PDE6B	R	1:2000	Thermo Fischer, PA1-722
PDE6B	M	1:200	Santa Cruz, sc-377486
Cone Arrestin	R	1:500	Merck, AB15282
PDE6G/H	M	1:50	Santa Cruz, sc-166350
PKCα	M	1:500	Santa Cruz, sc-8393
GFP	G	1:500	Biomol, 600-101-215
Calbindin D-28k	M	1:4000	Swant, 300
GARP, clone 4B1	M	1:400	Sigma Aldrich, MABN2429
ß-Catenin	R	1:500	CellSignalingTechnology, 8480S
Glutamine synthetase	R	1:2000	Abcam, ab228590
Iba1	R	1:500	Fujifilm Wako, WAKO019-19741
SCGN	R	1:5000	[non-commercial; from Prof. Wagner (University of Vienna)]
GLUT1	M	1:200	Abcam, ab40084

Table 4. Secondary antibodies used for retinal sections. All antibodies in 1:1 glycerol.

Name	Dilution	Manufacturer, #
Anti-rabbit Alexa Fluor 488	1:500	ThermoFisher, A-11070
Anti-mouse Alexa Fluor 555	1:500	ThermoFisher, A-2425
Anti-rabbit Alexa Fluor 647	1:500	ThermoFisher, A-21245
Anti-mouse Alexa Fluor 405	1:500	ThermoFisher, A-31553
Anti-goat Alexa Fluor 488	1:500	ThermoFisher, A-11055
Anti-mouse Alexa Fluor 647	1:500	ThermoFisher, A-21240

4.2.1.3 Image acquisition

Sections were imaged with on Leica TCS SP8 MP confocal microscope with lasers emitting at wavelengths 405, 488, 555 and 647, using an objective magnification of 40x. Same settings were used for all sections. Leica Application Suite X 3.5.5.19976 software was used with the microscope. GLUT1 images were taken as z-stacks (1 µm thickness in wildtype, 3 µm thickness in mutant and partially treated) and 1-4 stacks were combined.

4.2.2 ONL thickness measurements

Temporal-nasal orientated retinal sections (prepared by Michelle Jentzsch) from 48-week-old wildtype, mutant and partially treated mice were imaged with Keyence BZ-X810, 10x magnification combined with stitching tool. ONL thickness was defined in every 50 µm starting from optic nerve and continued until the end of the section at 2200 µm in length in both nasal and temporal sites by using ImageJ. Analyses and graphs were made with GraphPad Prism 8.4.2.

4.3 RPE morphology

4.3.1 RPE wholemount preparation

Mice were sacrificed and the temporal site was marked by pressing it gently with a heated needle. Then, the eyes were isolated gently by tweezers and put to 4% paraformaldehyde (PFA, Carl Roth GmbH, #0335.2) in 1xPBS, pH 7.4. Preparation was done under a dissecting microscope (dry) at RT. After making a hole into the cornea by using a needle, eyes were put back into 4% PFA for 5min. Cornea was cut away and vitreous was removed. Temporal mark cut was made. Eye cup was fixed in 4% PFA at RT for 45 min and washed three times with 1xPBS. Retina was gently separated by using tweezers in 1xPBS. Optic nerve and fat tissue were removed from the remaining RPE/sclera/choroid tissue.

ß-Catenin antibody (1:500, CellSignalingTechnology, 8480S) was diluted in 5% ChemiBlocker; 0,3% Triton X-100; 3% DMSO in 1xPBS and incubated on RPE wholemount at +4 °C overnight. After three times washing with 1xPBS, secondary antibody anti-rabbit Alexa Fluor 647 diluted in 3% ChemiBlocker in 1xPBS was added and incubated at RT for 1.5 h. Following three times washing with 1xPBS, 5 µg/ml Hoechst 33342 was added and incubated 5 min at RT. RPE wholemounts were washed three times with 1xPBS and mounted with mounting medium.

4.3.1.1 Image acquisition

RPE wholemounts were imaged with Leica TCS SP8 MP confocal microscope with lasers emitting at wavelengths 405 and 647, using an objective magnification of 40x. Leica Application Suite X 3.5.5.19976 software was used with the microscope. Same settings were used for all wholemounts. Images were processed with the ImageJ 1.53c software and finalized with GIMP 2.10.22.

4.3.2 Cell size and shape measurements

RPE cell sizes was defined from confocal images from ß-Catenin-stained RPE wholemounts (imaged by Michelle Jentzsch) by using CellProfiler software. GraphPad Prism 8.4.2 was used for the analyses and graphs ($p<0.05$ was considered as significant, 2-way ANOVA). n-values in center: wildtype, 9; mutant, 5, partially treated, 5 and in temporal periphery: wildtype, 10; mutant, 5; partially treated, 5.

Solidity and eccentricity values were defined defined from confocal images from ß-Catenin-stained RPE wholemounts by using CellProfiler software. GraphPad Prism 8.4.2 was used for the analyses and graphs ($p<0.05$ was considered as statistically significant, 2-way ANOVA).

n-numbers in eccentricity measurements: wildtype, n = 9; mutant, n = 5, partially treated, n = 5 in center and wildtype, n = 10; mutant, n = 5, partially treated, n = 5 in temporal periphery. n-values in solidity measurements in center: wildtype, n = 7; mutant, n = 5, partially treated, n = 5 and in temporal periphery: wildtype, n = 8; mutant, n = 3, partially treated, n = 5. periphery.

Additional solidity measurements were conducted manually by using ImageJ 1.53c. Analyses and graphs were made as described above.

4.3.3 Nuclei number

Relative number of nuclei per RPE was defined from confocal images from ß-Catenin- and Hoechst stained RPE wholemounts (imaged by Michelle Jentzsch) manually by using ImageJ. GraphPad

Prism 8.4.2 was used for the analyses and graphs ($p<0.05$ was considered as significant, 2-way ANOVA).

4.3.4 Temporal and nasal comparisons of *Pde6*$^{ST/ST}$ RPE morphology

RPE wholemounts were imaged with Keyence BZ-X810 using 10x magnification with combination of stitching tool to illustrate four different cell areas. The cell areas were measured manually by using the ImageJ 1.53c software. GraphPad Prism 8.4.2 was used for the analyses and graphs ($p<0.05$ was considered as significant, 2-way ANOVA, n=3 in nasal, n=5 in temporal).

4.4 POS Phagocytosis Assay

4.4.1 Solutions

Five POS isolation stock solutions were prepared:
1. 100 mM glucose (Carl Roth GmbH, #HN06.2)
2. 200mM Tris/Acetate pH 7.2 (Tris Base: Carl Roth GmbH, #3738.4. Acetic acid: Carl Roth GmbH, #3738.4)
3. 70% sucrose (Carl Roth GmbH, #4621.1)
4. 0.1 M Na2CO3 pH 11.5 (Carl Roth GmbH, #HN01.1)
5. 0.1 M NaHCO3 pH 8.4 (Carl Roth GmbH, #8563.1)

Nine POS isolation working solutions were prepared:
1. Homogenization solution: 20% sucrose, 20 mM Tris/Acetate pH 7.2; 2 mM $MgCl_2$ (Carl Roth GmbH, #KK36.2), 10 mM glucose, 5 mM taurine (Carl Roth GmbH, #4721.2)
2. 25% sucrose solution: 25% sucrose, 20 mM Tris/Acetate pH 7.2; 10 mM glucose, 5 mM taurine
3. 60% sucrose solution: 48 g of sucrose in a solution of 20 mM Tris–Acetate pH 7.2; 10 mM glucose, 5 mM taurine
4. WASH1: 20 mM Tris–Acetate pH 7.2; 5 mM taurine
5. WASH2: 10% sucrose, 20 mM Tris–Acetate pH 7.2; 5 mM taurine
6. WASH3: 10% sucrose, 20 mM phosphate buffer pH 7.2; 5 mM taurine
7. DMEM: DMEM/F-12 (ThermoFisher Scientific, # 11320, LOT 2401971), 4.5 g/L glucose
8. FITC stock solution: 10 mg of FITC isomer I (Invitrogen, #F1906, LOT 2291415) dissolved in 5 ml of 0.1 M Na-carbonate buffer, pH 9.5
9. PBS-CM: 1 mM $MgCl_2$ (Carl Roth GmbH, # KK36.2) 0.2 mM $CaCl_2$ (Carl Roth GmbH, # CN93.1) in 1xPBS

4.4.2 Isolation of POS from porcine eyes (Fig. S1)

58 porcine eyes were dissected under a dim red light and retinas were isolated using a scalp. Retinas were collected into a falcon containing 15ml of homogenization solution. Suspension was shaken gently for 2 min and then filtered three times through 1-layer gauze. Next, three 24ml of linear gradient of 25–60% sucrose, 20 mM Tris/Acetate pH 7.2, 10 mM glucose, 5mM taurine in 30ml ultracentrifuge tubes. Under dim red light equal volumes of retina isolate were pipetted on top of the sucrose gradient. Centrifugation tubes were balanced using homogenization solution. Tubes were spinned immediately at 25,000 rpm for 48min at +4°C (Beckman SW-28 rotor; Optima™ LE-80K Ultracentrifuge, serial No. COL00C28, Instance No. 825153). Two sharp, orange-like bands from the upper third of the gradient were collected using a needle through the tube. Collected samples were combined and diluted four times volume of ice-cold WASH 1. Solution was separated to two centrifugation tubes and spined at 3,000 x *g* for 10 min. Pellets were resuspended in 10 ml of WASH2, combined and spined at 3,000 x *g* for 10 min. Pellet was resuspended in 15 ml of WASH3, spined at 3,000 x *g* for 10 min. Pellet was resuspended in 5 ml of WASH3 and 1,5 ml of FITC stock solution was added. The tube was rotated for 1 h at RT in the dark. After rotation, labelled POSs were washed twice in WASH3 and twice in 2,5% sucrose in DMEM. After every wash, FITC-POSs were spined at 3,000 x *g* for 10 min. After washing, labelled POSs were resuspended in 2,5% sucrose in DMEM. Concentration of FITC-POSs was calculated under a microscope using a hemocytometer. FITC-POSs were aliquoted to units of 16,2 x 10^6 POS and stored in −80°C.

4.4.3 POS phagocytosis assay

RPE wholemounts were prepared in as defined in section 4.4.1 except the whole preparation process was conducted in DMEM. One aliquot (16,2 x 10^6 POS per RPE) was used. FITC-POS aliquots were thawed from −80°C and spined at 2,400 x *g* for 5 min at RT. Pellets were gently resuspended with 10% heat-inactivated FBS in DMEM. RPE wholemounts were incubated in FITC-POS suspension in 48-well plate at 37°C 5% CO_2 for 2 h.

Phagocytosis was terminated by washing 3 x with 1xPBS-CM at RT. RPE wholemounts were fixed with 4% PFA in PBS at RT for 20 min. Remaining fixative was quenched by incubating RPE wholemounts in 50 mM NH_4Cl in PBS-CM for 20 min at RT. Wholemounts were blocked with 1% BSA (Sigma, #A7030-50G) in PBS-CM for 10 min at RT. Wholemounts were incubated with anti-rhodopsin antibody (1D4, Santa Cruz, sc-57432) 1:500 in 5% ChemiBlocker; 0,3% Triton X-100; 3% DMSO in 1xPBS for 25min at RT. Wholemounts were washed two times with PBS-CM and once

with 1 % BSA in PBS-CM for 5 min per each. β-catenin antibody (1:500 in 5% ChemiBlocker; 0,3% Triton X-100; 3% DMSO in 1xPBS) was added and incubated at +4°C overnight. Anti-rabbit Alexa Fluor 647 and Anti-mouse Alexa Fluor 555 (both 1:500 in 3% ChemiBlocker in 1xPBS) were added and incubated 1.5h at RT. After washing with 1xPBS-CM, 5 µg/ml Hoechst 33342 was added and incubated at RT for 15min. Wells were washed three times with PBS-CM before mounting wholemounts on coverslips.

4.4.4 Image acquisition and quantification

The test experiments for defining the feasible amount of porcine-POS were images on Leica TCS SP8 MP confocal microscope with lasers emitting at wavelengths 405, 488, 555 and 647, using an objective magnification of 40x. Leica Application Suite X 3.5.5.19976 software was used with the microscope. For main experiments, Keyence BZ-X810 fluorescence microscope was used with 40x object. BZ-X800 Viewer and Analyzer software were used with Keyence. Images were processed with the ImageJ 1.53c software and finalized with GIMP 2.10.22.

4.5 TUNEL assay

4.5.1 Procedure

TUNEL assay was conducted using a commercial kit by Roche (*In Situ* Cell Death Detection Kit, Fluorescein, #11684795910) according to the manufacturer's instructions. RPE wholemounts were prepared as described in section 4.4.1. Then, wholemounts were bleached in 10% H_2O_2 (Carl Roth GmbH, # 9683.4) in 1xPBS at +55 °C for 1.5 h and then washed three times with 1xPBS. Wholemount were incubated in permeabilization solution (0.1% Triton X-100; 0,1% sodium citrate, 1xPBS) on ice using a 48-well plate. Wells were washed three times with 1xPBS. Wholemounts were incubated with TUNEL reaction mixture for 1 h at +37°C plate covered. After incubation wells were washed with 1xPBS three times.

After TUNEL assay, wholemounts were incubated with β-catenin antibody (1:500 in 5% ChemiBlocker; 0,3% Triton X-100; 3% DMSO in 1xPBS) at +4°C overnight. After primary antibody incubation wells were washed three times with 1xPBS. Secondary antibody anti-rabbit Alexa Fluor 647 was added and incubated for 1.5 h at RT. 5 µg/ml Hoechst 33342, ThermoFisher was added and incubated at RT for 15 min. Wholemounts were washed three times with 1xPBS after which mounted to cover slips.

4.5.2 Controls

In negative control, TUNEL reaction was conducted by using only Label Solution (without the TdT enzyme). Positive control was incubated with DNase 1 (50 U/ml in 50 mM Tris-HCl, pH 7.5, 1 mg/ml BSA, 5mM $Mg^{2+)}$ for 10 min at 37 °C in prior to TUNEL assay. A 48-week-old *Pde6b*$^{ST/WT}$ mouse was used for the negative control, and 4-week-old *Pde6b*$^{ST/WT}$ mouse for the positive control.

4.5.3 Image acquisition

RPE wholemounts were imaged by Leica TCS SP8 MP confocal microscope with lasers emitting at wavelengths 405, 488 and 647, using an objective magnification of 40x. Leica Application Suite X 3.5.5.19976 software was used with the microscope. Images were processed with the ImageJ 1.53c software and finalized with GIMP 2.10.22.

4.6 Fluorescence microscopy

Fluorescence imaging is a valuable tool to study cell physiology. Before the imaging process, samples are first labelled with a primary antibody which has a specific protein target. Depending on the host of the primary antibody, a secondary antibody is chosen according to that. The secondary antibody is conjugated with a fluorophore. When a sample is illuminated with a specific wavelength (emission), a fluorophore emits a longer wavelength which is then detected by the fluorescence microscope. (Sanderson et al., 2014) Autofluorescence is a phenomenon, in which a biological structure emits (without a fluorophore) light naturally when it is excited with suitable wavelength (Croce and Bottiroli, 2014).

In this research project, two different fluorescence microscopes were used. Leica TCS SP8 MP is a confocal fluorescence microscope, whereas Keyence BZ-X810 is a phase contrast fluorescence microscope. Although both can detect fluorescent signals, confocal microscope uses lasers as having more resolution and contrast in its images. In a confocal microscope, the illumination and detection optics are focused on the same point of a sample, which is then the only spot imaged. Whereas, in non-confocal microscope, everything emitting of a certain wavelength will be imaged despite are they in focus or not. After finding a perfect spot on from the sample, image is taken with a desired magnification (objective). (Elliott, 2020)

Acknowledgements

I want to thank my supervisor Prof. Susanne F. Koch for all the support and expertise during this thesis project. Also, I want to acknowledge Michelle Jentzsch for patient guidance in the laboratory. I'm grateful for the whole team Koch for memorable and educational six-month period that I was a part of the group.

Support of my dear friends and family has inspired and motivated me throughout these university years and finally, also through this Master's thesis. You are my superpower.

Abbreviation list

AAV	adeno-associated virus
AQP	aquaporin (receptor)
AMD	age-related macular degeneration
AMPA	α-amino-3-hydroxy-5-methyl-4 isoxazolepropionic acid
ATP	adenosine triphosphate
BSA	bovine serum albumin
CBC	cone bipolar cell
cGMP	cyclic guanosine monophosphate
CNG	cGMP gated cation channel
EGFP	enhanced green fluorescent protein
EMA	European Medicines Agency
FDA	U.S. Food and Drug Administration
GABA	γ-aminobutyric acid
GDP	guanosine diphosphate
GLUT1	glucose transporter 1
GS	glutamine synthetase
GDP	guanosine diphosphate
GTP	guanosine triphosphate
HC	horizontal cell
IBA1	Ionized calcium binding adaptor molecule 1
INL	inner nuclear layer
IPL	inner plexiform layer
IOP	intraocular pressure
IS	inner segment
IRD	inherited retinal degeneration
mGluR6	metabotropic glutamate receptor 6
mtDNA	mitochondrial DNA
NMR	nuclear magnetic resonance
ONL	outer nuclear layer
OPL	outer plexiform layer
OS	outer segment
PDE6	phosphodiesterase 6
PDE6*	phosphodiesterase, activated form
POS	photoreceptor outer segment
PtdSer	phosphatidylserine
R	rhodopsin
R*	rhodopsin, activated form
RBC	rod bipolar cell
RPC	retinal progenitor cell
RPE	retinal pigment epithelium
RP	retinitis pigmentosa
TdT	terminal deoxynucleotidyl transferase

References

Abeywickrama, C., H. Matsuda, S. Jockusch, J. Zhou, Y.P. Jang, B.X. Chen, Y. Itagaki, B.F. Erlanger, K. Nakanishi, N.J. Turro, and J.R. Sparrow. 2007. Immunochemical recognition of A2E, a pigment in the lipofuscin of retinal pigment epithelial cells. *Proc. Natl. Acad. Sci. U. S. A.* 104:14610–14615. doi:10.1073/PNAS.0706806104/ASSET/D71ABBD4-A5FF-4B61-B1EA-BF88E7FEEA17/ASSETS/GRAPHIC/ZPQ0350774710007.JPEG.

Almedawar, S., K. Vafia, S. Schreiter, K. Neumann, S. Khattak, T. Kurth, M. Ader, M.O. Karl, S.H. Tsang, and E.M. Tanaka. 2020. MERTK-Dependent Ensheathment of Photoreceptor Outer Segments by Human Pluripotent Stem Cell-Derived Retinal Pigment Epithelium. *Stem cell reports*. 14:374–389. doi:10.1016/J.STEMCR.2020.02.004.

Arslan, U., E. Özmert, S. Demirel, F. Örnek, and F. Şermet. 2018. Effects of subtenon-injected autologous platelet-rich plasma on visual functions in eyes with retinitis pigmentosa: preliminary clinical results. *Graefe's Arch. Clin. Exp. Ophthalmol.* 256:893–908. doi:10.1007/S00417-018-3953-5/TABLES/9.

Artero-Castro, A., K. Long, A. Bassett, A. Ávila-Fernandez, M. Cortón, A. Vidal-Puig, P. Jendelova, F.J. Rodriguez-Jimenez, E. Clemente, C. Ayuso, and E. Slaven. 2021. Gene Correction Recovers Phagocytosis in Retinal Pigment Epithelium Derived from Retinitis Pigmentosa-Human-Induced Pluripotent Stem Cells. *Int. J. Mol. Sci.* 22:1–13. doi:10.3390/IJMS22042092.

Asteriti, S., C. Gargini, and L. Cangiano. 2014. Mouse rods signal through gap junctions with cones. *Elife*. 2014:1386. doi:10.7554/ELIFE.01386.001.

Ayoub, A.B. 2003. The Eccentricity of a Conic Section. *Coll. Math. J.* 34:116–121. doi:10.1080/07468342.2003.11921994.

Baden, T., P. Berens, K. Franke, M. Román Rosón, M. Bethge, and T. Euler. 2016. The functional diversity of retinal ganglion cells in the mouse. *Nature*. 529:345–350. doi:10.1038/NATURE16468.

Baehr, W., M.J. Devlin, and M.L. Applebury. 1979. Isolation and characterization of cGMP phosphodiesterase from bovine rod outer segments. *J. Biol. Chem.* 254:11669–11677.

Baraas, R.C., Å. Horjen, S.J. Gilson, and H.R. Pedersen. 2021. The Relationship Between Perifoveal L-Cone Isolating Visual Acuity and Cone Photoreceptor Spacing—Understanding the Transition Between Healthy Aging and Early AMD. *Front. Aging Neurosci.* 13:573. doi:10.3389/FNAGI.2021.732287/BIBTEX.

Bäumer, N., T. Marquardt, A. Stoykova, R. Ashery-Padan, K. Chowdhury, and P. Gruss. 2002. Pax6 is required for establishing naso-temporal and dorsal characteristics of the optic vesicle. *Development*. 129:4535–4545. doi:10.1242/DEV.129.19.4535.

Baylor, D.A., T.D. Lamb, and K.W. Yau. 1979. Responses of retinal rods to single photons. *J. Physiol.* 288:613. doi:10.1113/jphysiol.1979.sp012716.

Benedicto, I., G.L. Lehmann, M. Ginsberg, D.J. Nolan, R. Bareja, O. Elemento, Z. Salfati, N.M. Alam, G.T. Prusky, P. Llanos, S.Y. Rabbany, A. Maminishkis, S.S. Miller, S. Rafii, and E. Rodriguez-Boulan.

2017. Concerted regulation of retinal pigment epithelium basement membrane and barrier function by angiocrine factors. *Nat. Commun. 2017 81*. 8:1–12. doi:10.1038/ncomms15374.

Bosch, E., J. Horwitz, and D. Bok. 1993. Phagocytosis of outer segments by retinal pigment epithelium: phagosome-lysosome interaction. *J. Histochem. Cytochem.* 41:253–263. doi:10.1177/41.2.8419462.

Bosco, A., K. Cusato, G.P. Niccbia, A. Frigeri, and D.C. Spray. 2005. A developmental switch in the expression of aquaporin-4 and Kir4.1 from horizontal to Müller cells in mouse retina. *Invest. Ophthalmol. Vis. Sci.* 46:3869–3875. doi:10.1167/IOVS.05-0385.

Bowes, C., T. Li, M. Danciger, L.C. Baxter, M.L. Applebury, and D.B. Farber. 1990. Retinal degeneration in the rd mouse is caused by a defect in the beta subunit of rod cGMP-phosphodiesterase. *Nature*. 347:677–680. doi:10.1038/347677A0.

Brancati, N., M. Frucci, D. Gragnaniello, D. Riccio, V. Di Iorio, and L. Di Perna. 2018. Automatic segmentation of pigment deposits in retinal fundus images of Retinitis Pigmentosa. *Comput. Med. Imaging Graph.* 66:73–81. doi:10.1016/J.COMPMEDIMAG.2018.03.002.

Bringmann, A., A. Grosche, T. Pannicke, and A. Reichenbach. 2013. GABA and glutamate uptake and metabolism in retinal glial (Müller) cells. *Front. Endocrinol. (Lausanne).* 4:48. doi:10.3389/FENDO.2013.00048/BIBTEX.

Bringmann, A., T. Pannicke, J. Grosche, M. Francke, P. Wiedemann, S.N. Skatchkov, N.N. Osborne, and A. Reichenbach. 2006. Müller cells in the healthy and diseased retina. *Prog. Retin. Eye Res.* 25:397–424. doi:10.1016/J.PRETEYERES.2006.05.003.

Burke, J.M. 2008. Epithelial phenotype and the RPE: Is the answer blowing in the Wnt? *Prog. Retin. Eye Res.* 27:579–595. doi:10.1016/J.PRETEYERES.2008.08.002.

Burkhardt, D.A. 1994. Light adaptation and photopigment bleaching in cone photoreceptors in situ in the retina of the turtle. *J. Neurosci.* 14:1091–1105. doi:10.1523/JNEUROSCI.14-03-01091.1994.

Burns, M.E. 2010. Deactivation Mechanisms of Rod Phototransduction: The Cogan Lecture. *Invest. Ophthalmol. Vis. Sci.* 51:1283. doi:10.1167/IOVS.09-4366.

Caberoy, N.B., Y. Zhou, and W. Li. 2010. Tubby and tubby-like protein 1 are new MerTK ligands for phagocytosis. *EMBO J.* 29:3898–3910. doi:10.1038/EMBOJ.2010.265.

Carrella, S., A. Indrieri, B. Franco, and S. Banfi. 2020. Mutation-Independent Therapies for Retinal Diseases: Focus on Gene-Based Approaches. *Front. Neurosci.* 14:1015. doi:10.3389/FNINS.2020.588234/BIBTEX.

Carullo, G., S. Federico, N. Relitti, S. Gemma, S. Butini, and G. Campiani. 2020. Retinitis Pigmentosa and Retinal Degenerations: Deciphering Pathways and Targets for Drug Discovery and Development. *ACS Chem. Neurosci.* 11:2173–2191. doi:10.1021/ACSCHEMNEURO.0C00358.

Chaitin, M.H., and M.O. Hall. 1983. The distribution of actin in cultured normal and dystrophic rat pigment epithelial cells during the phagocytosis of rod outer segments. *Invest. Ophthalmol. Vis. Sci.* 24:821–831.

Chan-Ling, T., S. Hughes, L. Baxter, E. Rosinova, I. McGregor, Y. Morcos, P. van Nieuwenhuyzen, and P.

Hu. 2007. Inflammation and breakdown of the blood-retinal barrier during “physiological aging” in the rat retina: a model for CNS aging. *Microcirculation*. 14:63–76. doi:10.1080/10739680601073451.

Chen, M., D. Rajapakse, M. Fraczek, C. Luo, J. V. Forrester, and H. Xu. 2016. Retinal pigment epithelial cell multinucleation in the aging eye – a mechanism to repair damage and maintain homoeostasis. *Aging Cell*. 15:436. doi:10.1111/ACEL.12447.

Chen, S. Der, J.H. Yin, C.S. Hwang, C.M. Tang, and D.I. Yang. 2012. Anti-apoptotic and anti-oxidative mechanisms of minocycline against sphingomyelinase/ceramide neurotoxicity: implication in Alzheimer’s disease and cerebral ischemia. *Free Radic. Res.* 46:940–950. doi:10.3109/10715762.2012.674640.

Cherry, J.D., J.A. Olschowka, and M.K. O’Banion. 2014. Neuroinflammation and M2 microglia: The good, the bad, and the inflamed. *J. Neuroinflammation*. 11:1–15. doi:10.1186/1742-2094-11-98/COMMENTS.

Crane, R., S.M. Conley, M.R. Al-Ubaidi, and M.I. Naash. 2021. Gene Therapy to the Retina and the Cochlea. *Front. Neurosci.* 15:247. doi:10.3389/FNINS.2021.652215/BIBTEX.

Croce, A.C., and G. Bottiroli. 2014. Autofluorescence Spectroscopy and Imaging: A Tool for Biomedical Research and Diagnosis. *Eur. J. Histochem.* 58:320–337. doi:10.4081/EJH.2014.2461.

da Cruz, L., J.D. Dorn, M.S. Humayun, G. Dagnelie, J. Handa, P.O. Barale, J.A. Sahel, P.E. Stanga, F. Hafezi, A.B. Safran, J. Salzmann, A. Santos, D. Birch, R. Spencer, A. V. Cideciyan, E. de Juan, J.L. Duncan, D. Eliott, A. Fawzi, L.C. Olmos de Koo, A.C. Ho, G. Brown, J. Haller, C. Regillo, L. V. Del Priore, A. Arditi, and R.J. Greenberg. 2016. Five-Year Safety and Performance Results from the Argus II Retinal Prosthesis System Clinical Trial. *Ophthalmology*. 123:2248–2254. doi:10.1016/J.OPHTHA.2016.06.049.

Dacey, D. 2004. Origins of Perception: Retinal Ganglion Cell Diversity and the Creation of Parallel Visual Pathways. *In* The Cognitive Neurosciences. M. Gazzaniga, editor. The MIT Press. 281–301.

Davis, R.J., C.W. Hsu, Y.T. Tsai, K.J. Wert, J. Sancho-Pelluz, C.S. Lin, and S.H. Tsang. 2013. Therapeutic margins in a novel preclinical model of retinitis pigmentosa. *J. Neurosci.* 33:13475–13483. doi:10.1523/JNEUROSCI.0419-13.2013.

Deguchi, J., A. Yamamoto, T. Yoshimori, K. Sugasawa, Y. Moriyama, M. Futai, T. Suzuki, K. Kato, M. Uyama, and Y. Tashiro. 1994. Acidification of phagosomes and degradation of rod outer segments in rat retinal pigment epithelium. *Investig. Ophthalmol. Vis. Sci.* 35:568–579.

Dekhuijzen, P.N.R. 2004. Antioxidant properties of N-acetylcysteine: their relevance in relation to chronic obstructive pulmonary disease. *Eur. Respir. J.* 23:629–636. doi:10.1183/09031936.04.00016804.

Deterre, P., J. Bigay, F. Forquet, M. Robert, and M. Chabre. 1988. cGMP phosphodiesterase of retinal rods is regulated by two inhibitory subunits. *Proc. Natl. Acad. Sci. U. S. A.* 85:2424–2428. doi:10.1073/pnas.85.8.2424.

Du, J., A. Yanagida, K. Knight, A.L. Engel, A.H. Vo, C. Jankowski, M. Sadilek, V.T.B. Tran, M.A. Manson, A. Ramakrishnan, J.B. Hurley, and J.R. Chao. 2016. Reductive carboxylation is a major metabolic

pathway in the retinal pigment epithelium. *Proc. Natl. Acad. Sci. U. S. A.* 113:14710–14715. doi:10.1073/PNAS.1604572113/-/DCSUPPLEMENTAL.

Eden, S., R. Rohatgi, A. V. Podtelejnikov, M. Mann, and M.W. Kirschner. 2002. Mechanism of regulation of WAVE1-induced actin nucleation by Rac1 and Nck. *Nature*. 418:790–793. doi:10.1038/NATURE00859.

Elliott, A.D. 2020. Confocal Microscopy: Principles and Modern Practices. *Curr. Protoc. Cytom.* 92:e68. doi:10.1002/CPCY.68.

Elner, S.G., A. Yoshida, Z.M. Bian, A.L. Kindezelskii, H.R. Petty, V.M. Elner, S.E. Wilson, R. Klein, and M.B. Mets. 2003. Human RPE cell apoptosis induced by activated monocytes is mediated by caspase-3 activation. *Trans. Am. Ophthalmol. Soc.* 101:77.

Escher, P., P. Gouras, R. Roduit, L. Tiab, S. Bolay, T. Delarive, S. Chen, C.C. Tsai, M. Hayashi, J. Zernant, J.E. Merriam, N. Mermod, R. Allikmets, F.L. Munier, and D.F. Schorderet. 2009. Mutations in NR2E3 can cause dominant or recessive retinal degenerations in a same family. *Hum. Mutat.* 30:342. doi:10.1002/HUMU.20858.

Fain, G., and A.P. Sampath. 2018. Rod and cone interactions in the retina. *F1000Research 2018 7657*. 7:657. doi:10.12688/f1000research.14412.1.

Farber, D.B., J.G. Flannery, and C. Bowes-Rickman. 1994. The rd mouse story: Seventy years of research on an animal model of inherited retinal degeneration. *Prog. Retin. Eye Res.* 13:31–64. doi:10.1016/1350-9462(94)90004-3.

Fernández-Sánchez, L., P. Lax, L. Campello, I. Pinilla, and N. Cuenca. 2015. Astrocytes and Müller cell alterations during retinal degeneration in a transgenic rat model of retinitis pigmentosa. *Front. Cell. Neurosci.* 9:484. doi:10.3389/FNCEL.2015.00484/BIBTEX.

Ferrer-Martín, R.M., D. Martín-Oliva, A. Sierra-Martín, M.C. Carrasco, M. Martín-Estebané, R. Calvente, S.M. Martín-Guerrero, J.L. Marín-Teva, J. Navascués, and M.A. Cuadros. 2015. Microglial Activation Promotes Cell Survival in Organotypic Cultures of Postnatal Mouse Retinal Explants. *PLoS One*. 10:e0135238. doi:10.1371/JOURNAL.PONE.0135238.

Finn, A.P., D.S. Grewal, and L. Vajzovic. 2018. Argus II retinal prosthesis system: a review of patient selection criteria, surgical considerations, and post-operative outcomes. *Clin. Ophthalmol.* 12:1089. doi:10.2147/OPTH.S137525.

Finnemann, S.C., L.W. Leung, and E. Rodriguez-Boulan. 2002. The lipofuscin component A2E selectively inhibits phagolysosomal degradation of photoreceptor phospholipid by the retinal pigment epithelium. *Proc. Natl. Acad. Sci. U. S. A.* 99:3842–3847. doi:10.1073/PNAS.052025899/SUPPL_FILE/0258FIG6LEGEND.HTML.

Flores-Bellver, M., L. Bonet-Ponce, J.M. Barcia, J.M. Garcia-Verdugo, N. Martinez-Gil, S. Saez-Atienzar, J. Sancho-Pelluz, J. Jordan, M.F. Galindo, and F.J. Romero. 2014. Autophagy and mitochondrial alterations in human retinal pigment epithelial cells induced by ethanol: implications of 4-hydroxy-nonenal. *Cell Death Dis. 2014 57*. 5:e1328–e1328. doi:10.1038/cddis.2014.288.

Florido, A. 2021. Mesenchymal Stem Cells for Treatment of Retinitis Pigmentosa: Short Review. *J. Stem Cells Res. Dev. Ther.* 7:1–6. doi:10.24966/SRDT-2060/100066.

Fontainhas, A.M., M. Wang, K.J. Liang, S. Chen, P. Mettu, M. Damani, R.N. Fariss, W. Li, and W.T. Wong. 2011. Microglial morphology and dynamic behavior is regulated by ionotropic glutamatergic and GABAergic neurotransmission. *PLoS One*. 6. doi:10.1371/JOURNAL.PONE.0015973.

Fung, B.K.K., J.B. Hurley, and L. Stryer. 1981. Flow of information in the light-triggered cyclic nucleotide cascade of vision. *Proc. Natl. Acad. Sci. U. S. A.* 78:152–156. doi:10.1073/pnas.78.1.152.

Gao, J., R.M. Hussain, and C.Y. Weng. 2020. Voretigene Neparvovec in Retinal Diseases: A Review of the Current Clinical Evidence. *Clin. Ophthalmol.* 14:3855. doi:10.2147/OPTH.S231804.

Gargini, C., E. Terzibasi, F. Mazzoni, and E. Strettoi. 2007. Retinal organization in the retinal degeneration 10 (rd10) mutant mouse: A morphological and ERG study. *J. Comp. Neurol.* 500:222–238. doi:10.1002/CNE.21144.

Ghosh, K.K., S. Bujan, S. Haverkamp, A. Feigenspan, and H. Wässle. 2004. Types of bipolar cells in the mouse retina. *J. Comp. Neurol.* 469:70–82. doi:10.1002/CNE.10985.

Gilhooley, M.J., D.G. Hickey, M. Lindner, T. Palumaa, S. Hughes, S.N. Peirson, R.E. MacLaren, and M.W. Hankins. 2021. ON-bipolar cell gene expression during retinal degeneration: Implications for optogenetic visual restoration. *Exp. Eye Res.* 207:108553. doi:10.1016/J.EXER.2021.108553.

Gillespie, P.G., and J.A. Beavo. 1988. Characterization of a bovine cone photoreceptor phosphodiesterase purified by cyclic GMP-sepharose chromatography. *J. Biol. Chem.* 263:8133–8141.

Giovanna Valentini, C., E. Rosa Nuzzolo, M. Bianchi, N. Orlando, M. Grazia Iachininoto, P. Pinci, and L. Teofili. 2019. Cord Blood Platelet Lysate: In Vitro Evaluation to Support the Use in Regenerative Medicine. *Mediterr. J. Hematol. Infect. Dis.* 11. doi:10.4084/MJHID.2019.021.

Glick, D., S. Barth, and K.F. Macleod. 2010. Autophagy: cellular and molecular mechanisms. *J. Pathol.* 221:3. doi:10.1002/PATH.2697.

Glickman, R.D., S.L. Jacques, R.M. Hall, and N. Kumar. 2001. Revisiting the internal absorption coefficient of the retinal pigment epithelium melanosome. *https://doi.org/10.1117/12.434697*. 4257:134–141. doi:10.1117/12.434697.

Golestaneh, N., Y. Chu, Y.Y. Xiao, G.L. Stoleru, and A.C. Theos. 2017. Dysfunctional autophagy in RPE, a contributing factor in age-related macular degeneration. *Cell Death Dis. 2017 81*. 8:e2537–e2537. doi:10.1038/cddis.2016.453.

Gorczyca, W.A., A.S. Polans, I.G. Surgucheva, I. Subbaraya, W. Baehr, and K. Palczewski. 1995. Guanylyl cyclase activating protein: A calcium-sensitive regulator of phototransduction. *J. Biol. Chem.* 270:22029–22036. doi:10.1074/jbc.270.37.22029.

Gospe, S.M., S.A. Baker, and V.Y. Arshavsky. 2010. Facilitative glucose transporter Glut1 is actively excluded from rod outer segments. *J. Cell Sci.* 123:3639–3644. doi:10.1242/JCS.072389.

Greferath, U., U. Grünert, and H. Wässle. 1990. Rod bipolar cells in the mammalian retina show protein kinase C-like immunoreactivity. *J. Comp. Neurol.* 301:433–442. doi:10.1002/CNE.903010308.

Guan, Z., Y. Li, S. Jiao, N. Yeasmin, P.J. Rosenfeld, S.R. Dubovy, B.L. Lam, and R. Wen. 2020. A2E Distribution in RPE Granules in Human Eyes. *Molecules*. 25. doi:10.3390/MOLECULES25061413.

Gulati, S., K. Palczewski, A. Engel, H. Stahlberg, and L. Kovacik. 2019. Cryo-EM structure of phosphodiesterase 6 reveals insights into the allosteric regulation of type I phosphodiesterases. *Sci. Adv.* 5. doi:10.1126/SCIADV.AAV4322.

Guo, L.W., J.E. Grant, A.R. Hajipourt, H. Muradov, M. Arbabian, N.O. Artemyev, and A.E. Ruoho. 2005. Asymmetric Interaction between Rod Cyclic GMP Phosphodiesterase γ Subunits and αβ Subunits *. *J. Biol. Chem.* 280:12585–12592. doi:10.1074/JBC.M410380200.

Gupta, N., K.E. Brown, and A.H. Milam. 2003. Activated microglia in human retinitis pigmentosa, late-onset retinal degeneration, and age-related macular degeneration. *Exp. Eye Res.* 76:463–471. doi:10.1016/S0014-4835(02)00332-9.

Gupta, N., S. Shyamasundar, R. Patnala, A. Karthikeyan, T. V. Arumugam, E.A. Ling, and S.T. Dheen. 2018. Recent progress in therapeutic strategies for microglia-mediated neuroinflammation in neuropathologies. *Expert Opin. Ther. Targets*. 22:765–781. doi:10.1080/14728222.2018.1515917.

Gurevich, V. V., S.B. Dion, J.J. Onorato, J. Ptasienski, C.M. Kim, R. Sterne-Marr, M.M. Hosey, and J.L. Benovic. 1995. Arrestin interactions with G protein-coupled receptors. Direct binding studies of wild type and mutant arrestins with rhodopsin, beta 2-adrenergic, and m2 muscarinic cholinergic receptors. *J. Biol. Chem.* 270:720–731. doi:10.1074/JBC.270.2.720.

Hall, M.O., M.S. Obin, M.J. Heeb, B.L. Burgess, and T.A. Abrams. 2005. Both protein S and Gas6 stimulate outer segment phagocytosis by cultured rat retinal pigment epithelial cells. *Exp. Eye Res.* 81:581–591. doi:10.1016/J.EXER.2005.03.017.

Hamel, C. 2006. Retinitis pigmentosa. *Orphanet J. Rare Dis.* 1:40. doi:10.1186/1750-1172-1-40.

Han, J.Y.S., J. Kinoshita, S. Bisetto, B.A. Bell, R.A. Nowak, N.S. Peachey, and N.J. Philp. 2020. Role of monocarboxylate transporters in regulating metabolic homeostasis in the outer retina: Insight gained from cell-specific Bsg deletion. *FASEB J.* 34:5401. doi:10.1096/FJ.201902961R.

Hanus, J., C. Anderson, D. Sarraf, J. Ma, and S. Wang. 2016. Retinal pigment epithelial cell necroptosis in response to sodium iodate. *Cell Death Discov. 2016 21*. 2:1–9. doi:10.1038/cddiscovery.2016.54.

He, Y., Y. Zhang, X. Liu, E. Ghazaryan, Y. Li, J. Xie, and G. Su. 2014. Recent Advances of Stem Cell Therapy for Retinitis Pigmentosa. *Int. J. Mol. Sci.* 15:14456. doi:10.3390/IJMS150814456.

Hinkle, J.W., R. Mahmoudzadeh, and A.E. Kuriyan. 2021. Cell-based therapies for retinal diseases: a review of clinical trials and direct to consumer “cell therapy” clinics. *Stem Cell Res. Ther.* 12:1–9. doi:10.1186/S13287-021-02546-9/TABLES/3.

Hollborn, M., M. Francke, I. Iandiev, E. Bühner, C. Foja, L. Kohen, A. Reichenbach, P. Wiedemann, A. Bringmann, and S. Uhlmann. 2008. Early Activation of Inflammation- and Immune Response-Related Genes after Experimental Detachment of the Porcine Retina. *Invest. Ophthalmol. Vis. Sci.* 49:1262–1273. doi:10.1167/IOVS.07-0879.

Howell, G.R., D.G. Macalinao, G.L. Sousa, M. Walden, I. Soto, S.C. Kneeland, J.M. Barbay, B.L. King, J.K.

Marchant, M. Hibbs, B. Stevens, B.A. Barres, A.F. Clark, R.T. Libby, and S.W.M. John. 2011. Molecular clustering identifies complement and endothelin induction as early events in a mouse model of glaucoma. *J. Clin. Invest.* 121:1429–1444. doi:10.1172/JCI44646.

Inana, G., C. Murat, W. An, X. Yao, I.R. Harris, and J. Cao. 2018. RPE phagocytic function declines in age-related macular degeneration and is rescued by human umbilical tissue derived cells. *J. Transl. Med.* 16:63. doi:10.1186/S12967-018-1434-6.

Jackson, H., D. Garway-Heath, P. Rosen, A.C. Bird, and S.J. Tuft. 2001. Outcome of cataract surgery in patients with retinitis pigmentosa. *Br. J. Ophthalmol.* 85:936–938. doi:10.1136/bjo.85.8.936.

Jeon, C.J., E. Strettoi, and R.H. Masland. 1998. The Major Cell Populations of the Mouse Retina. *J. Neurosci.* 18:8936–8946. doi:10.1523/JNEUROSCI.18-21-08936.1998.

Jiang, Y., X. Qi, M.A. Chrenek, C. Gardner, J.H. Boatright, H.E. Grossniklaus, and J.M. Nickerson. 2013. Functional Principal Component Analysis Reveals Discriminating Categories of Retinal Pigment Epithelial Morphology in Mice. *Invest. Ophthalmol. Vis. Sci.* 54:7274–7283. doi:10.1167/IOVS.13-12450.

Kahraman, N.S., and A. Oner. 2020. Umbilical cord derived mesenchymal stem cell implantation in retinitis pigmentosa: a 6-month follow-up results of a phase 3 trial. *Int. J. Ophthalmol.* 13:1423–1429. doi:10.18240/IJO.2020.09.14.

Kalloniatis, M., L. Nivison-Smith, J. Chua, M.L. Acosta, and E.L. Fletcher. 2016. Using the rd1 mouse to understand functional and anatomical retinal remodelling and treatment implications in retinitis pigmentosa: A review. *Exp. Eye Res.* 150:106–121. doi:10.1016/J.EXER.2015.10.019.

Kamermans, M., and H. Spekreijse. 1999. The feedback pathway from horizontal cells to cones: A mini review with a look ahead. *Vision Res.* 39:2449–2468. doi:10.1016/S0042-6989(99)00043-7.

Kaneko, A. 1970. Physiological and morphological identification of horizontal, bipolar and amacrine cells in goldfish retina. *J. Physiol.* 207:623–633. doi:10.1113/JPHYSIOL.1970.SP009084.

Kang, C., and L.J. Scott. 2020. Voretigene Neparvovec: A Review in RPE65 Mutation-Associated Inherited Retinal Dystrophy. *Mol. Diagn. Ther.* 24:487–495. doi:10.1007/S40291-020-00475-6.

Kanow, M.A., M.M. Giarmarco, C. Jankowski, K. Tsantilas, A.L. Engel, J. Du, J.D. Linton, C.C. Farnsworth, S.R. Sloat, K.J. Lindsay, E.D. Parker, S.E. Brockerhoff, M. Sadilek, J.R. Chao, and J.B. Hurley. 2017. Biochemical adaptations of the retina and retinal pigment epithelium support a metabolic ecosystem in the vertebrate eye. *bioRxiv*. 143347. doi:10.1101/143347.

Karunadharma, P.P., C.L. Nordgaard, T.W. Olsen, and D.A. Ferrington. 2010. Mitochondrial DNA Damage as a Potential Mechanism for Age-Related Macular Degeneration. *Invest. Ophthalmol. Vis. Sci.* 51:5470. doi:10.1167/IOVS.10-5429.

Kawamura, S., and S. Tachibanaki. 2008. Rod and cone photoreceptors: molecular basis of the difference in their physiology. *Comp. Biochem. Physiol. A. Mol. Integr. Physiol.* 150:369–377. doi:10.1016/J.CBPA.2008.04.600.

Kevany, B.M., and K. Palczewski. 2010. Phagocytosis of retinal rod and cone photoreceptors. *Physiology*.

25:8–15. doi:10.1152/PHYSIOL.00038.2009/ASSET/IMAGES/LARGE/Y0038-9-04.JPEG.

Kim, H., M. Kim, S.-K. Im, and S. Fang. 2018. Mouse Cre-LoxP system: general principles to determine tissue-specific roles of target genes. *Lab. Anim. Res.* 34:147. doi:10.5625/LAR.2018.34.4.147.

Kim, Y.N., J.S. Song, S.H. Oh, Y.J. Kim, Y.H. Yoon, E.J. Seo, C.A. Seol, S.M. Lee, J.M. Choi, G.H. Seo, C. Keum, B.H. Lee, and J.Y. Lee. 2020. Clinical characteristics and disease progression of retinitis pigmentosa associated with PDE6B mutations in Korean patients. *Sci. Reports 2020 101*. 10:1–12. doi:10.1038/s41598-020-75902-z.

Klenchin, V.A., P.D. Calvert, and M.D. Bownds. 1995. Inhibition of rhodopsin kinase by recoverin. Further evidence for a negative feedback system in phototransduction. *J. Biol. Chem.* 270:16147–16152. doi:10.1074/JBC.270.27.16147.

Koch, S.F., J.K. Duong, C.W. Hsu, Y.T. Tsai, C.S. Lin, C.A. Wahl-Schott, and S.H. Tsang. 2017. Genetic rescue models refute nonautonomous rod cell death in retinitis pigmentosa. *Proc. Natl. Acad. Sci. U. S. A.* 114:5259–5264. doi:10.1073/pnas.1615394114.

Koch, S.F., Y.T. Tsai, J.K. Duong, W.H. Wu, C.W. Hsu, W.P. Wu, L. Bonet-Ponce, C.S. Lin, and S.H. Tsang. 2015. Halting progressive neurodegeneration in advanced retinitis pigmentosa. *J. Clin. Invest.* 125:3704–3713. doi:10.1172/JCI82462.

Kofuji, P., P. Ceelen, K.R. Zahs, L.W. Surbeck, H.A. Lester, and E.A. Newman. 2000. Genetic inactivation of an inwardly rectifying potassium channel (Kir4.1 subunit) in mice: phenotypic impact in retina. *J. Neurosci.* 20:5733–5740. doi:10.1523/JNEUROSCI.20-15-05733.2000.

Komeima, K., B.S. Rogers, L. Lu, and P.A. Campochiaro. 2006. Antioxidants reduce cone cell death in a model of retinitis pigmentosa. *Proc. Natl. Acad. Sci. U. S. A.* 103:11300–11305. doi:10.1073/PNAS.0604056103.

Kuehlewein, L., D. Zobor, K. Stingl, M. Kempf, F. Nasser, A. Bernd, S. Biskup, F.P.M. Cremers, M.I. Khan, P. Mazzola, K. Schäferhoff, T. Heinrich, T.B. Haack, B. Wissinger, E. Zrenner, N. Weisschuh, and S. Kohl. 2021. Clinical Phenotype of PDE6B-Associated Retinitis Pigmentosa. *Int. J. Mol. Sci.* 22:1–15. doi:10.3390/IJMS22052374.

Kurihara, T., P.D. Westenskow, M.L. Gantner, Y. Usui, A. Schultz, S. Bravo, E. Aguilar, C. Wittgrove, M.S.H. Friedlander, L.P. Paris, E. Chew, G. Siuzdak, and M. Friedlander. 2016. Hypoxia-induced metabolic stress in retinal pigment epithelial cells is sufficient to induce photoreceptor degeneration. *Elife*. 5. doi:10.7554/ELIFE.14319.

Kwon, W., and S.A. Freeman. 2020. Phagocytosis by the Retinal Pigment Epithelium: Recognition, Resolution, Recycling. *Front. Immunol.* 11:2985. doi:10.3389/FIMMU.2020.604205/BIBTEX.

Langlois, G., C.K. Chen, K. Palczewski, J.B. Hurley, and T.M. Vuong. 1996. Responses of the phototransduction cascade to dim light. *Proc. Natl. Acad. Sci. U. S. A.* 93:4677. doi:10.1073/PNAS.93.10.4677.

Lee, S.J., and S.Y. Kim. 2021. Non-separate Mouse Sclerochoroid/RPE/Retina Staining and Whole Mount for the Integral Observation of Subretinal Layer. *Bio-protocol*. 11. doi:10.21769/BIOPROTOC.3872.

Lehtonen, J. V., D.J. Still, V. V. Rantanen, J. Ekholm, D. Björklund, Z. Iftikhar, M. Huhtala, S. Repo, A. Jussila, J. Jaakkola, O. Pentikäinen, T. Nyrönen, T. Salminen, M. Gyllenberg, and M.S. Johnson. 2004. BODIL: A molecular modeling environment for structure-function analysis and drug design. *J. Comput. Aided. Mol. Des.* 18:401–419. doi:10.1007/s10822-004-3752-4.

Li, S., S. Datta, E. Brabbit, Z. Love, V. Woytowicz, K. Flattery, J. Capri, K. Yao, S. Wu, M. Imboden, A. Upadhyay, R. Arumugham, W.B. Thoreson, M.M. DeAngelis, and N.B. Haider. 2021a. Nr2e3 is a genetic modifier that rescues retinal degeneration and promotes homeostasis in multiple models of retinitis pigmentosa. *Gene Ther.* 28:223–241. doi:10.1038/S41434-020-0134-Z.

Li, X., S. Cai, Z. He, J. Reilly, Z. Zeng, N. Strang, and X. Shu. 2021b. Metabolomics in Retinal Diseases: An Update. *Biology (Basel).* 10. doi:10.3390/BIOLOGY10100944.

Lin, B., and R.H. Masland. 2006. Populations of wide-field amacrine cells in the mouse retina. *J. Comp. Neurol.* 499:797–809. doi:10.1002/CNE.21126.

Lin, B., and E.B. Peng. 2013. Retinal Ganglion Cells are Resistant to Photoreceptor Loss in Retinal Degeneration. *PLoS One*. 8. doi:10.1371/JOURNAL.PONE.0068084.

Liu, J., D.A. Copland, S. Theodoropoulou, H.A.A. Chiu, M.D. Barba, K.W. Mak, M. Mack, L.B. Nicholson, and A.D. Dick. 2016. Impairing autophagy in retinal pigment epithelium leads to inflammasome activation and enhanced macrophage-mediated angiogenesis. *Sci. Rep.* 6. doi:10.1038/SREP20639.

Ma, Y., R. Kawasaki, L.P. Dobson, J.B. Ruddle, L.S. Kearns, T.Y. Wong, and D.A. Mackey. 2012. Quantitative analysis of retinal vessel attenuation in eyes with retinitis pigmentosa. *Investig. Ophthalmol. Vis. Sci.* 53:4306–4314. doi:10.1167/iovs.11-8596.

MacNeil, M.A., and R.H. Masland. 1998. Extreme diversity among amacrine cells: implications for function. *Neuron*. 20:971–982. doi:10.1016/S0896-6273(00)80478-X.

Majumdar, S., J. Weiss, and H. Wässle. 2009. Glycinergic input of widefield, displaced amacrine cells of the mouse retina. *J. Physiol.* 587:3831. doi:10.1113/JPHYSIOL.2009.171207.

Mantych, G.J., S.U. Devaskar, and S.U. Devaskar. 1993. Characterization of glucose transporter isoforms in the adult and developing human eye. *Endocrinology*. 133:600–607. doi:10.1210/ENDO.133.2.8344201.

Mao, Y., and S.C. Finnemann. 2012a. Analysis of Photoreceptor Outer Segment Phagocytosis by RPE Cells in Culture. *Methods Mol. Biol.* 935:285–295. doi:10.1007/978-1-62703-080-9_20.

Mao, Y., and S.C. Finnemann. 2012b. Essential diurnal Rac1 activation during retinal phagocytosis requires αvβ5 integrin but not tyrosine kinases focal adhesion kinase or Mer tyrosine kinase. *Mol. Biol. Cell*. 23:1104–1114. doi:10.1091/MBC.E11-10-0840.

Mao, Y., and S.C. Finnemann. 2016. Live Imaging of LysoTracker-Labelled Phagolysosomes Tracks Diurnal Phagocytosis of Photoreceptor Outer Segment Fragments in Rat RPE Tissue Ex Vivo. *Adv. Exp. Med. Biol.* 854:717. doi:10.1007/978-3-319-17121-0_95.

Marc, R.E., J.R. Anderson, B.W. Jones, C.L. Sigulinsky, and J.S. Lauritzen. 2014. The All amacrine cell connectome: A dense network hub. *Front. Neural Circuits*. 8:104. doi:10.3389/FNCIR.2014.00104/ABSTRACT.

Marc, R.E., B.W. Jones, C.B. Watt, and E. Strettoi. 2003. Neural remodeling in retinal degeneration. *Prog. Retin. Eye Res.* 22:607–655. doi:10.1016/S1350-9462(03)00039-9.

Marquardt, T., R. Ashery-Padan, N. Andrejewski, R. Scardigli, F. Guillemot, and P. Gruss. 2001. Pax6 Is Required for the Multipotent State of Retinal Progenitor Cells. *Cell*. 105:43–55. doi:10.1016/S0092-8674(01)00295-1.

Masu, M., H. Iwakabe, Y. Tagawa, T. Miyoshi, M. Yamashita, Y. Fukuda, H. Sasaki, K. Hiroi, Y. Nakamura, R. Shigemoto, M. Takada, K. Nakamura, K. Nakao, M. Katsuki, and S. Nakanishi. 1995. Specific deficit of the ON response in visual transmission by targeted disruption of the mGluR6 gene. *Cell*. 80:757–765. doi:10.1016/0092-8674(95)90354-2.

Matsumoto, B., D.M. Defoe, and J.C. Besharse. 1987. Membrane turnover in rod photoreceptors: ensheathment and phagocytosis of outer segment distal tips by pseudopodia of the retinal pigment epithelium. *Proc. R. Soc. London. Ser. B, Biol. Sci.* 230:339–354. doi:10.1098/RSPB.1987.0023.

Mazzoni, F., H. Safa, and S.C. Finnemann. 2014. Understanding photoreceptor outer segment phagocytosis: Use and utility of RPE cells in culture. *Exp. Eye Res.* 0:51. doi:10.1016/J.EXER.2014.01.010.

Milićević, N., O. Ait-Hmyed Hakkari, U. Bagchi, C. Sandu, A. Jongejan, P.D. Moerland, J.B. ten Brink, D. Hicks, A.A. Bergen, and M.P. Felder-Schmittbuhl. 2021. Core circadian clock genes Per1 and Per2 regulate the rhythm in photoreceptor outer segment phagocytosis. *FASEB J.* 35:e21722. doi:10.1096/FJ.202100293RR.

Milićević, N., N. Mazzaro, I. de Bruin, E. Wils, J. ten Brink, A. ten Asbroek, J. Mendoza, A. Bergen, and M.P. Felder-Schmittbuhl. 2019. Rev-Erbα and Photoreceptor Outer Segments modulate the Circadian Clock in Retinal Pigment Epithelial Cells. *Sci. Rep.* 9. doi:10.1038/S41598-019-48203-3.

Mills, S.L., and S.C. Massey. 1995. Differential properties of two gap junctional pathways made by AII amacrine cells. *Nature*. 377:734–737. doi:10.1038/377734A0.

Mitchell, C.K., C.L. Rowe-Rendleman, S. Ashraf, and D.A. Redburn. 1995. Calbindin immunoreactivity of horizontal cells in the developing rabbit retina. *Exp. Eye Res.* 61:691–698. doi:10.1016/S0014-4835(05)80020-X.

Moreno, M.L., S. Mérida, F. Bosch-Morell, M. Miranda, and V.M. Villar. 2018. Autophagy Dysfunction and Oxidative Stress, Two Related Mechanisms Implicated in Retinitis Pigmentosa. *Front. Physiol.* 9. doi:10.3389/FPHYS.2018.01008.

Murenu, E., S. Kostidis, S. Lahiri, A.S. Geserich, A. Imhof, M. Giera, and S. Michalakis. 2021. Metabolic Analysis of Vitreous/Lens and Retina in Wild Type and Retinal Degeneration Mice. *Int. J. Mol. Sci.* 22:1–22. doi:10.3390/IJMS22052345.

Nagelhus, E.A., M.L. Veruki, R. Torp, F.M. Haug, J.H. Laake, S. Nielsen, P. Agre, and O.P. Ottersen. 1998. Aquaporin-4 Water Channel Protein in the Rat Retina and Optic Nerve: Polarized Expression in Müller Cells and Fibrous Astrocytes. *J. Neurosci.* 18:2506–2519. doi:10.1523/JNEUROSCI.18-07-02506.1998.

Negoescu, A., P. Lorimier, F. Labat-Moleur, C. Drouet, C. Robert, C. Guillermet, C. Brambilla, and E.

Brambilla. 1996. In situ apoptotic cell labeling by the TUNEL method: improvement and evaluation on cell preparations. *J. Histochem. Cytochem.* 44:959–968. doi:10.1177/44.9.8773561.

Nikonov, S.S., R. Kholodenko, J. Lem, and E.N. Pugh. 2006. Physiological Features of the S- and M-cone Photoreceptors of Wild-type Mice from Single-cell Recordings. *J. Gen. Physiol.* 127:359–374. doi:10.1085/JGP.200609490.

Ohguro, H., K. Palczewski, L.H. Ericsson, K.A. Walsh, and R.S. Johnson. 1993. Sequential phosphorylation of rhodopsin at multiple sites. *Biochemistry*. 32:5718–5724. doi:10.1021/BI00072A030.

Ohsawa, K., Y. Imai, Y. Sasaki, and S. Kohsaka. 2004. Microglia/macrophage-specific protein Iba1 binds to fimbrin and enhances its actin-bundling activity. *J. Neurochem.* 88:844–856. doi:10.1046/J.1471-4159.2003.02213.X.

Oner, A., Z.B. Gonen, N. Sinim, M. Cetin, and Y. Ozkul. 2016. Subretinal adipose tissue-derived mesenchymal stem cell implantation in advanced stage retinitis pigmentosa: a phase I clinical safety study. *Stem Cell Res. Ther.* 7:1–12. doi:10.1186/S13287-016-0432-Y/FIGURES/7.

Özmert, E., and U. Arslan. 2020. Management of retinitis pigmentosa by Wharton's jelly derived mesenchymal stem cells: preliminary clinical results. *Stem Cell Res. Ther.* 11. doi:10.1186/S13287-020-1549-6.

Panda-Jonas, S., J.B. Jonas, and M. Jakobczyk-Zmija. 1996. Retinal pigment epithelial cell count, distribution, and correlations in normal human eyes. *Am. J. Ophthalmol.* 121:181–189. doi:10.1016/S0002-9394(14)70583-5.

Pandit, S.K., B. Westendorp, and A. De Bruin. 2013. Physiological significance of polyploidization in mammalian cells. *Trends Cell Biol.* 23:556–566. doi:10.1016/J.TCB.2013.06.002.

Parmeggiani, F., F. S. Sorrentino, D. Ponzin, V. Barbaro, S. Ferrari, and E. Di Iorio. 2011. Retinitis Pigmentosa: Genes and Disease Mechanisms. *Curr. Genomics*. 12:238. doi:10.2174/138920211795860107.

Patel, J.C., A. Hall, and E. Caron. 2002. Vav regulates activation of Rac but not Cdc42 during FcgammaR-mediated phagocytosis. *Mol. Biol. Cell*. 13:1215–1226. doi:10.1091/MBC.02-01-0002.

Petit, C. 2001. Usher syndrome: from genetics to pathogenesis. *Annu. Rev. Genomics Hum. Genet.* 2:271–297. doi:10.1146/ANNUREV.GENOM.2.1.271.

Petrukhin, K. 2013. Pharmacological inhibition of lipofuscin accumulation in the retina as a therapeutic strategy for dry AMD treatment. *Drug Discov. Today. Ther. Strateg.* 10:e11. doi:10.1016/J.DDSTR.2013.05.004.

Pfeiffer, R.L., R.E. Marc, M. Kondo, H. Terasaki, and B.W. Jones. 2016. Müller cell metabolic chaos during retinal degeneration. *Exp. Eye Res.* 150:62–70. doi:10.1016/J.EXER.2016.04.022.

Phillips, M.J., D.C. Otteson, and D.M. Sherry. 2010. Progression of Neuronal and Synaptic Remodeling in the rd10 Mouse Model of Retinitis Pigmentosa. *J. Comp. Neurol.* 518:2071. doi:10.1002/CNE.22322.

Di Pierdomenico, J., A. Martínez-Vacas, D. Hernández-Muñoz, A.M. Gómez-Ramírez, F.J. Valiente-Soriano, M. Agudo-Barriuso, M. Vidal-Sanz, M.P. Villegas-Pérez, and D. García-Ayuso. 2020.

Coordinated Intervention of Microglial and Müller Cells in Light-Induced Retinal Degeneration. *Invest. Ophthalmol. Vis. Sci.* 61. doi:10.1167/IOVS.61.3.47.

Pittler, S.J., and W. Baehr. 1991. Identification of a nonsense mutation in the rod photoreceptor cGMP phosphodiesterase β-subunit gene of the rd mouse. *Proc. Natl. Acad. Sci. U. S. A.* 88:8322–8326. doi:10.1073/PNAS.88.19.8322.

Pow, D. V., and D.K. Crook. 1995. Immunocytochemical evidence for the presence of high levels of reduced glutathione in radial glial cells and horizontal cells in the rabbit retina. *Neurosci. Lett.* 193:25–28. doi:10.1016/0304-3940(95)11657-I.

Prigge, J.R., J.A. Wiley, E.A. Talago, E.M. Young, L.L. Johns, J.A. Kundert, K.M. Sonsteng, W.P. Halford, M.R. Capecchi, and E.E. Schmidt. 2013. Nuclear double-fluorescent reporter for in vivo and ex vivo analyses of biological transitions in mouse nuclei. *Mamm. Genome*. 24:389–399. doi:10.1007/S00335-013-9469-8.

Pugh, E.N., and T.D. Lamb. 2000. Chapter 5 Phototransduction in vertebrate rods and cones: Molecular mechanisms of amplification, recovery and light adaptation. *Handb. Biol. Phys.* 3:183–255. doi:10.1016/S1383-8121(00)80008-1.

Puthussery, T., J. Gayet-Primo, and W.R. Taylor. 2010. Localization of the Calcium-binding Protein Secretagogin in Cone Bipolar Cells of the Mammalian Retina. *J. Comp. Neurol.* 518:513–525. doi:10.1002/CNE.22234.

Queirós, A., J.M. González-Méijome, P. Fernandes, J. Jorge, R. Montés-Micó, J.B. Almeida, and M.A. Parafita. 2007. Technical note: a comparison of central and peripheral intraocular pressure using rebound tonometry. *Ophthalmic Physiol. Opt.* 27:506–511. doi:10.1111/J.1475-1313.2007.00508.X.

Qureshi, B.M., E. Behrmann, J. Schöneberg, J. Loerke, J. Bürger, T. Mielke, J. Giesebrecht, F. Noé, T.D. Lamb, K.P. Hofmann, C.M.T. Spahn, and M. Heck. 2018. It takes two transducins to activate the cGMP-phosphodiesterase 6 in retinal rods. *Open Biol.* 8. doi:10.1098/RSOB.180075.

Rashid, K., I. Akhtar-Schaefer, and T. Langmann. 2019. Microglia in retinal degeneration. *Front. Immunol.* 10:1975. doi:10.3389/FIMMU.2019.01975/BIBTEX.

Rauen, T., and M. Wießner. 2000. Fine tuning of glutamate uptake and degradation in glial cells: common transcriptional regulation of GLAST1 and GS. *Neurochem. Int.* 37:179–189. doi:10.1016/S0197-0186(00)00021-8.

Raviola, E., and N.B. Gilula. 1973. Gap Junctions between Photoreceptor Cells in the Vertebrate Retina. *Proc. Natl. Acad. Sci. U. S. A.* 70:1677. doi:10.1073/PNAS.70.6.1677.

Reichenbach, A., and A. Bringmann. 2013. New functions of Müller cells. *Glia*. 61:651–678. doi:10.1002/GLIA.22477.

Reilander, H., A. Achilles, U. Friedel, G. Maul, F. Lottspeich, and N.J. Cook. 1992. Primary structure and functional expression of the Na/Ca,K-exchanger from bovine rod photoreceptors. *EMBO J.* 11:1689. doi:10.1002/j.1460-2075.1992.tb05219.x.

Riepe, R.E., and M.D. Norenburg. 1977. Müller cell localisation of glutamine synthetase in rat retina. *Nat.*

1977 2685621. 268:654–655. doi:10.1038/268654a0.

Rizzolo, L.J. 2007. Development and Role of Tight Junctions in the Retinal Pigment Epithelium. *Int. Rev. Cytol.* 258:195–234. doi:10.1016/S0074-7696(07)58004-6.

Ruggiero, L., M.P. Connor, J. Chen, R. Langen, and S.C. Finnemann. 2012. Diurnal, localized exposure of phosphatidylserine by rod outer segment tips in wild-type but not Itgb5-/- or Mfge8-/- mouse retina. *Proc. Natl. Acad. Sci. U. S. A.* 109:8145–8148. doi:10.1073/PNAS.1121101109.

Sahel, J.A., E. Boulanger-Scemama, C. Pagot, A. Arleo, F. Galluppi, J.N. Martel, S.D. Esposti, A. Delaux, J.B. de Saint Aubert, C. de Montleau, E. Gutman, I. Audo, J. Duebel, S. Picaud, D. Dalkara, L. Blouin, M. Taiel, and B. Roska. 2021. Partial recovery of visual function in a blind patient after optogenetic therapy. *Nat. Med. 2021 277*. 27:1223–1229. doi:10.1038/s41591-021-01351-4.

Sakai, N., J. Decatur, K. Nakanishi, and G.E. Eldred. 1996. Ocular age pigment "A2-E": An unprecedented pyridinium bisretinoid. *J. Am. Chem. Soc.* 118:1559–1560. doi:10.1021/JA953480G/SUPPL_FILE/JA1559.PDF.

Sanderson, M.J., I. Smith, I. Parker, and M.D. Bootman. 2014. Fluorescence Microscopy. *Cold Spring Harb. Protoc.* 2014:pdb.top071795. doi:10.1101/PDB.TOP071795.

Sarfare, S., A.S. McKeown, J. Messinger, G. Rubin, H. Wei, T.W. Kraft, and S.J. Pittler. 2014. Overexpression of rod photoreceptor glutamic acid rich protein 2 (GARP2) increases gain and slows recovery in mouse retina. *Cell Commun. Signal.* 12. doi:10.1186/S12964-014-0067-5.

Sato, K., D. Saigusa, R. Saito, A. Fujioka, Y. Nakagawa, K.M. Nishiguchi, T. Kokubun, I.N. Motoike, K. Maruyama, K. Omodaka, Y. Shiga, A. Uruno, S. Koshiba, M. Yamamoto, and T. Nakazawa. 2018. Metabolomic changes in the mouse retina after optic nerve injury. *Sci. Reports 2018 81*. 8:1–13. doi:10.1038/s41598-018-30464-z.

Schmitz, Y., and P. Witkovsky. 1997. Dependence of photoreceptor glutamate release on a dihydropyridine-sensitive calcium channel. *Neuroscience*. 78:1209–1216. doi:10.1016/S0306-4522(96)00678-1.

Schneider, B.G., A.W. Shyjan, and R. Levenson. 1991. Co-localization and polarized distribution of Na,K-ATPase alpha 3 and beta 2 subunits in photoreceptor cells. *J. Histochem. Cytochem.* 39:507–517. doi:10.1177/39.4.1848572.

Schütte, M., and P. Werner. 1998. Redistribution of glutathione in the ischemic rat retina. *Neurosci. Lett.* 246:53–56. doi:10.1016/S0304-3940(98)00229-8.

Shekhar, K., S.W. Lapan, I.E. Whitney, N.M. Tran, E.Z. Macosko, M. Kowalczyk, X. Adiconis, J.Z. Levin, J. Nemesh, M. Goldman, S.A. McCarroll, C.L. Cepko, A. Regev, and J.R. Sanes. 2016. COMPREHENSIVE CLASSIFICATION OF RETINAL BIPOLAR NEURONS BY SINGLE-CELL TRANSCRIPTOMICS. *Cell*. 166:1308. doi:10.1016/J.CELL.2016.07.054.

Shevell, S.K., and F.A.A. Kingdom. 2007. Color in Complex Scenes. *http://dx.doi.org/10.1146/annurev.psych.59.103006.093619*. 59:143–166. doi:10.1146/ANNUREV.PSYCH.59.103006.093619.

Song, X., F. Ma, and K. Herrup. 2019. Accumulation of Cytoplasmic DNA Due to ATM Deficiency

Activates the Microglial Viral Response System with Neurotoxic Consequences. *J. Neurosci.* 39:6378. doi:10.1523/JNEUROSCI.0774-19.2019.

Sparrow, J.R., A. Blonska, E. Flynn, T. Duncker, J.P. Greenberg, R. Secondi, K. Ueda, and F.C. Delori. 2013. Quantitative fundus autofluorescence in mice: correlation with HPLC quantitation of RPE lipofuscin and measurement of retina outer nuclear layer thickness. *Invest. Ophthalmol. Vis. Sci.* 54:2812–2820. doi:10.1167/IOVS.12-11490.

Sparrow, J.R., and M. Boulton. 2005. RPE lipofuscin and its role in retinal pathobiology. *Exp. Eye Res.* 80:595–606. doi:10.1016/J.EXER.2005.01.007.

Sparrow, J.R., D. Hicks, and C.P. Hamel. 2010. The Retinal Pigment Epithelium in Health and Disease. *Curr. Mol. Med.* 10:802. doi:10.2174/156652410793937813.

Steinberg, R.H., I. Wood, and M.J. Hogan. 1977. Pigment epithelial ensheathment and phagocytosis of extrafoveal cones in human retina. *Philos. Trans. R. Soc. Lond. B. Biol. Sci.* 277:459–474. doi:10.1098/RSTB.1977.0028.

Sternberg, N., and D. Hamilton. 1981. Bacteriophage P1 site-specific recombination. I. Recombination between loxP sites. *J. Mol. Biol.* 150:467–486. doi:10.1016/0022-2836(81)90375-2.

Stone, J., A. Itin, T. Alon, J. Pe'er, H. Gnessin, T. Chan-Ling, and E. Keshet. 1995. Development of retinal vasculature is mediated by hypoxia-induced vascular endothelial growth factor (VEGF) expression by neuroglia. *J. Neurosci.* 15:4738–4747. doi:10.1523/JNEUROSCI.15-07-04738.1995.

Strauss, O. 2005. The Retinal Pigment Epithelium in Visual Function. *https://doi.org/10.1152/physrev.00021.2004*. 85:845–881. doi:10.1152/PHYSREV.00021.2004.

Sung, C.H., and J.Z. Chuang. 2010. Review series: The cell biology of vision. *J. Cell Biol.* 190:953. doi:10.1083/JCB.201006020.

Tan, S.Z., P. Begley, G. Mullard, K.A. Hollywood, and P.N. Bishop. 2016. Introduction to metabolomics and its applications in ophthalmology. *Eye 2016 306*. 30:773–783. doi:10.1038/eye.2016.37.

Tanida, I., T. Ueno, and E. Kominami. 2008. LC3 and Autophagy. *Methods Mol. Biol.* 445:77–88. doi:10.1007/978-1-59745-157-4_4.

Tchedre, K.T., S. Batabyal, M. Galicia, D. Narcisse, S.M. Mustafi, A. Ayyagari, S. Chavala, and S.K. Mohanty. 2021. Biodistribution of adeno-associated virus type 2 carrying multi-characteristic opsin in dogs following intravitreal injection. *J. Cell. Mol. Med.* 25:8676–8686. doi:10.1111/JCMM.16823.

Thoreson, W.B., N. Babai, and T.M. Bartoletti. 2008. Feedback from Horizontal Cells to Rod Photoreceptors in Vertebrate Retina. *J. Neurosci.* 28:5691. doi:10.1523/JNEUROSCI.0403-08.2008.

Tohari, A.M., X. Zhou, and X. Shu. 2016. Protection against oxidative stress by vitamin D in cone cells. *Cell Biochem. Funct.* 34:82–94. doi:10.1002/CBF.3167.

Tsujikawa, M., Y. Wada, M. Sukegawa, M. Sawa, F. Gomi, K. Nishida, and Y. Tano. 2008. Age at Onset Curves of Retinitis Pigmentosa. *Arch. Ophthalmol.* 126:337–340. doi:10.1001/ARCHOPHT.126.3.337.

Tuekprakhon, A., S. Sangkitporn, A. Trinavarat, A.R. Pawestri, V. Vamvanij, M. Ruangchainikom, P. Luksanapruksa, P. Pongpaksupasin, A. Khorchai, A. Dambua, P. Boonchu, C. Yodtup, M.

Uiprasertkul, S. Sangkitporn, and L. ongsri Atchaneeyasakul. 2021. Intravitreal autologous mesenchymal stem cell transplantation: a non-randomized phase I clinical trial in patients with retinitis pigmentosa. *Stem Cell Res. Ther.* 12:1–15. doi:10.1186/S13287-020-02122-7/FIGURES/8.

Tuohy, G.P., and R. Megaw. 2021. A Systematic Review and Meta-Analyses of Interventional Clinical Trial Studies for Gene Therapies for the Inherited Retinal Degenerations (IRDs). *Biomolecules*. 11. doi:10.3390/BIOM11050760.

Twig, G., H. Levy, and I. Perlman. 2003. Color opponency in horizontal cells of the vertebrate retina. *Prog. Retin. Eye Res.* 22:31–68. doi:10.1016/S1350-9462(02)00045-9.

Uy, H., M.; Pik, S. Chan, M.; Franz, and M. Cruz. 2013. Stem Cell Therapy: a Novel Approach for Vision Restoration in Retinitis Pigmentosa. *Med. Hypothesis, Discov. Innov. Ophthalmol.* 2:52.

Vecino, E., F.D. Rodriguez, N. Ruzafa, X. Pereiro, and S.C. Sharma. 2016. Glia-neuron interactions in the mammalian retina. *Prog. Retin. Eye Res.* 51:1–40. doi:10.1016/J.PRETEYERES.2015.06.003.

Verbakel, S.K., R.A.C. van Huet, C.J.F. Boon, A.I. den Hollander, R.W.J. Collin, C.C.W. Klaver, C.B. Hoyng, R. Roepman, and B.J. Klevering. 2018. Non-syndromic retinitis pigmentosa. *Prog. Retin. Eye Res.* 66:157–186. doi:10.1016/j.preteyeres.2018.03.005.

Veske, A., S.E.G. Nilsson, K. Narfström, and A. Gal. 1999. Retinal dystrophy of Swedish briard/briard-beagle dogs is due to a 4-bp deletion in RPE65. *Genomics*. 57:57–61. doi:10.1006/GENO.1999.5754.

Viegas, F.O., and S.C.F. Neuhauss. 2021. A Metabolic Landscape for Maintaining Retina Integrity and Function. *Front. Mol. Neurosci.* 14:60. doi:10.3389/FNMOL.2021.656000/BIBTEX.

Volland, S., J. Esteve-Rudd, J. Hoo, C. Yee, and D.S. Williams. 2015. A Comparison of Some Organizational Characteristics of the Mouse Central Retina and the Human Macula. *PLoS One*. 10. doi:10.1371/JOURNAL.PONE.0125631.

Wang, A.L., M.E. Boulton, W.A. Dunn, H.V. Rao, J. Cai, T.J. Lukas, and A.H. Neufeld. 2009. Using LC3 to Monitor Autophagy Flux in the Retinal Pigment Epithelium. *Autophagy*. 5:1190. doi:10.4161/AUTO.5.8.10087.

Wang, T., J. Reingruber, M.L. Woodruff, A. Majumder, A. Camarena, N.O. Artemyev, G.L. Fain, and J. Chen. 2018. The PDE6 mutation in the rd10 retinal degeneration mouse model causes protein mislocalization and instability and promotes cell death through increased ion influx. *J. Biol. Chem.* 293:15332–15346. doi:10.1074/JBC.RA118.004459.

Whitaker, C.M., G. Nobles, M. Ishibashi, and S.C. Massey. 2021. Rod and Cone Connections With Bipolar Cells in the Rabbit Retina. *Front. Cell. Neurosci.* 15:155. doi:10.3389/FNCEL.2021.662329/BIBTEX.

Wilkinson, C.P., D.R. Hinton, S.R. Sadda, and P. Wiedemann. 2018. Ryan's Retina 6th Edition. 6th ed. Elsevier.

Winkler, P.A., L.M. Occelli, and S.M. Petersen-Jones. 2020. Large Animal Models of Inherited Retinal Degenerations: A Review. *Cells*. 9. doi:10.3390/CELLS9040882.

Van Wyk, M., H. Wässle, and W.R. Taylor. 2009. Receptive field properties of ON- and OFF-ganglion cells in the mouse retina. *Vis. Neurosci.* 26:297–308. doi:10.1017/S0952523809990137.

Xiong, W.H., J.J. Pang, M.E. Pennesi, R.M. Duvoisin, S.M. Wu, and C.W. Morgans. 2015. The Effect of PKCα on the Light Response of Rod Bipolar Cells in the Mouse Retina. *Invest. Ophthalmol. Vis. Sci.* 56:4961–4974. doi:10.1167/IOVS.15-16622.

Xue, Y., S. Sato, D. Razafsky, B. Sahu, S.Q. Shen, C. Potter, L.L. Sandell, J.C. Corbo, K. Palczewski, A. Maeda, D. Hodzic, and V.J. Kefalov. 2017. The role of retinol dehydrogenase 10 in the cone visual cycle. *Sci. Reports 2017 71*. 7:1–13. doi:10.1038/s41598-017-02549-8.

Yao, J., Y. Qiu, E. Frontera, L. Jia, N.W. Khan, D.J. Klionsky, T.A. Ferguson, D.A. Thompson, and D.N. Zacks. 2018. Inhibiting autophagy reduces retinal degeneration caused by protein misfolding. *Autophagy*. 14:1226–1238. doi:10.1080/15548627.2018.1463121.

Yee, R., and P.A. Liebman. 1978. Light-activated phosphodiesterase of the rod outer segment. Kinetics and parameters of activation and deactivation. *J. Biol. Chem.* 253:8902–8909.

Zdilla, M.J., S.A. Hatfield, K.A. McLean, L.M. Cyrus, J.M. Laslo, and H.W. Lambert. 2016. Circularity, solidity, axes of a best fit ellipse, aspect ratio, and roundness of the foramen ovale: a morphometric analysis with neurosurgical considerations. *J. Craniofac. Surg.* 27:222. doi:10.1097/SCS.0000000000002285.

Zhang, L., X. Cui, R. Jauregui, K.S. Park, S. Justus, Y.T. Tsai, J.K. Duong, C.W. Hsu, W.H. Wu, C.L. Xu, C.S. Lin, and S.H. Tsang. 2018. Genetic Rescue Reverses Microglial Activation in Preclinical Models of Retinitis Pigmentosa. *Mol. Ther.* 26:1953–1964. doi:10.1016/J.YMTHE.2018.06.014.

Zhao, T., Q. Liang, X. Meng, P. Duan, F. Wang, S. Li, Y. Liu, and Z.Q. Yin. 2020. Intravenous Infusion of Umbilical Cord Mesenchymal Stem Cells Maintains and Partially Improves Visual Function in Patients with Advanced Retinitis Pigmentosa. *Stem Cells Dev.* 29:1029–1037. doi:10.1089/SCD.2020.0037.

Zhi, Z., W.O. Cepurna, E.C. Johnson, J.C. Morrison, and R.K. Wang. 2012. Impact of intraocular pressure on changes of blood flow in the retina, choroid, and optic nerve head in rats investigated by optical microangiography. *Biomed. Opt. Express*. 3:2220. doi:10.1364/BOE.3.002220.

Supplementary material

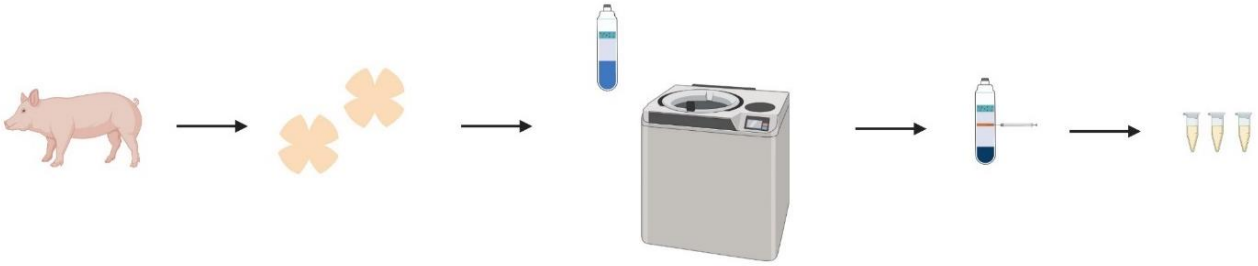

Fig. S1. POS isolation from porcine retinas and labelling with FITC isomer. Retinae were isolated from porcine eyes, and mixed with homogenization solutions, and filtered. Next, glucose gradient was created, and the filtered solution was pipetted above glucose gradient. Tubes were centrifuged with an ultracentrifuge, and sharp, orangish layers was collected with a needle. After multiple dilution and resuspension rounds, FITC-label was added. Then, washing and resuspension was done once again, and finally POS concentration was defined under a microscope. Created with BioRender.com.

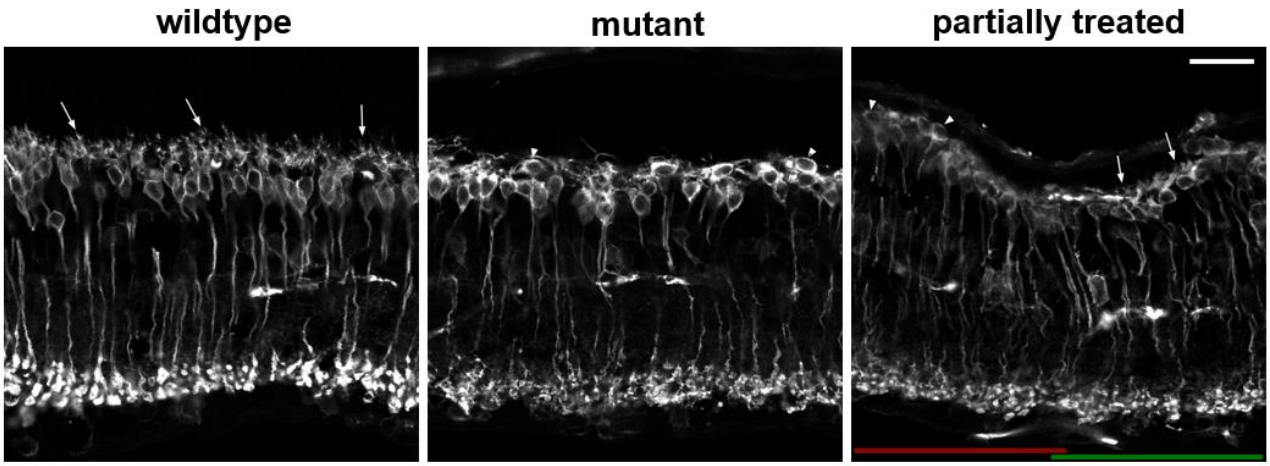

Fig. S2. RBC dendrites are lost in the mutant mouse retina and partially degenerated in the treated mouse retina at 48 weeks of age. Arrows show that in wildtype abundant RBC dendrites in wildtype, whereas in mutant retina the RBC dendrites are lost (arrowhead). In treated mouse retina, a difference between recombined area (green) and non-recombined area (red) in the RBC dendrites is noticeable; recombined area consist of more dendrites in its RBCs. Red and green lines illustrates the non-recombined and recombined areas of the retina. Arrow, RBC dendrites. Arrowhead, dendrite-lacking RBC. Scalebar, 25µm.

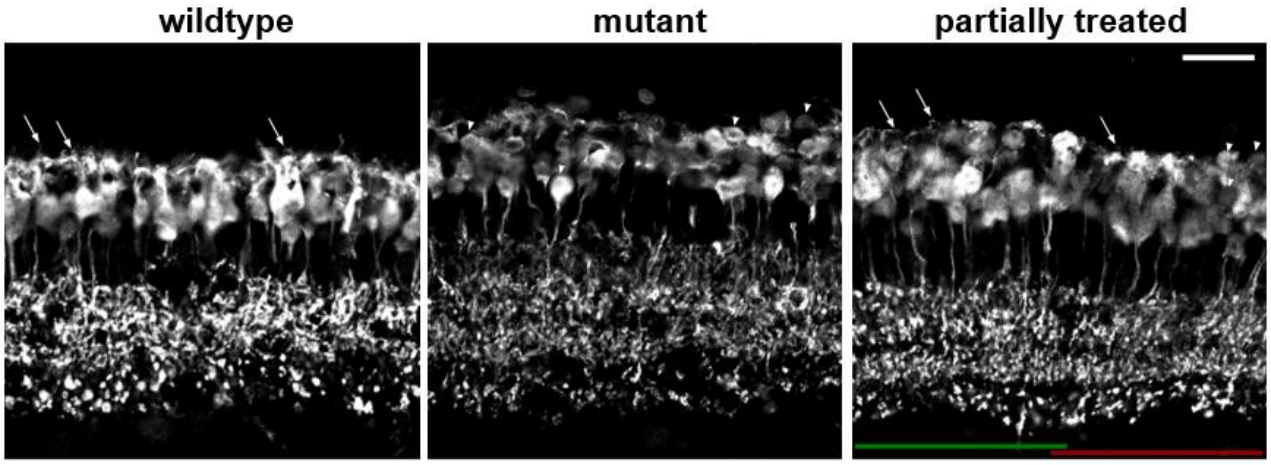

Fig. S3. CBC dendrite loss in 48-week-old mutant and treated mice is notable. CBC dendrites are lost in mutant retinae. Also, CBC axons and axon terminals in mutant have started to degenerate. CBC dendritic loss can be detected from non-recombined area of treated mouse retinae, but in recombined area dendrites can be seen. Red and green lines illustrates the non-recombined and recombined areas of the retina. Arrow, CBC dendrites. Arrowhead, dendrite-lacking CBC Scalebar, 25μm.

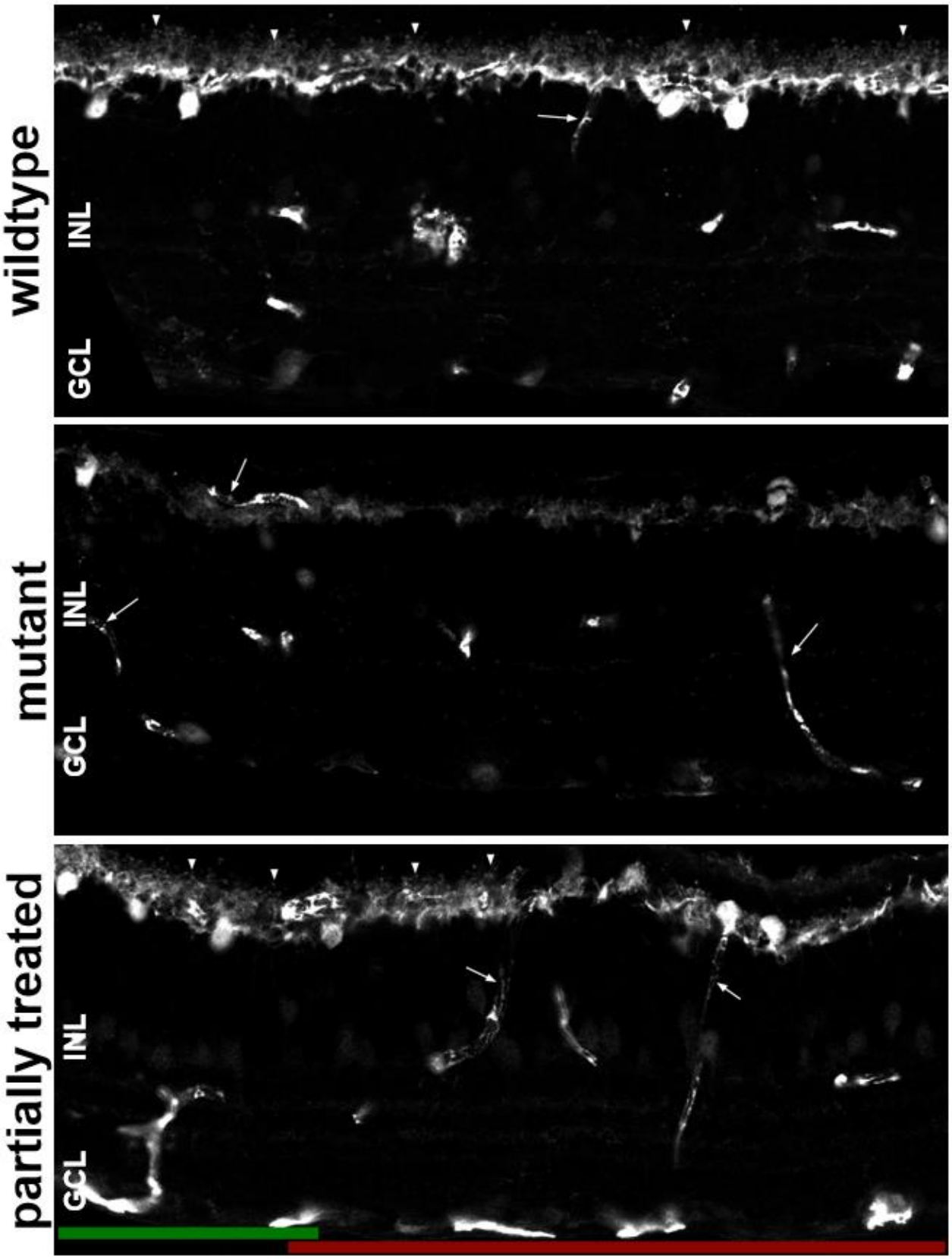

Fig. S4. Horizontal cells are almost completely degenerated in mutant retina and have less HC dendrites in the non-recombined area of partially treated retina at 48 weeks of age. Additional, long ectopic branches of HCs can be observed in both mutant and non-recombined area of partially treated retina. Arrow, ectopic branches of HCs. Arrowhead, dendritic branches of HCs. HC, horizontal cell. Scalebar, 20μm.

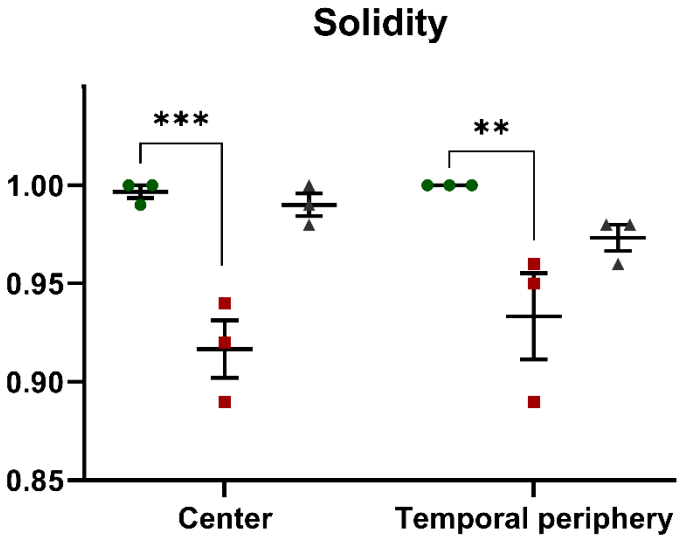

Fig. S5. RPE cells of partially treated resembles wildtype solidity values in center, whereas mutant has significantly lower solidity values in both center and periphery compared to wildtype at 48 weeks of age. Additional solidity measurement conducted by using ImageJ. Means with SEMs. In center, significant difference between wildtype and mutant (p=0.0009) was shown (wildtype, n = 3; mutant, n = 3, partially treated, n = 3) with 2-way ANOVA. In temporal periphery, significant difference between wildtype and mutant (p=0.0036) was shown (wildtype, n = 3; mutant, n = 3, treated, n = 3; 2-way ANOVA). Green, wildtype; red, mutant; grey, partially treated.